Environmental Chemistry Letters
https://doi.org/10.1007/s10311-020-01045-2

REVIEW

Fabrication, functionalization and performance of doped photocatalysts for dye degradation and mineralization: a review

Ackmez Mudhoo[1] · Sonam Paliya[2,3] · Prittam Goswami[4] · Mukesh Singh[4] · Giusy Lofrano[5] · Maurizio Carotenuto[5] · Federica Carraturo[6] · Giovanni Libralato[6] · Marco Guida[6] · Muhammad Usman[7] · Sunil Kumar[3]

Received: 28 March 2020 / Accepted: 23 June 2020

Abstract

Textile wastewaters contain refractory dyes that cause pollution and socio-economic issues, thus calling for efficient remediation techniques such as photocatalysis. We review the fabrication, functionalization, performance and limitations of doped catalysts for degrading and mineralizing dyes. We present developments in photocatalyst immobilization and photocatalytic reactor design. Methods such as microwave irradiation, sonication and use of ionic liquids are emerging for the preparation of doped photocatalysts. Whilst single-dye systems have been extensively studied, there is limited knowledge on multiple-dye systems. Immobilization of photocatalysts is gaining popularity for large-scale application, but faces issues of erosion, corrosion, mechanical strength and structure integrity. Ecotoxicological studies are required in real environments to validate the potential applications of nanostructured doped photocatalysts.

Keywords Doping · Composites · Dye · Photocatalytic degradation · Reactor design · Scalability · Ecotoxicity

Introduction

The contamination and pollution of water bodies and soils caused by dyes have been continually emphasized and so have been the related environmental impacts (Lofrano et al. 2016). Such pressing socio-economic and environmental issues related to dye-induced water and soil milieus' pollution have bolstered research towards probing for more and more remediation routes. With the coining and advent of the Green Chemistry Principles (Anastas and Eghbali 2010), the search and assessment of dye pollution remediation strategies have been particularly progressing on many fronts, especially with the new material synthesis techniques offered by nanoscience and thermal processing. The aim of these efforts is, most comprehensibly, to come up with such a remediation and detoxification package which can allow the degradation, mineralization and eventually near-complete removal of the parent dye moieties and their respective degradation intermediates and by-products. Amongst the various remediation approaches for removing dye molecules, heterogeneous photocatalysis has been receiving significant importance in the scientific research ambit (Reddy et al. 2016; Kumar et al. 2019). Indeed, heterogeneous photocatalysis has been employed for the degradation of different dyes (Wang et al. 2010; Barbosa et al. 2015; Al-Kahtani

✉ Ackmez Mudhoo
a.mudhoo@uom.ac.mu

1 Department of Chemical and Environmental Engineering, Faculty of Engineering, University of Mauritius, Réduit 80837, Mauritius

2 Rajiv Gandhi National Research Fellow, Academy of Scientific and Innovative Research (AcSIR), Ghaziabad 201002, India

3 CSIR-National Environmental Engineering Research Institute (CSIR-NEERI), Nehru Marg, Nagpur 440 020, India

4 Department of Biotechnology, Haldia Institute of Technology, HIT Campus, Hatiberia, Purba Medinipur, Haldia 721657, India

5 Department of Chemistry and Biology, University of Salerno, Fisciano, SA 84084, Italy

6 Department of Biology, University of Naples Federico II, Via Cinthia 21, 80126 Naples, Italy

7 PEIE Research Chair for the Development of Industrial Estates and Free Zones, Center for Environmental Studies and Research, Sultan Qaboos University, Al-Khoud 123, Muscat, Oman

Published online: 08 July 2020

and Abou Taleb 2016; Ajmal et al. 2016) by virtue of the greenness traits emanating from the unique morphologies and outstanding physico-chemical characteristics of the novel photocatalysts. Yet, the relatively high economic costs associated with the novel photocatalysts (Fan et al. 2016; Lin et al. 2017), the wide energy band gaps (Fang et al. 2015; Nguyen et al. 2018), low adsorption capacity (Khataee et al. 2018; Mohamed et al. 2018) and poor reusability (Mohamed et al. 2018) seem to pose certain limitations to their wide use and full-fledged application in large-scale photocatalytic dye remediation processes.

One set of research approaches which has been fast progressing for crafting more potent and chemically stable photocatalysts intended for the degradation and mineralization of environmental pollutants such as dyes is in engineering different synthetic modifications to the structural topology of the parent catalysts (Malwal and Gopinath 2016; Gnanasekaran et al. 2017; Magdalane et al. 2017; Sorbiun et al. 2018; Bilal Tahir and Sagir 2019; Vasantharaj et al. 2019; Adam et al. 2020; Yang et al. 2020). One single material can exhibit significantly superior catalytic activity for a specific (single, dual, ternary and even quaternary) dye system. However, that same single material may not always be capable of delivering the same superior catalytic activity for another single-, dual-, ternary- and even four-dye system, with or without common dyes or other non-dyestuff organic and inorganic species. Therefore, continuous research and material science and engineering efforts are deployed to formulate such materials which can unleash much acceptable and superior photocatalytic degradation performances by encompassing more and more of the dyes contained within a specific multi-dye system. Moreover, synthetic modifications occur in the form of doping the parent catalyst with specific heteroatoms (Yao et al. 2016; Pham and Yeom 2016; Di et al. 2017; Zeng et al. 2017; Cao et al. 2017; Nguyen and Ngo 2018; Qian et al. 2018), in combining the catalyst with other compounds to generate composites with enhanced and adjustable catalytic properties such as improved interfacial surface areas and more favourable band gaps (Tanwar et al. 2017; Hossain et al. 2018; Azzam et al. 2019) and enhanced electronic movement (Hu et al. 2015; Saleh et al. 2016; Sankar et al. 2016; Chai et al. 2017; Bhanvase et al. 2017; Qian et al. 2018; Zeng et al. 2018).

A corollary to the outcome of such innovative ongoing research is that highly effective and green doped photocatalysts can be synthesized and these can be thereafter of significant importance in curbing the detrimental effects of dye-related pollution and in eventually bringing remedial benefits to the environment, economy and community, at large. Given the ongoing progress logged in the literature on the synthesis of a very wide array of novel photocatalysts modified by doping (or codoping), this review has the intent to revisit and analyse selected recently published laboratory-scale works (essentially from 2015 to 2020) which have reported the green and relatively facile fabrication, functionalization and performance metrics of several types of doped catalysts (including photocatalysts) designed to assist the degradation and mineralization processes of a wide number of dyes in different dye systems. Hence, the next sections in this article discuss: (1) the novel fabrication approaches for (co)doping catalysts, (2) the various techniques employed for functionalizing the photocatalysts, (3) the performances of the different types of doped and functionalized photocatalysts in the degradation and mineralization of a wide range of dye molecules in single- and mixed-dye systems, (4) the ecotoxicological aspects related to the use of doped photocatalysts when assessing dye degradation systems, (5) the progress made in reactor system design for photocatalytic dye-degrading systems and (6) a handful of the key limitations associated with the development and use of photocatalysts. The analysis ends by highlighting some research avenues which could make way for an adapted application of the more potent doped photocatalysts in assisting with the degradation of dyes in more complex (real) dye systems.

The broad approach towards data curation and analysis for this review has been to consider largely original peer-reviewed articles and abstracts, and only those written and eventually obtained in their corresponding English version. An extensive and progressive literature search was conducted on Scopus, Web of Science and Google Scholar for articles and abstracts published essentially from 2015 to date in view to produce a review of recent findings and trends. Many search words and phrases were used to gather an initial pool of articles and abstracts. The main keywords were 'dye pollution', 'photocatalyst', 'doping catalysts', 'doped photocatalysts', 'photocatalyst functionalization', 'dye degradation', 'photocatalytic reactor', 'green dye degradation', 'green photocatalysts', 'photocatalytic dye degradation' and 'photocatalyst ecotoxicological assessment'. Relevant data were retrieved by the authors working on the different sections, and the manuscript was continually crafted with text, tabular and graphics materials being synthesized after mutual consultations and regular proofreading, inputs and edits from all the authors.

Upgrading photocatalytic characteristics

Internal factors such as physical structure and composition of the photocatalytic crystal can greatly influence the photocatalytic activity of the photocatalyst. To be an ideal photocatalyst, it should have the following properties: it should have low band gap energy so that it can be easily excited by photons; it should be able to harness visible light and it should have a high charge separation efficiency and a low

recombination rate. Many of the photocatalytic materials such as TiO_2 have high band gap energy; hence, they can be excited exclusively by UV rays and not by visible light (Zheng et al. 2015). Furthermore, there is a high rate of recombination in these materials due to the weak separation efficiency between the photogenerated electron–hole pairs (Huang et al. 2016). To overcome these limitations, several techniques such as doping, heterostructuring and shape modification have been developed (Marschall and Wang 2014).

Doping schemes

Doping is an effective way to overcome the latter problems. Doping involves 'adulterating' the material with self or foreign ions. Doping modifies the band gap energy and the atomic structure of the material, thus making it possible to harvest visible light. Furthermore, it can introduce additional energy levels which help to trap excitons in separate carriers, thus preventing recombination (Huang et al. 2016; Li et al. 2017). Based on the type of materials used, doping can be classified as self-doping, non-metal doping, rare earth metal doping, transitional metal doping and codoping (Yu et al. 2012; Borlaf et al. 2014; Li et al. 2015; Ahmad 2019). In self-doping, the semiconductor crystal is doped with the same cation that makes the bulk of the crystal material. For example, in the case of TiO_2 self-doping, Ti^{3+} is used as a dopant. This leads to higher oxygen vacancies, which can lead to better absorption of light (de Brites-Nóbrega et al. 2013). Non-metal doping involves doping the intrinsic semiconductors with non-metals such as boron, nitrogen, carbon, sulphur, fluorine and chlorine which have high ionization potential and high electronegativities (Huang et al. 2016). They generally act by interacting with the 2*p* electrons of oxygen present in the lattice (Khan et al. 2015a). The different mechanisms by which non-metal doping is speculated to work are: (1) introduction of localized states above the valence band or below the conduction band which causes band narrowing, (2) introduction of oxygen vacancies leading to the formation of colour centres, which increases light absorption, and (3) surface modification through the introduction of coordination sites on the surface (Serpone and Emeline 2012; Li et al. 2018).

Transitional metal doping involves the use of transition metals such as iron, chromium, niobium, zinc, tungsten, manganese and molybdenum to modify the electronic configuration of the photocatalyst by modulating the band gap energy, band position, Fermi level and d orbital configuration (Huang et al. 2016). The partially filled d orbitals present in the transition metals lead to the formation of new energy bands below the conduction band leading to a redshift in band gap energy, which makes it possible for the photocatalyst to absorb photons in the visible range. Rare earth metal doping is one of the most efficient doping techniques which involves the use of rare earth metal such as cerium, erbium, gadolinium, europium and ytterbium (de Brites-Nóbrega et al. 2013). The 4*f*, 5*d* and 6*s* orbitals of the rare earth metal interact with the atomic structure of the intrinsic semiconductor through the formation of mid-gaps states within the conduction and valence band, and this can lead to visible light absorption, decrease in band gap energy and increase in charge separation efficiency (de Brites-Nóbrega et al. 2013). The rare earth metals exposed on the surface of the photocatalyst can also form complexes with organic compounds leading to higher adsorption, thus enhancing the photocatalytic activity (Liu et al. 2012). Codoping is another prominent doping strategy in which more than one type of ions are used for doping (de Brites-Nóbrega et al. 2013). Codoping can be classified as non-metal–non-metal, metal–non-metal and metal–metal codoping. It works in a similar mechanism as the previously described doping techniques and used to combine the effects of two or more dopants in a single crystal.

For example, Shah et al. (2019) have recently fabricated N-doped and N–B-co-doped WO_3 and Mn_2O_3 nanoparticles (NPs) following a precipitation and hydrothermal procedure. Shah et al. (2019) reported excellent photocatalytic performances of the new nanomaterial in that the codoping of the WO_3 and Mn_2O_3 had led to high photocatalytic activity in contrast to the photodegradation of methylene blue that reached nearly three and half times greater for in the case of the W-based materials and three times more in the case of the Mn-based materials in relation to their pure state compounds, respectively. In a study reported earlier, Movahed et al. (2018) had shown that a novel, effective and reusable Cu_X/*N*-PC composite could be employed as a heterogeneous photocatalyst for the degradation of methyl orange and rhodamine B and in the C–H activation of formamides. Movahed et al. (2018) also reported that the most noteworthy photocatalytic activity of a $Cu_{0.25}$/*N*-PC composite could be plausibly set on account of the high crystallinity of Cu_2O, the absence of agglomeration, the high BET surface area of the composite and probable synergetic effects between Cu_2O and hollow carbon. In another study, Krishnakumar et al. (2017) synthesized magnesium-doped cadmium sulphide composites and functionalized them with polyvinyl alcohol. Characterization results obtained from FTIR analysis thereafter indicated the presence of stretching bond of cadmium sulphide and polyvinyl alcohol, and FESEM data showed the presence of homogeneously grown films (Krishnakumar et al. 2017). Krishnakumar et al. (2017) also found that the functionalized composite had very good visible light-driven photocatalytic properties towards the degradation of methylene blue.

Nsabimana et al. (2019) have recently synthesized a multifunctional Fe_3O_4/N-doped porous carbon nanocomposite with excellent adsorption, magnetic and catalytic features

using 4′,5,7-trihydroxyflavanone-7-rhamnoglucosid as the carbon precursor. Some of the notable features of this novel catalyst composite material are, in a first instance, its mesoporous morphology (BET specific surface area of nearly 187.1 $m^2\ g^{-1}$, pore widths between 2 and 50 nm and total pore volume of 0.49 $cm^3\ g^{-1}$, Fig. 1), the various

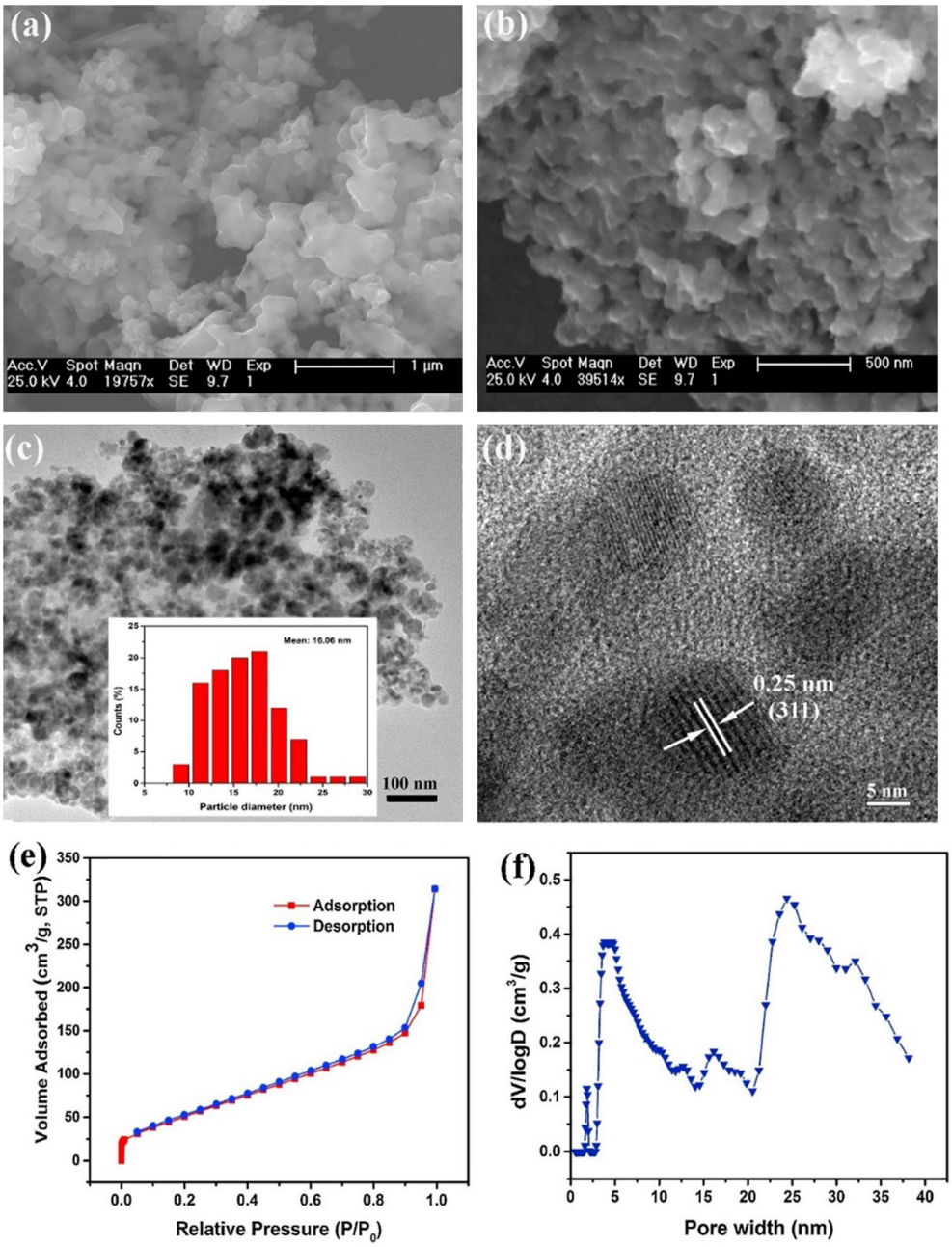

Fig. 1 Scanning electron microscopy (SEM) image (**a**) and the corresponding enlarged magnification in image (**b**) showing that the Fe_3O_4/N-PCNC nanocomposites fabricated by Nsabimana et al. (2019) vary in size and shape, and which cluster to form a three-dimensional porous structure; transmission electron microscopy (TEM) image (**c**) with inset showing the particle size distribution whereby characteristic particle size of nanocomposites ranges from 8.66 to 29.96 nm with a mean of 16.06 nm; high-resolution TEM image (**d**) wherefrom it can be observed that Fe_3O_4 NPs are crystalline in character and are closely attached to Fe_3O_4/N-PCNC surface, and with lattice fringes of Fe_3O_4/N-PCNC displaying an interplane distance of around 0.25 nm coming from (3 1 1) plane of Fe_3O_4; and nitrogen sorption isotherms (image (**e**)) demonstrating a type IV isotherm having an H3-type hysteresis loop, suggesting a mesoporous structure for Fe_3O_4/N-PCNC, and pore size distribution in image (**f**) eventually leading to pore widths determined between 2 and 50 nm of Fe_3O_4/N-PCNC. This figure has been reproduced from Nsabimana et al. (2019) with the permission of Elsevier (© 2018 Elsevier B.V. All rights reserved) under licence number 4855150592439 (for both print and electronic formats)

functional groups (attributed in being C=C/C–C in aromatic rings, C–N, C–C, C–O, O–C=O, pyrrolic N, pyridinic N and quaternary N) it has, its ability to remove more than 99.7% rhodamine B and crystal violet, 100% thionine from aqueous solutions and its high recyclability (Nsabimana et al. 2019). In another work, Fan et al. (2017) have synthesized sulphur-doped graphitic C_3N_4 porous rods in a one-pot pyrolysis process of melamine–trithiocyanuric acid complex at different temperatures. It was found that the sulphur-doped graphitic C_3N_4 consisted of porous rod structures with a larger surface area ranging 20–52 $m^2\ g^{-1}$ in comparison with the bulk graphitic C_3N_4 and that the surface area of the sulphur-doped graphitic C_3N_4 structures was greater at higher heating temperatures. Fan et al. (2017) also noted that since the sulphur-doped graphitic C_3N_4 structures had a narrowed band gap, the latter materials had an enhanced physical adsorption and visible light-driven photocatalytic degradation activity for rhodamine B dye.

Uniform doping is normally regarded as being an efficient strategy for enhancing the properties of parent photocatalysts, whilst non-uniform doping is usually assumed to be inefficient as a result of the dispersion of dopants being inhomogeneous. Very much interestingly, the study of Zhang et al. (2017) demonstrated that non-uniform doping with gold had yielded enhanced photocatalysis of TiO_2 nanotubes in contrast to the uniform doping case. According to the discussions put forward by Zhang et al. (2017) to explain their findings, Au-non-uniformly doped TiO_2 nanotubes exhibited better photocatalytic activity when compared with the performance of the Au-uniformly doped species, and this enhanced performance (of non-uniform doping) was principally because of interfaces which get generated between pure phase TiO_2 and Au-doped TiO_2, together with the '*platinum island*' contribution (described and discussed earlier in Egerton and Mattinson (2010)), leading to a more efficient separation of charge carriers. Amongst the several novel results reported by Zhang et al. (2017), it was found that the collective effects of liquid phase deposition processing, non-uniform doping with gold and heat treatment had yielded a photocatalyst which had outstandingly high $K_{Au\text{-}TND340}$ (TND340 standing for TiO_2 nanotubes heat treated at 340 °C) being 9.81-fold greater than K_{TNT60} (TNT60 standing for pure TiO_2 nanotubes and K value being a measure of photocatalytic activity analysed for the degradation of methyl orange using first-order kinetic equation $\ln(C_o/C) = Kt$).

Heterostructuring

Heterostructuring is another technique to increase the photocatalytic efficiency by increasing the charge separation efficiency. Heterostructures are created by combining the semiconductor with metals or non-metals which introduces new energy states that help in the separation of photogenerated charges by delocalizing them into different carriers and thus preventing them from recombining with each other (Dutta et al. 2015; Ola and Maroto-Valer 2015). For example, Ruzimuradov et al. (2017) have fabricated visible light-active lanthanum- and N-co-doped strontium titanate–titanium dioxide heterostructured macroporous monolithic materials having a bicontinuous morphology. Based on the results from X-ray powder diffraction characterization, Ruzimuradov et al. (2017) observed that the impregnation of Sr, La and N had effectively delayed phase transformation of titanium dioxide from anatase to rutile and growth of crystallites. Moreover, the XPS analysis revealed that the La atoms had been impregnated into the strontium–titanate lattice following substitution of the Sr atoms, and N had been incorporated in the titanium dioxide lattice (1) substitutionally through the formation of Ti–N bonds and (2) interstitially. In a work completed recently, Shende et al. (2019) have synthesized a novel magnetically separable visible light-active In-doped ZnS–$NiFe_2O_4$ photocatalyst. Based on the findings of the characterization studies of the latter nanocomposite, Shende et al. (2019) indicated that In-doped ZnS existed in the hexagonal structure, whereas the $NiFe_2O_4$ was in a cubic structure, and both were in a very much dispersed state. Interestingly, (1) the optical property of the ZnS–$NiFe_2O_4$ composite was enhanced as a result of In doping (and a significant degree of visible light absorption had been surveyed) and (2) it also had ferrimagnetic property which imparted to it the feature of being easily separated and recyclable from aqueous suspensions under the action of an external magnetic field. Some additional merits of the novel nanocomposite as reported by Shende et al. (2019) are: photodegradation kinetics of acid violet 7 was better in comparison with that observed with In-doped ZnS, ZnS–$NiFe_2O_4$ and $NiFe_2O_4$; based on the total organic carbon analysis, a complete mineralization of the acid violet 7 had occurred within 60 min under visible light illumination (Fig. 2); electrochemical analysis data suggested enhanced charge-storage capacitance property, enhanced charge carrier transport and improved aqueous phase stability *vis-à-vis* those of ZnS and $NiFe_2O_4$, and significant separation of electron–hole pair over In-doped ZnS.

The efficiency of photocatalysis is also greatly modulated by the physical structure of the crystal surface (Cui et al. 2016; Zhong et al. 2018). Table 1 summarizes certain points of some studies (not solely dealing with dye degradation) wherein a parent compound has been engineered to enhance its structural properties with a view to upgrade its photocatalytic ability for some processes. The flat microscopic faces on the surface of crystals are called facets. According to Kumar et al. (2017), the surface energy of facets varies from one crystal to the other and this difference results in a corresponding difference in photocatalytic behaviour. The

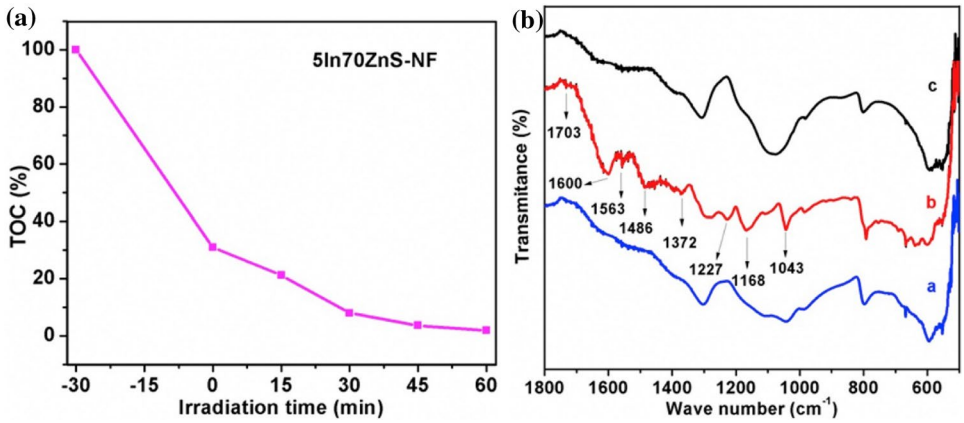

Fig. 2 Data in image (**a**) report the percentage total organic carbon (TOC) changes which occur during the photocatalytic degradation process of acid violet by the nanocomposite 5In70ZnS–$NiFe_2O_4$ wherein the total organic carbon content decreases with irradiation time and drops to quasi-nil after 60 min, hence suggesting total mineralization of acid violet 7 (Shende et al. 2019); the FTIR spectra in image (**b**) are for fresh 5In70ZnS–$NiFe_2O_4$ (line **a** in blue), for 5In70ZnS–$NiFe_2O_4$ (line **b** in red) after stirring with acid violet at a concentration of 400 mg L^{-1} for 30 min in dark conditions and for 5In70ZnS–$NiFe_2O_4$ (line **c** in black) after the photocatalytic degradation of the dye (Shende et al. 2019). As per interpretations reported in Shende et al. (2019), some band attributions made are follows: 1486 cm^{-1} to –N=N– stretching vibration, 1168 cm^{-1} to S–O symmetric stretching vibration, both the 1600 cm^{-1} and 1563 cm^{-1} to aromatic C=C stretching vibration, 1227 cm^{-1} to C–N stretching vibration and 1043 cm^{-1} to C–O stretching vibration (for more details with regard to FTIR results, the online version of this article can be consulted at https://doi.org/10.1016/j.matchemphys.2018.09.032). This figure has been reproduced from Shende et al. (2019) with the permission of Elsevier (© 2018 Published by Elsevier B.V.) under licence number 4855150807776 (for both print and electronic formats)

facets expressed on the surface of the semiconductor lattice are of many types, out of which {110} and {101} are highly stable with the lowest surface energy, whereas facet {001} has the highest surface energy and is highly reactive (Liu et al. 2011). A highly reactive facet possesses a higher number of uncoordinated atoms, which leads to a higher rate of dye adsorption (Liu et al. 2011). However, during crystal growth, the surface tends to achieve the maximum stability by acquiring the configuration with the lowest surface energy, due to this the presence of highly reactive facets are minimized (Liu et al. 2011). An effective way to overcome this is through facet engineering. The physical structure of the crystal being formed is dependent on the nature of the reaction environment under which the crystal is being produced (Liu et al. 2011). Facet engineering is an effective strategy for increasing the photocatalytic activity of the crystal by artificially inducing the formation of the facet of interest through the modulation of the environment under which the crystal is being formed.

Scanning electron microscopy (SEM) images of TiO_2 powders synthesized under different fluorinion concentrations by Cui et al. (2016) indicated the way in which fluorinion had regulated the phase constituent of TiO_2 and how different concentrations of fluorinion had significantly changed the morphology and exposed facets. As per descriptions in Cui et al. (2016), in the sample with no fluorinion, crystals appeared as elongated tetragonal crystal structures (ETCS) having a pyramid habit with the {110} face exposed at tetragonal prism and the {111} facet at bipyramid habit; with the incorporation of fluorinion, the {111} facet reduced and the ETCS became shorter in length and 'thicker'; at [fluorinion] = 3.5 mmol L^{-1}, some brookite crystals were surveyed; for [fluorinion] = 8.75 mmol L^{-1}, the morphology was transformed to nearly cubic crystals, and some truncated octahedral crystals (TOCrys) were also observed, and this was characteristic of the anatase morphology; subsequent increases in [fluorinion] of 8.75–52.5 mmol L^{-1} resulted in more crystals being transformed to the TOCrys morphology with grain sizes becoming gradually bigger; and as [fluorinion] was increased, the TOCrys became thinner and eventually turned into a nanosheet, with the ratio of {001} facet increasing continuously. In another interesting work, using a facile solvothermal and chemical precipitation process, Qi et al. (2017) fabricated facet-dominated AgBr/BiOCl composites with exposed {101} (BiOCl-101) and {001} (BiOCl-001) facets. Besides noting that AgBr/BiOCl heterojunctions yielded in significantly better photocatalytic performance for the visible light photodegradation of rhodamine B in comparison with those of pure AgBr and BiOCl, Qi et al. (2017) also observed that the AgBr–{001}BiOCl with mole ratio of 1:2 gave the best (and complete) photocatalytic rhodamine B degradation in 15 min, and such a performance was plausibly associated with the {001} facet of BiOCl having facilitated the separation of photogenerated carriers and formation of additional oxygen vacancy on the surface {001} facets of BiOCl. Kumar et al. (2017) have conducted a brilliant work

Table 1 Reports showing enhanced photocatalytic capacity by structural modification of a parent material. Applications are not restricted to the degradation of dyes

Species	Modification (or modulation) approach	Observed effects of modification	References
Er^{3+}:$YAlO_3$/Fe- and Co-doped TiO_2-coated composites	Er^{3+}:$YAlO_3$ content, heat-treated temperature, heat-treated time	Findings demonstrated that Er^{3+}:$YAlO_3$/Fe- and Co-doped TiO_2-coated composites were capable than Fe- and Co-doped TiO_2 powders in the photocatalytic degradation of azo fuchsine Better performance was attributed to Er^{3+}:$YAlO_3$ being able to convert visible light into UV light for improving photocatalytic activities of Fe- and Co-doped TiO_2 powders	Xu et al. (2010)
g-C_3N_4/$Co_xMo_{1-x}S_2$ with different exposed facets of Co–Mo	C_3N_4/$Co_xMo_{1-x}S_2$ composites with different g-C_3N_4 mass ratios (10–50%) were fabricated	Effect of mass ratio of g-C_3N_4 to $Co_{0.04}Mo_{0.96}S_2$ in g-C_3N_4/$Co_{0.04}Mo_{0.96}S_2$ on hydrogen production revealed that g-C_3N_4 content had considerable bearing for optimal photocatalytic activity Photocatalytic hydrogen production rose with g-C_3N_4 content increase (peaking for a mass ratio of g-C_3N_4 to $Co_{0.04}Mo_{0.96}S_2$ of around 30 wt%	Hao et al. (2016)
Well-defined $Bi_2O_2(OH)(NO_3)$ nanosheets with dominantly exposed {001} active facet	Sodium-dodecyl-benzenesulfonate-assisted soft-chemical route	Extremely enhanced photocatalytic activity was mostly due to a shorter pathway for the diffusion of photogenerated electrons and holes, which facilitated their migration from the bulk system to the catalyst surface under the influence of an internal electric field between $[Bi_2O_2(OH)]^+$ and NO_3^- layers along [001] direction	Hao et al. (2018)
Ti^{3+} self-doped TiO_2	Varying fluorinion concentrations during hydrothermal synthesis of TiO_2	Fluorinion incorporation led to F-doping and phase transformation F-doping also influenced Ti^{3+} ions content in TiO_2 TiO_2 fabricated with 17.5 mmol L^{-1} fluorinion gave remarkable good photocatalytic activity for the full spectrum illumination	Cui et al. (2016)
Anatase TiO_2 nanocatalyst having dominantly exposed (001) reactive facets	Self-assembly of cellulose nanocrystal; Control of cellulose nanocrystal concentration	Synthesized nanocatalyst can efficiently catalyse visible light rhodamine B degradation *Biotemplating* strategy of huge value in developing novel functional catalysts with tunable structures and properties for environmental applications	Xue et al. (2019)
Ag@AgBr/$BiVO_4$/Co_3O_4 visible light photocatalyst	Selective doping of Ag@AgBr and Co_3O_4 on {010} and {110} facets of $BiVO_4$	Z-scheme structured Ag@AgBr/$BiVO_4$/Co_3O_4 (0.15 wt%) yielded very good photodegradation rate of organic molecules and retain high photocatalytic activity (90% degradation of oxytetracycline within 24 min) even after ninth cycle	Chen et al. (2019)
Zinc oxide (ZnO) nano- and microstructures	Variables control in microwave hydrothermal fabrication process of microstructures: time, NaOH concentration and synthesis temperature	Difference noted in volume/surface area ratio and specific surface area of different microstructures	Rangel et al. (2017)

Table 1 (continued)

Species	Modification (or modulation) approach	Observed effects of modification	References
$Ag_xAu_{1-x}/ZnIn_2S_4/TiO_2$ photocatalyst	Dual modification of $ZnIn_2S_4$ and Ag_xAu_{1-x}; Variation of ratio of silver and gold in Ag_xAu_{1-x} NPs	Extremely significant enhancement in the photocatalytic activity for hydrogen generation noted in the sense that H_2 production quantity and rate of $Ag_{0.2}Au_{0.8}/ZnIn_2S_4/TiO_2$ with 60 wt% ternary sulphide $ZnIn_2S_4$ after 10 h reach 9862 μmol g^{-1} and 986.2 μmol g^{-1} h^{-1}, respectively (2098 times that of virgin TiO_2)	An et al. (2019)
Cu_2O nanoparticles (COPNP)	Adjustment of the quantity of hydroxylamine hydrochloride and surfactant used	COPNP having Cu-terminated (110) or (111) surfaces very good exhibit photocatalytic activity, whereas the other exposed facets yield low reactivity	Su et al. (2017)
TiO_2/graphene nanocomposites	Modulation brought about with addition of hydrofluoric acid; Sizes of TiO_2 nanocrystals controlled based on contents of GO functionalized with *p*-phenylenediamine	Nanocomposites had been endowed with significantly more pronounced photocatalytic activity and stability for methyl blue and fulvic acids degradation in comparison with other TiO_2 samples under Xe-lamp irradiation For the third cycle, the 10 wt% N-reduced graphene oxide/TiO_2 catalyst retains 87% photoactivity for fulvics acid degradation v/s 61% activity of the TiO_2-N/F (61%) in 3 h	Yan et al. (2016)
Cu-doped α-MnO_2 NPs	Variation of copper doping and post-sintering temperature	Degradation efficiency of 73.1% obtained for Brilliant Green (5 ppm) when using ultra-diluted aqueous solution (2.5 mg L^{-1}) of active fabricated material	Mondal et al. (2019)
B-doped BiOCl nanosheets with exposed (001) facets	Doping of B into BiOCl	B-doping could adjust and control (001) crystal facet growth, raise specific surface areas and improve charge separation efficiency $B_{1.0}$-BiOCl gave significantly promoted degradation of organics, namely bisphenol A, phenol and rhodamine B than that obtained with pure BiOCl	Yu et al. (2019)
Co-doped BiOBr (0 1 0)	Effect of Co doping	As-prepared Co-doped BiOBr (010) could bring about 83% photocatalytic degradation of tetracycline hydrochloride within 30 min	Shao et al. (2020)

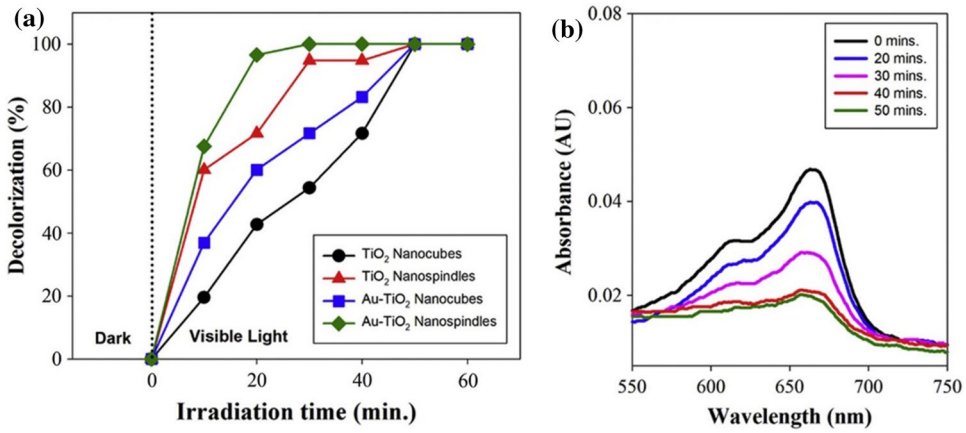

Fig. 3 **a** Decolourization profiles of methylene blue under the action of fabricated nano Au–TiO_2 heterostructured nanocatalysts; and **b** time dependent ultraviolet–visible absorption spectra of methylene blue photodegradation under the action of Au-TiO_2 nanospindles (Khalil et al. 2019). From image (**a**), it is evident that the TiO_2 nanospindles present in the catalyst had a significantly better degradation capability towards methylene blue when compared to the TiO_2 nanocubes. This figure has been reproduced from Khalil et al. (2019) with the permission of Elsevier (© 2019 Elsevier B.V. All rights reserved) under licence number 4855151017498 (for both print and electronic formats)

wherein, amongst others, the photocatalytic degradation of a test dye under the influence of $NaNbO_3$/CdS core/shell heterostructures was analysed for surface energies of the (110) and (114) facets of the orthorhombic phase and the {100} family of facets of the cubic phase of $NaNbO_3$. Besides discussing the various mechanisms which bring about the improvement in catalytic activity of the two phases, Kumar et al. (2017) observed that the very reactive facets of the cubic phase of the $NaNbO_3$ present in the $NaNbO_3$/CdS core/shell heterostructures contribute to enhanced photocatalytic activity in comparison with the orthorhombic phase.

Amongst the different observations made (e.g. synergistic plasmonic resonance effect of the gold NPs analysed) and explanations provided thereof, Khalil et al. (2019) also reported that the 'nanospindles' morphology of the synthesized nano Au–TiO_2 heterostructures had significantly superior photocatalytic activity than the 'nanocubes' morphology (Fig. 3). Khalil et al. (2019) explained the latter difference in photocatalytic activity on basis of the presence of co-facet characteristic of TiO_2 whereby less stable and yet catalytically active (001) facets were available together with the presence of more stable but less reactive (101) facets. According to Khalil et al. (2019), the (001) facet surface facilitates both migration and separation of charge carriers generated during the process, and these hinder fast electron–hole recombination and eventually bring about better methylene blue degradation. More recently, Zhu et al. (2020) have used a one-step hydrothermal procedure facilitated by thionyl chloride for the carbonization process and doping effect to prepare S- and Cl-co-doped carbon dots with wood powders of palm veneers serving as source of carbon. Zhu et al. (2020) reported that the bio-carbon dots had been suitably doped with the heteroatoms within their structures, hence leading to a successful functionalization of the biomass-derived carbon dots. In this same study, it was reported that well-distributed and quasi-spherical NPs had been formed and that crystalline structures of bio-carbon dots had been obtained as backed by transmission electron microscopy (TEM) results which demonstrated that carbon dots had been endowed with identical well-resolved lattice fringes (interplanar spacing 0.21 nm) approaching that of the (100) facet of graphitic carbon (Zhu et al. 2020). Moreover, a number of absorption peaks were observed: stretching vibration bands originating from O–H (3403 cm^{-1}), C–H (2929 cm^{-1}), C=O (1711 cm^{-1}), C=C (1631 cm^{-1}); bending vibration of –COOH at 1385 cm^{-1}; band at 2488 cm^{-1} corresponding to S–H, peak at 1068 cm^{-1} attributed to C=S vibration, and the peak at 1174 cm^{-1} was associated with C–S bonds (Zhu et al. 2020). Another interesting result reported in Zhu et al. (2020) is that the bio-carbon dots were endowed with many functional groups, which promoted formation of different surface-defect states, which, in turn, plausibly lead to the formation of numerous luminescent centres in the structures. Also, under visible light conditions, the degradation of rhodamine B was almost 71.7%, whereas that of methylene blue was practically complete (ca. 94.2%) (Zhu et al. 2020).

Fabrication methods of doped photocatalysts

The literature abounds with a diverse range of methods for the preparation of doped photocatalysts (e.g. as summarized in Khaki et al. (2017) and Wen et al. (2017)). Amongst the

several methods surveyed when writing this review, the sol–gel, hydrothermal-based, electrochemical, microemulsion, precipitation methods and combinations thereof are apparently the most popular ones. With the openings brought by the Principles of Green Chemistry in material synthesis, new facile methods such as microwave irradiation-assisted, ionic liquid-mediated, and ultrasound irradiation-assisted photocatalyst material synthesis are also being frequently developed and reported to give materials endowed with superior photocatalytic activity. Besides the discussions which follow in this section and which intend to highlight some of the salient features of the former methods, a few of the novel green and facile approaches recently reported for the synthesis of doped photocatalysts are presented in Table 2.

Sol–gel method

The sol–gel method has been used by different workers for catalysts preparation (e.g. Sangchay 2016; Liau and Huang 2017; Kayani et al. 2018; Louangsouphom et al. 2019) and is a well-established synthetic approach to prepare nanocomposites. The process is a wet chemical technique also known as chemical solution deposition and involves the following steps (in chronological order): hydrolysis and condensation, drying and crystallization. Low reaction temperatures and very mild reaction conditions are particularly useful for the incorporation of inorganic species into organic materials or organic materials into inorganic matrices (Xu 2001). Based on the solvent being used, the sol–gel method can be either the aqueous sol–gel (this is when water is used) or the non-aqueous sol–gel method (this is when an organic solvent is used). In the aqueous sol–gel method, hydrolysis, condensation and drying can happen simultaneously and this may lead to some extent of difficulty being experienced when attempting to control particle morphology and reproducibility of the final procedure involved in the sol–gel process (Rao et al. 2017).

The sol–gel approach is a relatively simple, cheap, reliable and repeatable method for the synthesis of the nanocomposites. It has been observed to maintain high purity, homogeneity and even particle size of synthesized nanocomposites (Rani and Manjunatha 2018). Hassan and Mannaa (2016) also prepared a doped catalyst of TiO_2 by incorporating varying concentration (0–20 wt%) of SnO_2 using the sol–gel method. In the next step, samples were calcinated at 500 °C, and structural analysis was carried out by using UV–Vis absorption spectroscopy. Evaluation of photodegradation capacity of synthesized doped NPs showed 100% degradation of Brilliant Green dye after 120 min with 10% SnO_2/TiO_2, but degradation efficiency of the catalyst was found to be reduced by increasing concentration of the dye (Hassan and Mannaa 2016). In a study conducted by Meshesha et al. (2017), a doped catalyst of TiO_2 by codoping with Mg^{2+} and Zr^{4+} was prepared using sol–gel synthesis method, and it was found that 0.1 g of doped TiO_2 catalysts with 1.0 wt% Mg^{2+} and 0.25 wt% Zr^{4+} dopant concentration showed higher photocatalytic degradation of 10 mg L^{-1} methylene blue dye (Meshesha et al. 2017). Another doped TiO_2 nanocomposite was prepared by Moradi et al. (2016) using the sol–gel fabrication method in varying amounts (0. 0.1, 1, 5 and 10 wt%) of Fe as a dopant, and it was found that the doped nanocomposites revealed that doping of Fe in TiO_2 lattice stimulated the redshift of the absorption spectra from UV to the visible region, which led to decreasing the band gap energy from 3 to 2.1 eV. Moreover, results of degradation study revealed that native TiO_2 was found highly effective in degrading RR 198 under UV light irradiation whilst degradation efficiency of Fe-doped TiO_2 composites observed to be higher under visible light irradiation. The decolourization capability of TiO_2 initially increased with the doping of Fe and then was lowered with increasing the dopant concentration with the 1 wt% concentration of Fe as dopant eventually found to be most suitable for enhancing the degradation capacity of TiO_2 (Moradi et al. 2016). In Raza et al. (2016), results indicated that ZnO nanorods doped with erbium (Er)/neodymium (Nd) dopants exhibited higher photocatalytic activity for the catalytic degradation of methylene blue and RR 241 dyes under visible light illumination. Also, the doped ZnO NPs with both rare earth metals displayed smaller particle size leading to enhanced absorption of both the dyes on the surface of newly synthesized composites with redshift from UV to visible light which allowed enhanced separation of electron–hole pairs (Raza et al. 2016). Table 3 reports the main features reported in other studies with respect to the doping approach employed in the fabrication of titanium and/or titania-based and graphene oxide-based doped catalyst nanosized composites using sol–gel-based, hydrothermal and a few 'green' methods.

Hydrothermal preparation

The hydrothermal method is one of the most promising methods for the fabrication of doped NPs as it comprises simple operation, lower cost, lower temperature, excellent control over the architecture and dimension of the particles and efficiency for broad-scale production. Cu–P25–graphene nanocomposites (CPG) were fabricated by Jin et al. (2015) using the hydrothermal method for the degradation of methyl blue. Initially, the binary composite of 25-graphene (PG) was synthesized by P25 and graphite oxide followed by PG composite was impregnated with Cu^{2+} ions. Jin et al. (2015) reported protracted light absorption efficiency of Cu–P25–graphene (CPG) nanocomposites than native systems. The highest

Table 2 Green methods recently designed to prepare doped photocatalytic materials having enhanced properties and thereafter examined for their capabilities in assisting dye degradation processes

Doped photocatalyst	Model dye	Synthesis method	Novelty feature(s) of method	Key observations	References
Iron-doped rutile TiO_2	Methyl orange	Relatively easy and mild in situ method	Rutile preparation temperature less than 100 °C (which was itself significantly less than calcination temperature of 600 °C in conventional preparation method	Methyl orange decomposed by around 90% under 40 min of UV light irradiation in contrast to only 70% decomposition rate of methyl orange yielded by P25 (under same reaction conditions) Specific surface area of Fe-doped catalysts was larger than that of control sample	Shi et al. (2019a)
Sulphur-doped porous TiO_2 NPs	Malachite green	Scaffold template technique	Doping with S and then calcination at different temperatures for tuning anatase/rutile content	Photocatalytic tests demonstrated that doped materials (corresponding to a calcination performed at 700 °C) gave the best performances 20 mg L^{-1} Malachite green decomposed in 30 min under UV irradiation at pH 9 and these results were superior than those obtained with P25	McManamon et al. (2015)
Er–Al-co-doped ZnO NPs	Methyl orange	Solvothermal preparation method	Simple, facile, non-toxic and surfactant-free method for doped photocatalyst synthesis	Er–Al-co-doped ZnO gave significantly better photocatalytic activity in the degradation of methyl orange in comparison with undoped ZnO	Zhang et al. (2015a)
Carbon-doped ZnO	Methylene blue	Urea-assisted thermal decomposition of zinc acetate	One-step method using different percentage weight of urea	Significant enhancement obtained for visible light-driven photocatalytic activity as a result of C-doping	Zhang et al. (2015b)
V-doped TiO_2-based nanosheets	Rhodamine B	Facile one-pot hydrothermal preparation process	Preparation process should be generally appropriate for synthesizing other advanced functional materials intended to give optimized performance when doped with an optimal dopant content	Photoactivity rose gradually with V concentration and thereafter declined from a peak performance corresponding to V at 1.0 at% for the dye	Lu et al. (2015)
Magnesium-doped ZrO_2 NPs	Rhodamine B	Green-assisted route	Effects of magnesium doping and *Aloe vera* gel concentration on phase formation, optical properties and morphology of NPs examined	2 mol% magnesium-doped ZrO_2 yielded 93% UV light-driven photocatalytic degradation rate of rhodamine B	Renuka et al. (2016)

Table 2 (continued)

Doped photocatalyst	Model dye	Synthesis method	Novelty feature(s) of method	Key observations	References
N-doped carbon quantum dots (NCQDs)	Rose Bengal	Fast and easy approach for synthesizing NCQDs in glucose–water solution with microwave heating for only 1 min at low temperature and applied MW power	Dots show dual behaviour with respect to interaction with dye at different pHs of solution	Under visible light irradiation for only 30 min, nearly 93% of the Rose Bengal was degraded	Prekodravac et al. (2019)
Au@Fe_2O_3 nanocomposite	Methylene blue	Green synthetic route using *Citrus sinensis* fruit extract (both as a reducing and stabilizing agent)	Presence of organic acids (namely citric acids) had a major part in stabilizing Au@Fe_2O_3, and *Citrus sinensis Var Kozan yerly*, and having such components may be more effective in the green synthesis of the gold nanocomposites fabricated in this study	First cycle: 94% decrease in methylene blue within 50 min Second cycle: methylene blue removal efficiency diminished; 50.71% of methylene blue was degraded after 50 min	Shams et al. (2019)
B-doped g-C_3N_4 nanosheets	Rhodamine B	Ultra-fast and environmentally friendly microwave heating method	Quite simple a method which used carbon fibres as microwave absorbent and boric-acid-modified melamine (as the raw materials)	Visible light-driven photocatalytic test showed that 92.9% rhodamine B had been degraded (in 30 min at room temperature) under the action of the B-doped g-C_3N_4 nanosheets Photodegradation rate constant of B-doped g-C_3N_4 nanosheets was 3.3-fold more than that obtained with pristine g-C_3N_4	Zou et al. (2019)

Table 3 Studies reporting the sol–gel method employed in the fabrication of titanium and/or titania-based and graphene oxide-based doped catalyst nanocomposites for use in processes involving the degradation of dyes

Nanocomposite catalysts	Doping agents	Final treatment	Target dye	References
Zr/Ti/chitosan	Zr, Ti (doping amount: 0.5 g zirconium oxychloride octahydrate)	Zr/Ti/CHT was dried and calcined at 500 °C for 2 h	Orange II	Demircivi and Simsek (2018)
Zr/CHT	Zr (0.5 g zirconium oxychloride octahydrate)	The solution was dried and calcined at 500 °C for 2 h	Orange II	Demircivi and Simsek (2018)
Ti/CHT	Ti	The solution was dried and calcined at 500 °C for 2 h	Orange II	Demircivi and Simsek (2018)
Fe^{3+}-doped TiO_2	TiO_2	In the end part of the procedure, the materials were calcined at 450 °C for 3 h, then cooled down and, lastly, ground into fine powder	Acid orange 7	Han et al. (2018)
Zr–TiO_2/rGO	Zr	The obtained gel was dried in air oven at 70 °C for 24 h, to convert graphene oxide (GO) to reduced rGO	Eosin blue	Prabhakarrao et al. (2017)
Fe–TiO_2/rGO	Fe	The powder was annealed at 400 °C for 2 h	Rhodamine B	Isari et al. (2018)
S, N/graphene aerogel (SN-rGO-A)	S, N	SN-rGO-A was achieved by a freeze-drying process for 48 h	Rhodamine B, methylene blue, methyl orange	Ren et al. (2018)

degradation efficiency (98%) for methyl blue was observed in CPG-4 (4 mM $Cu(NO_3)_2$) composition with 7.9 times higher hydrogen evolution rate as compared to native compositions in the duration 100 min (Jin et al. 2015). Brindha and Sivakumar (2017) fabricated a N, S-co-doped TiO_2/GO photocatalyst using a one-step facile hydrothermal method using low-cost chemicals, which was then assessed for its photodegradation efficiency for the decolourization of methylene blue, Congo red and reactive orange 16 dyes. Brindha and Sivakumar (2017) reported that the N, S-co-doped TiO_2/GO photocatalyst had higher photocatalytic activity than graphene/TiO_2, N- and S-co-doped TiO_2 and commercial TiO_2. Kaur et al. (2019) recently synthesized rGO-CdS heterostructure for the degradation of the synthetic food colourant sunset yellow (SY). In the latter work, the heterostructure was fabricated by employing a facile hydrothermal process on native graphene oxide (GO), Cd and C_2H_5NS. The obtained heterostructure was observed as an excellent fluorescent sensor for selective detection and degradation of SY. The detection and degradation efficiencies of composites for SY were found 7.89 µM and 82.7%, respectively. Kaur et al. (2019) observed approximately 66% degradation of SY in 270 min under visible light. It was the first report, in which RGO-CdS heterostructure was used for sensing fluorescence and the degradation of SY (Kaur et al. 2019). In the study conducted by Dodoo-Arhin et al. (2018), the degradation efficiency of titanium dioxide (TiO_2) nanostructured catalysts prepared by hydrothermal and sol–gel methods were compared for the degradation of rhodamine B and Sudan III dyes. Particles were fabricated with a specific surface area of 2 nm and 30 nm crystallite domain size and were characterized by using BET surface area analysis, FTIR, X-ray diffraction (XRD), SEM and Raman spectroscopy. The degradation of rhodamine B dye solution was observed higher (100%) in sol–gel prepared catalysts in 150-min duration with ultraviolet (UV) light irradiation, whilst the higher degradation efficiency (94%) for Sudan III dye solution was observed in catalysts prepared by hydrothermal fabrication method with the same UV irradiation (Dodoo-Arhin et al. 2018). Different doped composites of TiO_2 were fabricated by incorporating dopants Ni (1 wt%), Pt (1 wt%) and Ni–Pt (0.5 and 0.5 wt%, respectively) combinations through a two-step hydrothermal method (Pol et al. 2016). Structural analysis revealed that the surface area of TiO_2 post-doping was found to be enhanced and was in the range of 186–200 $m^2\ g^{-1}$. Fabricated catalysts were tested for photodegradation of rhodamine B dye under UV light illumination. Higher degradation of rhodamine B dye was observed in all doped combinations which was recorded as 63%, 57% and 54% in Pt-, Ni- and Ni–Pt-doped TiO_2, respectively, as compared to native TiO_2 (39%) (Pol et al. 2016).

Electrochemical method

A novel one-step anodization method for fabrication of copper-doped TiO_2 nanotube array using copper nitrate was utilized by Momeni et al. (2015). In the study, the researchers used different concentrations of copper nitrate with an aqueous solution of ammonium fluoride (NH_4F) for electrochemical oxidation of native Ti particles and characterized the morphology of synthesized doped $CuTiO_2$ nanotubes using XRD, XPS, SEM and EDX. The resulting doped nanocomposites showed the shift of diffuse reflectance spectra towards visible light in comparison with fundamental TiO_2 substrate with an enhanced photocatalytic degradation of methylene blue dye and evolution of hydrogen. The fabrication method developed in the study by Momeni et al. (2015) was a simple, feasible and effective method for the synthesis of inexpensive and reproducible doped TiO_2 nanotube arrays which can be effortlessly scaled up and utilized to lessen the pollutants (Momeni et al. 2015).

Electrospinning is a method to fabricate polymer fibres in the dimensions ranging from nano-metres to sub-micrometres, but the same has been applied in the fabrication of doped nanocomposites by several researchers (Panthi et al. 2015; Pascariu et al. 2016; Yildirim 2018; Baylan and Altintas Yildirim 2019). Panthi et al. (2015) used palladium (Pd) and zinc (Zn) as co-dopants with polyvinyl acetate (PVAc) for the synthesis of reusable photocatalyst hybrid electrospun nanofibre mat. Ammonium sulphide was added to the solution of PVAc, zinc acetate and palladium acetate; then, colloid was electrospun to obtain the PdS/ZnS-co-doped nanofibres with good morphology. The composite was tested for the degradation of methyl blue dye and found to be a good photocatalyst for the dye photodegradation. Panthi et al. (2015) reported that due to the hydrophobicity of synthesized hybrid electrospun nanofibre mat, it was floating on the surface of the water. Hence, it can be easily utilized to diminish the surface water pollution. Also, the used immobilization technique can be an efficient, low-cost and reusable solution, leading to solving the issue of secondary pollution caused by the nanostructural catalysts (Panthi et al. 2015). The electrospinning technique was adopted with a combination of calcination at 600 °C for the formulation of SnO_2-doped ZnO nanofibres (Pascariu et al. 2016). Synthesized nanofibres had the highest degradation efficiency for rhodamine B dye (0.01 mM solution) at the molar ratio of 0.030 (Sn/Zn) in 6 h. Also, the degradation rate was found to be dependent on the molar ratio of Sn/Zn (Pascariu et al. 2016). Pascariu et al. (2019) used electrospinning with calcination as a fabrication method for doped ZnO nanofibres, but with a different dopant substrate lanthanum (La^{3+}). The 0.02%, 1%, 2% and 4% concentrations were opted for preparing the doped nanofibres and mixed with polyvinylpyrrolidone (PVP) for electrospinning, followed by calcination at 700 °C for 3 h. The lifetime of La^{3+} ion-doped ZnO nanocomposites obtained from decay curves ranged from 2.69 to 2.80 ns with the increasing concentration of La^{3+} from 0 to 4% (Pascariu et al. 2019). The fabricated composite was also evaluated for dye degradation performance using Congo red dye under UV light illumination, and highest degradation potential (97.63%) of doped composite was observed at 2% La^{3+} dopant concentration in 0.283 g L^{-1} dosage, where the catalyst was recovered and reused successfully after 1-h activation at 700 °C (Pascariu et al. 2019). Another ZnO nanofibres were synthesized with different combinations of copper oxide (CuO) using one-step electrospinning method (Naseri et al. 2017). Morphological characterization revealed that fabricated nanocomposites had smooth beadles and monoclinic crystalline structure. A decline in electron–hole pair recombination was observed by incorporating CuO in ZnO nanostructure, and maximum attainment was achieved at 0.5 wt% of CuO. Furthermore, doped nanofibres with 0.5% CuO exhibited maximum degradation of methylene blue dye under sunlight irradiation (Naseri et al. 2017). Yildirim (2018) conducted a study for doping of ZnO with various silver (Ag) concentrations (1 and 3 wt%). Photocatalytic degradation study results revealed that synthesized composites were found to have higher degradation capacity for the methylene blue dye with the increasing Ag concentration (60% and 67% for 1 and 3 wt% of Ag, respectively) under UV light illumination, whereas it was observed to be much lower (52%) in the basic ZnO nanofibre (Yildirim 2018).

Microemulsion

Microemulsion is an innovative technique, used to fabricate extremely minute particles, which allows controlling the size when synthesizing nanocomposites and prevents the accumulation of these NPs. Sathish Kumar et al. (2018) used the microemulsion method for the synthesis of MgO-doped titanium oxide NPs, and these composites were evaluated for their photocatalytic dye degradation efficiency under UV–visible light illumination. Span 80 and Tween 80 were utilized to produce oil in water microemulsion, and their percentage was balanced by hydrophilic and hydrophobic equilibrium, followed by mechanical agitation. The calcination of microemulsion was carried out to obtain the fine doped particles, and different concentrations of synthesized catalyst (0.4, 0.6, 0.8, 1.0 and 1.2 g L^{-1}) were tested for the degradation of different amounts (20, 40, 60, 80, 100 mg L^{-1}) of methyl red dye. Amongst all the combinations, 1 g L^{-1} of catalyst load showed a maximum degradation potential (84.8%) for 20 mg L^{-1} concentration of methyl red dye in 60 min which was accounted as 11.3% more than native TiO_2 NPs (Sathish Kumar et al. 2018). The microemulsion method was also employed to synthesize carbon (C)-doped TiO_2/CdS core–shell NPs (Lavand et al. 2015), wherein the morphology characterization data

obtained by TEM revealed that C/TiO_2/CdS core–shell heterostructure composites with CdS as an inner core and C-doped TiO_2 as the outer shell were successfully obtained by the microemulsion method. Moreover, the fabricated heterostructure was successfully employed for the degradation of methylene blue and it was found to be stable and reusable (Lavand et al. 2015). More recently, Lavand et al. (2019) prepared co-doped nanocomposites of TiO_2 with C and iron (Fe) using microemulsion approach. In the synthesized structure, carbon atom was observed to occur as interstitial carbon in titanium oxide lattice, whilst the substitution of some Ti^{4+} by Fe^{3+} ions formed the structure in the lattice as Ti–O–Fe. In Lavand et al. (2019), doping of C and Fe with titanium oxide declined the band gap and enhanced the visible light absorption and photocatalytic degradation activity of fabricated catalysts for malachite green dye. Moreover, the results revealed 78% improved degradation capacity of C- and Fe-doped composite under visible light illumination as compared to bare titanium oxide particles (Lavand et al. 2019). A novel type of transparent nanocomposite film of polymethyl methacrylate (PMMA)/TiO_2/ionic liquid with different loads of TiO_2 NPs was prepared by Mirhoseini and Salabat (2015), using liquid-in-oil microemulsion approach. Formulated nanocomposites exhibited an exceptional photocatalytic degradation of methylene blue dye under visible light illumination (Mirhoseini and Salabat 2015). In another study, TiO_2 NPs were doped with palladium (Pd) using microemulsion technique and utilized it to degrade C.I. acid yellow 23 (AY23) dye under UV irradiation (Najjar et al. 2015). Doping of 0.75 wt% Pd with TiO_2 for doped catalyst synthesis and 600 mg L^{-1} loading of this synthesized catalyst for 0.05 mM AY23 dye concentration was found to be most effective for degradation in 30 min (Najjar et al. 2015).

Extending a little on the use of ionic liquids (which are essentially organic salts with melting points less than 100 °C (Kang et al. 2016)) as a novel green component in the fabrication of doped photocatalysts, there are a few more interesting works which support the superior photocatalytic dye degradation capacity of such catalysts. Indeed, a survey of the relevant literature will indicate that there has been a fast growing interest and successive examination of several ionic liquids as environmentally benign co-solvents or co-surfactants (Zhao et al. 2017a; Bento et al. 2020). Ionic liquids have been used in the preparation of various efficient and multifunctional materials endowed with tunable properties suiting a range of applications (Kang et al. 2016; Sobhani et al. 2017; Iannone et al. 2017; Manjunath et al. 2018; Nan et al. 2018). It has been found that ionic liquids are especially apt in efficiently stabilizing NPs and then guarding them from agglomeration (Sharma et al. 2017). For example, Rout et al. (2019) prepared a Au–Sn/ZnO nanocatalyst in a two-step method whereby Au–Sn alloy bimetallic nanoparticles were included into a pre-synthesized ZnO in the ionic liquid 1-butyl 3-methylimidazolium by combustion and thereafter observed that it required 90 min for rhodamine B to be degraded under the action of the novel catalyst to the extent of 95% under visible irradiation. Rout et al. (2019) attributed the high photoactivity of the 3Au–1Sn/ZnO catalyst to the collective influence of better light absorption intensity, a longer lifetime of e^{-}–h^{+} pair, a decreased recombination rate of e^{-}–h^{+}, higher stability, larger surface area and the synergistic effect developed between the Au–Sn NPs and the ZnO support. In another recent work, Ravishankar et al. (2019) report the preparation of niobium/TiO_2 NPs using 1-butyl-2,3-dimethylimidazolium tetrafluoroborate and niobium(V) nitrate and titanium(IV) isopropoxide as precursors by a hydrothermal method (140 °C). Thereafter, the optimized material prepared was found to have very good photocatalytic detoxification ability for rhodamine B dye and the 0.3 wt% niobium/TiO_2 photocatalyst had good photostability.

Sonochemical method

Ultrasonic irradiation has been used in sonochemical methods in order to control the reaction and the particle size for uniform dispersion of dopant and catalysts on supports such as graphene-based materials (Shende et al. 2018). High-intensity ultrasound can be used to prepare nanocatalysts and other nanomaterials (Xu et al. 2013) without bulk high temperatures, long reaction times or high pressures. During ultrasonic irradiation, several phenomena occur. Acoustic cavitation comprises the formation, growth and implosive collapse of bubbles (Sancheti et al. 2018) and can be categorized within the following: primary sonochemistry, secondary sonochemistry and physical modifications (induced under the effects of high-speed jets or shock waves originating from bubble collapse, Fig. 4) (Xu et al. 2013; Yusof et al. 2016).

The sonochemical approach is a relatively simple and environmentally friendly method in which an ultrasonic vibration bath is utilized to fabricate the materials (Sutanto et al. 2017). Sood et al. (2015) utilized the hydrothermal fabrication method in combination with an ultrasonic method for the synthesis of strontium-doped TiO_2 NPs. The synthesized Sr-doped TiO_2 was further tested for the photocatalytic degradation of Brilliant Green. The analysis for degradation revealed that the newly synthesized Sr-doped TiO_2 composite had a higher photocatalytic activity, which resulted in enhanced degradation efficiency up to 96%, within 60 min, and moreover, the doping of strontium with TiO_2 enhanced the quantum efficiency by inhibiting the recombination of photo developed charge carriers (Sood et al. 2015). Hidayanto et al. (2017) used the sonochemical method for the preparation of nitrogen (N) (5–9 wt%)-doped TiO_2 nanocomposites. The resulting particles were observed having a size of 21.42 nm and a polycrystalline structure with increased photocatalytic activity for methylene blue dye (20 ppm) degradation (0.024 ppm min^{-1}),

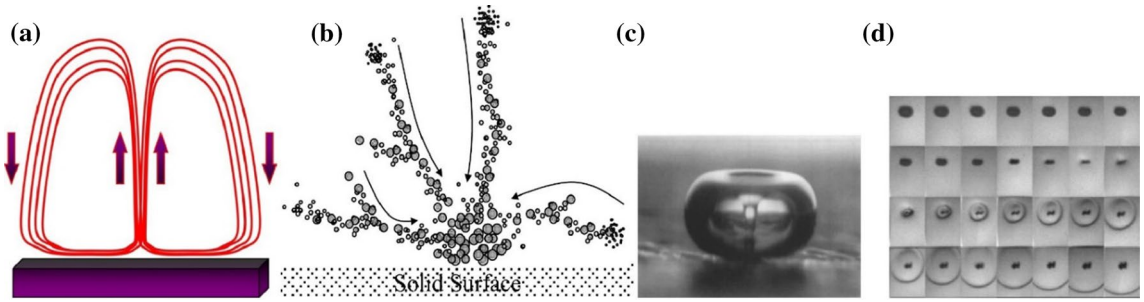

Fig. 4 **a** Acoustic streaming accompanied by considerable mass transfer effects (oscillator is positioned at the bottom and the liquid surface is located at the top), **b** microstreamers wherein bubble streamers are formed within an acoustic field as a result of the interactions occurring between the ultrasound waves and the gas bubbles; the generation of the oscillating gas bubble streamers happens because of primary and secondary Bjerknes forces where bubbles are in high-speed movement towards the pressure antinodes, and with the net microstreaming effect generating significant physical forces which influence the chemical reactions in progress within the ultrasound field, **c** high-speed microjets originating from the asymmetrical collapse of cavitation bubbles and **d** high-intensity shockwaves produced as a result of the symmetrically collapse of cavitation bubbles. The latter data and descriptions are compiled from Yusof et al. (2016), and this figure has been reproduced from Yusof et al. (2016) with the permission of Elsevier (Copyright © 2015 Elsevier B.V. All rights reserved) under licence number 4855151208397 (for both print and electronic formats)

as compared to bare TiO_2 (Hidayanto et al. 2017). Cerium-doped ZnO photocatalytic nanorods were synthesized by succinic acid, and a polyethylene glycol (PEG)-mediated sonochemical method was employed to degrade the hazardous pollutant dye crystal violet (Meshram et al. 2017). Morphology analysis by XRD revealed that doping of Ce up to 4% into ZnO particle did not result in any morphological change in pristine hexagonal ZnO morphology, whilst the increase in Ce concentration (6% and 8%) appeared in separate cubic cerium oxide (CeO_2) structure, and the maximum photocatalytic activity leading to higher degradation (99%) of crystal violet dye was also observed within 100 min at 4% doping of Ce with native ZnO (Meshram et al. 2017).

Snoussi et al. (2018) also utilized the versatility of sonochemical method to fabricate the unique core/double-layered shell NPs by accumulating the palladium-doped polypyrrole particles onto magnetite coated with mesoporous silica. In Snoussi et al. (2018), the fabrication of nanocomposites took only 1 h for complete synthesis by the sonochemical method which was a much lesser duration of reaction for metal-doped polypyrrole nanoparticle synthesis than other previously proclaimed fabrication methods in the several studies. Morphology analysis revealed the occurrence of zero-valent palladium in the exterior of magnetic NPs, and the results of degradation study showed that the fabricated composites were found to reduce almost 99% of the methyl orange dye in aqueous media (Snoussi et al. 2018). Perovskite morphology of zinc titanate ($ZnTiO_3$) was doped with cobalt (Co) and manganese (Mn) by adopting the sonochemical method (Wattanawikkam et al. 2019). Structural analysis of synthesized composites confirms the presence of Co and Mn in the lattice of $ZnTiO_3$ perovskite-structured composites. The degradation efficiency of composites was evaluated using rhodamine B (Rh B) dye deterioration, which showed that doped composites fabricated by sonochemical method had the higher photocatalytic activity for Rh B dye degradation under visible light illumination as compared to native zinc titanate (Wattanawikkam et al. 2019). The study conducted by Wattanawikkam et al. (2019) revealed that doping of metal ions into perovskite $ZnTiO_3$ using sonochemical method could be an effective solution for the enhancement of the photocatalytic activity of the composites.

Precipitation

Synthesis of nanocomposites using the co-precipitation method has various benefits over other existing fabrication methods. Co-precipitation of metal ions facilitates controlling the size and shape of newly synthesized particles by changing the pH of media. Also, it is an inexpensive and facile method which does not demand high pressure and temperature for the synthesis of particles. Jeyachitra et al. (2018) utilized the co-precipitation method for the synthesis of iron-doped ZnO NPs and employed these composites (Fe 0.02, 0.04 and 0.06%) as photocatalyst for the degradation of pollutant dye methylene blue. Doping of Fe at the concentration of 0.06 and 0.04 wt% in ZnO particles with the pH 4 exhibited the maximum degradation of methylene blue dye as compared to bare ZnO and other doped particle having different doping concentrations. Moreover, the increased degradation efficiency of doped nanocomposites might be the outcome of Fe integration into the Zn particles, which led to a decline in the recombination of electron–hole pairs and increment in the photocatalytic activity (Jeyachitra et al. 2018). Malika et al. (2016) also adopted the co-precipitation method for the fabrication of mono- and bimetal (Cu and Ni)-doped TiO_2 NPs. The use of the sonochemical method significantly expanded the anatase phase and crystallite size of doped composites

with enhanced stability of dopants within the crystal, and codoping of Cu and Ni dramatically increased the photocatalytic activity of bare TiO_2 for the degradation of eriochrome cyanine red (ECR) (Malika et al. 2016). Also, the photocatalytic activity of co-doped particles measured higher than mono-metal doping. Co-doped nanocomposites were found to have an efficiency of almost complete degradation of 100 mg L^{-1} ECR dye in 3 h (Malika et al. 2016).

There are other recent studies which have equally highlighted the outstanding photocatalytic properties and exceptional photocatalytic dye degradation capabilities of catalyst materials synthesized using precipitation-based methods, such as the works of Kundu and Mondal (2019) where layered sodium-intercalated Cu-doped titania was fabricated employing controlled precipitation and then examined in malachite green photodegradation, Franco et al. (2019) whereby ZnO photocatalyst was prepared through the thermal decomposition of zinc acetate NPs produced by a supercritical antisolvent precipitation method and then tested for its potential in the photocatalytic elimination of Crystal violet, Andrade Neto et al. (2020) where Ce^{4+}-, Co^{2+}-, Mn^{2+}- and Ni^{2+}-doped Fe_3O_4 NPs were synthesized using co-precipitation at 70 °C and assessed for their potential in bringing about discoloration of methylene blue containing solutions, and last but not least, Munawar et al. (2020) wherein ternary oxide NiO–CdO–ZnO nanocomposite was synthesized following a homogeneous co-precipitation procedure and then tested for its sunlight-driven photocatalytic degradation ability of rhodamine B and methylene blue.

Microwave-assisted synthesis

Microwave-assisted heating has been receiving more and more research attention and application in the synthesis of several nanomaterials over the last decade and more. The most significant merits of microwave-assisted heating warranting its application in material synthesis are the rapid heating effect (direct delivery of microwave energy to reacting materials (Lee and Wu 2017) and the direct absorption of microwave energy thereafter (Osman et al. 2017)), high rates of reaction, relatively shorter times for material preparation, homogeneity of materials fabricated, cost-effectiveness (Kadam et al. 2014; Xuan et al. 2015; Azadi and Habibi-Yangjeh 2015; Akhundi and Habibi-Yangjeh 2016) and high product yields (He et al. 2016). Other workers such as Zhang et al. (2018), McBride et al. (2017), Shkir et al. (2016), Liu et al. (2019), Parthibavarman et al. (2018a, b) and He et al. (2018) have also indicated that microwave irradiation time and temperature have important bearings in the surface morphology, crystallinity and photocatalytic activity of materials/catalysts prepared using microwave-assisted processes. A surfactant-free microwave-assisted synthesis method was successfully employed for the synthesis of Fe-doped ZnO photocatalysts for the degradation of tropaeolin O dye (Kwong and Yung 2015). Degradation analysis revealed that doping of Fe shifted the absorption spectra of composites from UV to visible range, thus raising the absorption of visible light and photocatalytic activity of the catalyst, and that the degradation of tropaeolin O dye was achieved almost to 99.8% with the 30 mg catalyst concentration at 0 cm light distance having initial pH 9 and 60 °C temperature in 3-h visible light irradiation (Kwong and Yung 2015). In another study, Liu et al. (2017) fabricated boron (B)-doped zinc tungstate ($ZnWO_4$) nanorods with the series length of 50–200 nm via microwave-assisted hydrothermal method. Therein, boron ions were smoothly integrated into $ZnWO_4$ lattice under microwave heating at the temperature of 180 °C with 1-h reaction time, and highly crystalline nanocomposites were obtained. Structural analysis thereafter revealed that tungsten ions were substituted by B ions in $ZnWO_4$ lattice, which resulted in decline of particle size and increment in specific surface area. Moreover, the obtained doped nanorods with 2.42 wt% B concentration showed higher photocatalytic activity for rhodamine B dye disintegration with the rate constant of 0.065 h^{-1}, which was four times higher than that exhibited by bare $ZnWO_4$ particles (0.016 h^{-1}) (Liu et al. 2017).

Functionalization of doped photocatalysts

The catalytic properties of pristine materials having some basic catalytic capabilities are usually relatively low and at times unsuitable for specific purposes. At this stage, and provided there is discernible merit in the gross catalytic properties of the pristine material, it becomes both interesting and worthwhile to devise some methods to functionalize the pristine material before their applications to simulated and/or real conditions. Broadly considered, the pristine catalysts are synthesized to prompt certain catalytic characteristics in view to initiate the intended catalysis for the degradation and/or mineralization of the dye molecules. However, with the specific set of steps serving the functionalization process, these original catalytic capabilities are enhanced and allowed to become more prominent in their effects on the dye degradation dynamics. In principle, the functionalization aims to improve significantly the surface properties and chemical attributes of the pristine catalyst. In a first instance, there is the aim to have an augmentation in the numbers of active catalysts sites which may then also offer the additional advantage of being endowed with more chemical active functional groups expected to enhance the dye degradation and mineralization kinetics. Based on the present analysis of the recent literature, it has been observed that there are some specific categories of functionalized doped-type photocatalysts which are very frequently analysed and have excellent photocatalytic

potentialities to assist with the degradation of a wide number of dyes. These categories are discussed in the following.

Titania-type photocatalysts

Based on a number of sources in the literature, titania has special photophysical and photochemical properties which enable its use in a number of situations as a potent photocatalyst (Fu et al. 2013; Paul and Choudhury 2014; Khaletskaya et al. 2015; Cao et al. 2016; Cargnello et al. 2016; Oblak et al. 2018; Sheng et al. 2019). Yet, there are two major limitations which impact on the photocatalytic capability of titania. In a first place, solely ultraviolet light is capable of giving rise to photocatalytic reactions on TiO_2. There is also the recombination phenomenon of the photoexcited electron (e^-)–holes (h^+) that lowers quantum efficiency (Iveland et al. 2013; Janczarek et al. 2016). The *good news* is that the latter limitation can be dealt with through the modification of the surface of TiO_2 with noble metals and their compounds which bring out an inhibition of the charge recombination process by augmenting photoexcited electrons transport from TiO_2 to the substrates (Bumajdad and Madkour 2014; Gonell et al. 2016; Luna et al. 2016). In recent times, doping of TiO_2 with rare earth (RE) metals has come out to be an efficient approach for enhancing the photocatalytic characteristics of TiO_2. According to Bellardita et al. (2011), Ramya et al. (2013) and Reszczyńska et al. (2015), the photocatalytic properties get improved by reason of the fact that f-orbitals of the lanthanide ions can produce complexes having different Lewis bases and hence allow for the build-up in concentration of the substrates onto the TiO_2 surface. Moreover, doping of TiO_2 with nonmetal such as nitrogen, carbon and sulphur has had excellent effects in improving the photocatalytic activity of TiO_2. For example, Chaudhary et al. (2016) have synthesized seaweed heteroatom-doped TiO_2 NPs wherein the remnant C-doping and S-doping from the seaweed carrageenan precursor in the TiO_2 composite implied larger surface areas for the effective degradation of dyes (namely methylene blue, reactive black-5 and methyl orange) in less than 20 min in daylight conditions. Chaudhary et al. (2016) explained the enhanced daylight dye-degrading photocatalytic activity of the λ-S–TiO_2 nanomaterial on the basis of the large surface area resulting from the graphite like carbon residue, greater S-content and suitable anatase crystallinity.

Yun et al. (2015) synthesized core–shell-type TiO_2@mercaptopropyl-functionalized silica particles in view to enhance the photocatalytic characteristics of TiO_2. Yun et al. (2015) observed that rhodamine 6G and rhodamine B dyes had been adsorbed significantly more onto the TiO_2@MPS particles than P25, by factors in the tune of 43 and 6, respectively, whereas the third dye under test, methyl orange, had been preferentially adsorbed more onto P25. These different adsorption behaviours were attributed by Yun et al. (2015) to the availability of functional groups and dye molecules, and their interactions thereafter with the specific sites on the test catalyst materials. Except in the case of methyl orange as the test dye, the photocatalytic activities of the core–shell-type TiO_2@mercaptopropyl-functionalized silica particles towards the two rhodamine dyes were significantly enhanced under both visible light and ultraviolet irradiations (Yun et al. 2015). It was also of particular practical importance to note that Yun et al. (2015) reported that their core–shell-type TiO_2@mercaptopropyl-functionalized silica particles had very good recyclability and were very much chemically stable even after at least three consecutive photocatalytic degradation experimental runs. Recently, in a novel work, Caschera et al. (2018) reported that functionalization of cotton textile with europium(III)-doped oleate-capped titanium dioxide TiO_2 nanocrystals had brought about many new functionalities including enhanced visible light-driven photocatalytic degradation of methylene blue, and changes in the structure of the parent cotton material.

Chen et al. (2017) fabricated nanofibrillated cellulose and had the surface of these nanostructures successfully functionalized with quaternary ammonium groups. Amongst the many nanofibrillated cellulose structures that had been prepared, the one endowed with nitrogen-doped TiO_2 demonstrated the optimum photodegradation performance for methyl orange under simulated sunlight, despite it having not as good adsorption properties in comparison with the pristine nanofibrillated cellulose (Chen et al. 2017). Besides other valuable features as an effective photodegradation catalyst, the nitrogen-doped nanofibrillated cellulose cryogel demonstrated very good reusability after multiple adsorption/photodegradation cycles and had also retained its mechanical durability and could also be recycled (Chen et al. 2017). Yang et al. (2015) reported that titanium dioxide-doped Fe_3O_4 NPs had sufficient potential to be used as a very effective Fenton-like catalyst for dye degradation and decolouration in near neutral milieu as a result of the titanium dioxide surface doping of the iron oxide species significantly enhancing the catalytic properties of the Fe_3O_4 in Fenton-like reactions. Yang et al. (2015) also reported green features of their synthesized catalytic nanostructures in that they favoured the decomposition of hydrogen peroxide for subsequent methylene blue oxidation without the need of an external source of energy, the nanocatalysts were versatile and effective at several pH values and even when radical scavengers were present in the reaction milieu. From their findings, Adyani and Ghorbani (2018) recently inferred that gadolinium and phosphorus doping had enhanced the surface textural characteristics of titanium dioxide by occasioning the formation of Ti–O–P and Ti–O–Gd bonds. Interestingly, Adyani and Ghorbani (2018) also observed that gadolinium had an important bearing in augmenting the oxygen vacancies and organic

moieties on the surface of the pristine titanium dioxide. The gadolinium doping had also successfully promoted the transfer of the photoinduced charge carriers to the species adsorbed on the TiO_2 surface (Adyani and Ghorbani 2018). Moreover, Adyani and Ghorbani (2018) also found that the Fe–Gd–P-tridoped titanium dioxide composite had brought about the most significant photodegradation rate of methyl orange amongst all experimental runs with a kinetic rate constant of 0.0128 min^{-1}. Adyani and Ghorbani (2018) explained these major findings based on the synergistic effects of significantly improved surface chemistry and surface textural properties, a higher count of organic species and hydroxyl groups adsorbed on the surface, enhanced absorption of visible light, higher lifetime of e^+/h^- pairs and better interfacial transfer of charge carriers. Patil et al. (2019) have also reported an interesting study wherein they fabricated TiO_2/WO_3 nanocomposites and had functionalized them with chlorosulfonic acid. Detailed characterization analysis and results thereof confirmed that active $–SO_3H$ groups had been successfully added to the surface of the titanium dioxide/WO_3 composites (Fig. 5), as a result

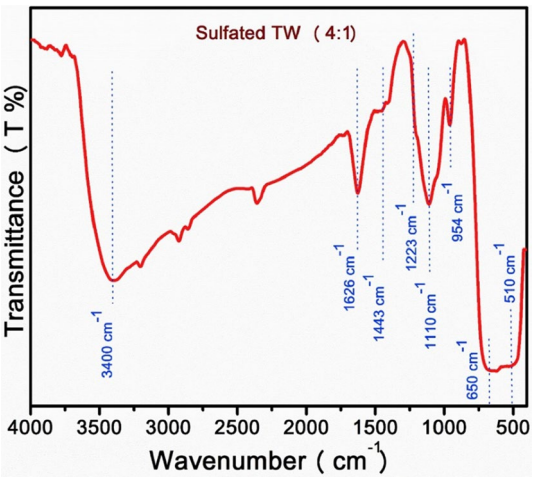

Fig. 5 FTIR spectra of sulphated TiO_2/WO_3 nanocomposite (4:1 wt% of TiO_2/WO_3) prepared by a simple sol–gel wet impregnation method (Patil et al. 2019). As per discussions and arguments in Patil et al. (2019), the broad peak recorded at 3400 cm^{-1} is attributable to surface-adsorbed water molecules (indicative of O–H stretching vibration); hydroxyl groups adsorbed onto the TiO_2/WO_3 nanocomposite (4:1 wt% of TiO_2/WO_3) surface are also detectable at the absorption band 1626 cm^{-1} (indicative of O–H bending vibrations); the typical Ti–O bending vibration band at 1443 cm^{-1} is also noted; peaks obtained at ~ 510 to ~ 650 cm^{-1} indicate the formation of TiO_2 NPs; W–O stretching and vibration bands are located in the section 960 cm^{-1} to 800 cm^{-1}; and the characteristic bands positioned at 1223 cm^{-1}, 1110 cm^{-1} and 954 cm^{-1} provide conclusive evidence of the presence of surface-anchored $–SO_3H$ groups onto the TiO_2/WO_3 nanocomposite (4:1 wt% of TiO_2/WO_3) surface. This figure has been reproduced from Patil et al. (2019) with the permission of Elsevier (© 2018 Published by Elsevier B.V.) under licence number 4855151417130 (for both print and electronic formats)

of which the novel nanocomposite material was able to degrade Congo red and methyl red very efficiently, and still possessed excellent catalytic efficiency of more than 90% even after five successive experimental cycles (Patil et al. 2019). Bakar and Ribeiro (2016) reported some actually interesting results wherein it was observed that in the case of cationic sulphur-doped TiO_2 photocatalysts, photoinduced holes and chemisorbed hydroxyls had played a key part in photocatalysis, whilst for anionic sulphur-doped TiO_2 photocatalysts, electrons and photoinduced holes were the species having quasi-equal parts played in photocatalysis. Moreover, based on the findings, it was found that sulphur atoms had been effectively incorporated into the TiO_2 crystal lattice and, consequently, there was substitution of Ti^{4+} by S^{6+} to form Ti–O–S bonds in the case of cationic sulphur doping, whilst for anionic sulphur doping, there had been substitution of S^{2-} by O^{2-} to form O–Ti–S bonds (Bakar and Ribeiro 2016).

Graphene-type photocatalysts

Graphene refers to a single layer of atoms of carbon closely packed into a benzene-ring structure (Faraldos and Bahamonde 2017). Graphene has forged itself a very prolific reputation as a unique material with outstanding physical properties and optical features. With the rate of progress in research and development have paced up very quickly with graphene and its various scientific and engineering applications, the reduction of exfoliated graphene oxide (GO) has come out to be a much effective, low-cost and dependable manner to fabricate graphene nanosheets having high stability (Faraldos and Bahamonde 2017). Moreover, through well-planned and executed chemical modifications, the surface characteristics of graphene can be tuned to reach novel graphene-based materials which embody remarkably feasible functionalization which eventually expand the scope of applications of these materials (Faraldos and Bahamonde 2017). To name a few, property-tuned graphene-type materials can find interesting uses in adsorption of environmental contaminants (Bai et al. 2012; Fakhri et al. 2017), thermal energy storage (Mehrali et al. 2013), catalysis (Li et al. 2010; Sun et al. 2012; Indrawirawan et al. 2015), biomass and organic biomolecules conversion (Zhu et al. 2015; Hou et al. 2016), bioenergy production processes (Ci et al. 2015) and nanomedical therapies (Rahmanian et al. 2017).

In the area of research on photocatalysis, graphene has been studied in the fabrication of several types of (nano) composite materials using a range of other compounds such as titania (Trapalis et al. 2016), zinc oxide (Moussa et al. 2016; Rokhsat and Akhavan 2016), $CH_3NH_3PbI_3$ (Wu et al. 2018), ZnS–Ag_2S (Amaranatha Reddy et al. 2015) and N–ZnO/CdS (Huo et al. 2016) for reaping better photocatalytic properties and performance. Graphene can be

considered a bank of photoelectrons which endow it with its observed high conductivity (Trapalis et al. 2016). Moreover, the photogenerated electrons become more readily accepted, stored and transported from the titania/graphene interface when using graphene which have a low defects content (Trapalis et al. 2016). The enhanced photocatalytic performance of TiO_2/graphene composite nanomaterials is attributed to the lowered extent of electron–hole recombination and the prolonged lifetime which are both entailed because of their separation (Zhang et al. 2010, 2011). In their work which involved the synthesis of gold NPs which had been functionalized with tannic acid and having graphene hydrogel as support, Luo et al. (2015) indicated that the tannic acid which contained many phenolic groups had achieved multiple green features. These green characteristics were reported to be that tannic acid functionalization had led to the reduction of the graphene oxide (GO) and brought about the self-assembly of the reduced GO into graphene hydrogel and that tannic acid had equally acted as the reducing agent and stabilizer for the in situ fabrication of the gold NPs in water at ambient reaction conditions. The additional green features of the gold nanocomposite material developed by Luo et al. (2015) are that it could catalyse the reduction of methylene blue and could equally be recycled and reused even after five cycles. Earlier, Zhao et al. (2017b) reported the development of a 3-D hemin-functionalized graphene hydrogel which possessed remarkable photodegradation capacity for methylene blue *vis-à-vis* the pristine graphene hydrogel and P25 catalyst. Moreover, it is important to highlight that the 3-D hemin-functionalized graphene hydrogel remained stable in its photocatalytic activity following multiple cycles of after photocatalytic reaction runs and that the photocatalytic degradation of methylene blue was mediated principally by the involvement of $O_2^{\cdot-}$ radicals (Zhao et al. 2017b) (Fig. 6). Cao et al. (2018) recently fabricated a new heterogeneous catalyst which they referred to as TEA/GO@Fe_3O_4. Cao et al. (2018) observed that the TEA/GO@Fe_3O_4 composite had an excellent contribution in a very rapid decomposition of methylene blue. Amongst other reasons, Cao et al. (2018) attributed the remarkable characteristics of the TEA/GO@Fe_3O_4 composite to the Fe_3O_4 NPs having been immobilized onto the graphene oxide surface and then functionalized by the triethanolamine (TEA). Furthermore, results of TEM analysis in this same work of the TEA/GO@Fe_3O_4 nanocomposite also indicated that the Fe_3O_4 NPs had characteristic spherical shapes and were distributed on the graphene oxide surface and particularly so on the edges (Fig. 7). Cao et al. (2018) rationalized this important observation to the abundance of functional groups which contained oxygen on the edge of the graphene oxide whilst the remaining of the Fe_3O_4 NPs had been immobilized by hydroxyl or epoxy groups found on the planar surface of the graphene oxide.

ZnO-based doped photocatalysts

ZnO is an important photocatalyst characterized by strong catalytic ability, large surface area, direct and suitable band gap ($E_g = 3.37$ eV), and large exciton binding energy (60 meV) (Lee et al. 2016a). In recent photocatalytic studies, it has emerged as a strong rival to TiO_2-based photocatalysts which are considered as the most-explored photocatalysts. However, ZnO is susceptible to chemical dissolution, especially under acidic conditions which affects its stability and efficiency (Wang et al. 2016). Moreover, like TiO_2-based photocatalysts, UV light is required for ZnO to become active due to wider band gap. Therefore, it is highly demanding to increase its stability and photocatalytic ability in visible light with narrow band gap. This section is devoted to review recent developments addressing this issue to effectively degrade the dyes.

For the degradation of dyes in aqueous solutions, ZnO exhibited better photocatalytic efficiency than TiO_2 alone (Aggelopoulos et al. 2017; Štrbac et al. 2018) or even their mixture as 2ZnO–TiO_2 containing zinc titanate (Zn_2TiO_4) as the dominant phase (Štrbac et al. 2018). This might be linked to higher electron mobility of ZnO (about two orders of magnitude) than TiO_2. However, inclusion of TiO_2 with ZnO was advocated in harsh acidic environments owing to its higher structural stability and better ability to change the band gap improving light absorption (Štrbac et al. 2018). Some other studies have also combined ZnO and TiO_2 for better stability. For example, Wang et al. (2016) reported much higher photocatalytic ability of iodine-doped ZnO (ZnO-I) to degrade rhodamine B (93% removal) than bare ZnO (54%). Pollutant removal was further enhanced to 97% by decorating TiO_2 (ZnO-I–TiO_2) due to suppressed charge recombination and higher light absorption. Though this increase in efficiency was not very prominent (from 93 to 97%), decorating with TiO_2 was particularly advantageous in improving the stability of ZnO-I–TiO_2. It retained its efficiency at a wide range of pH (5–10) and for five repeated runs, whilst ZnO-I was sensitive to pH variations (42% and 59% pollutant removal at pH 5 and 10, respectively) (Wang et al. 2016).

Photocatalytic efficiency of ZnO can also be improved by compositing it with the carbon materials where ZnO is allowed to grow and stabilize over these materials. Owing to the better efficiency of carbon materials as electron acceptors, photocatalytic ability of ZnO (as electron donor) is improved (Sushma and Girish Kumar 2017). For example, efficiency and stability of ZnO were significantly enhanced when it was composited with functionalized graphene oxide (GO) to degrade safranin-T dye under UV light (Nenavathu et al. 2018). Complete removal of dye was observed by nanocomposites based on functionalized GO/ZnO as compared to 80% removal by pristine ZnO. They associated this to improved dye adsorption by inclusion of GO and decrease in band gap of composite sample (3.10 eV) than pristine ZnO (3.16 eV) which improved the

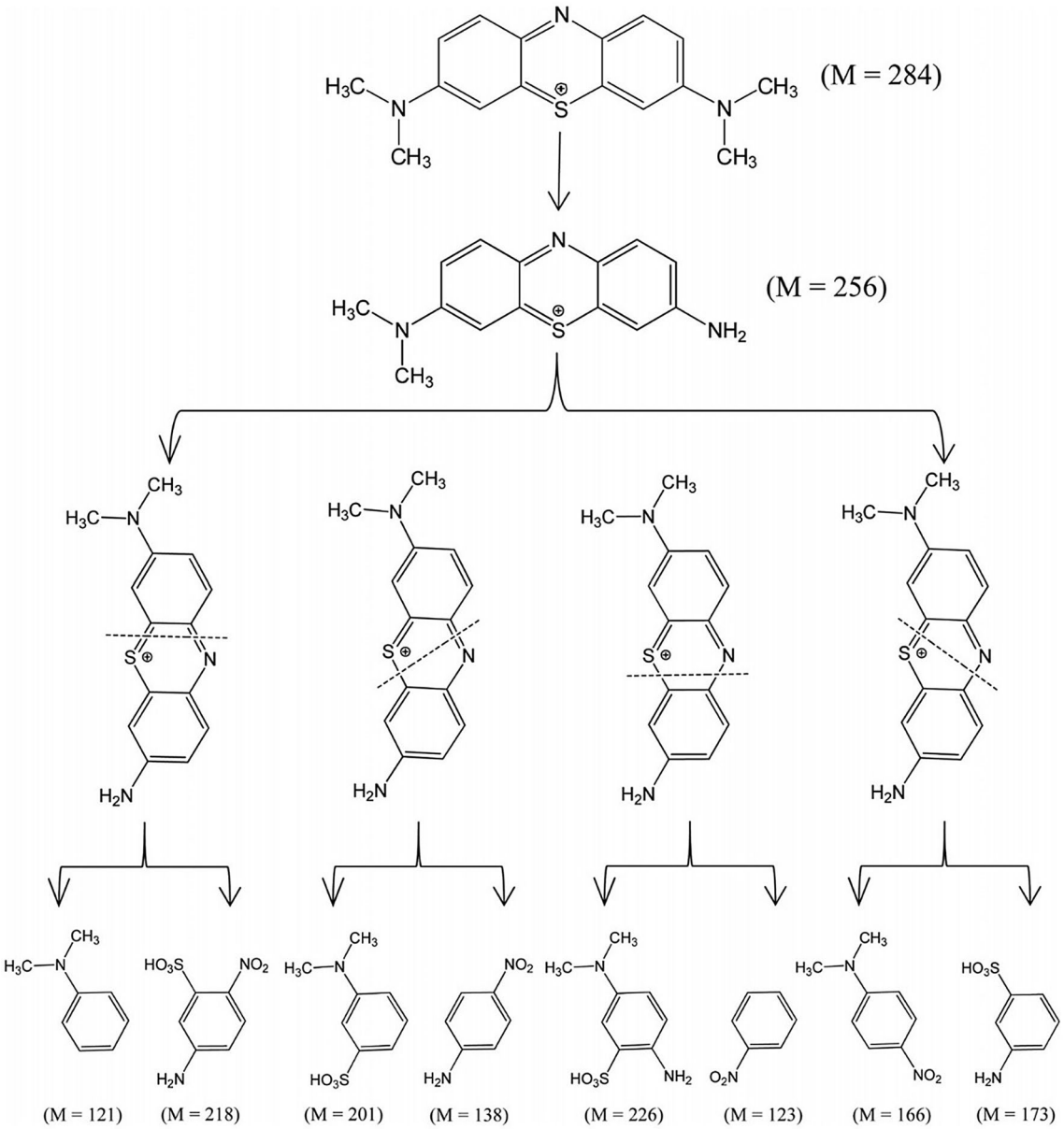

Fig. 6 Photodegradation pathway of methylene blue solution under the action of a hemin/graphene hydrogel proposed by Zhao et al. (2017b). As per discussions in Zhao et al. (2017b), two $-CH_3$ functional groups in methylene blue likely to falling off and chemical species with MS peak at 256 were obtained; then, the much bioactive superoxide anions could attack and bring about the catalytic oxidation of demethylation products, which then split into two parts to produce acidic molecules; and finally, the different pyrolysis products were reached. Based on the results obtained, Zhao et al. (2017b) inferred that although the methylene blue solution had turned colourless and transparent and no UV–Vis absorption occurred, the extent of degradation had not reached completion. (Just 10% total organic carbon had been left in solution.) This figure has been reproduced from Zhao et al. (2017b) with the permission of American Chemical Society (Copyright © 2017, American Chemical Society) obtained on June 24, 2020 (for both print and electronic formats)

absorbance in visible range. Efficiency of composite samples varied according to the contents of GO where 0.09 wt% gave the best efficiency amongst the tested compositions (GO: 0.05, 0.09, 0.10, 0.5 and 5 wt%). Increasing the GO contents beyond 0.09% decreased the catalytic ability because excess amounts of GO can block the active sites of ZnO due to a shielding effect. It is also interesting to point out that tested composites were highly stable as they retained the catalytic ability for five treatment cycles (only 4% decrease in degradation), whilst a drastic reduction was reported for pristine ZnO (from 80 to 40%) (Nenavathu et al. 2018). However, GO sheets are susceptible to agglomeration which can reduce their efficiency. For this, Chauhan et al. (2019) proposed that agglomeration can be avoided by coating of GO over Si substrate followed by

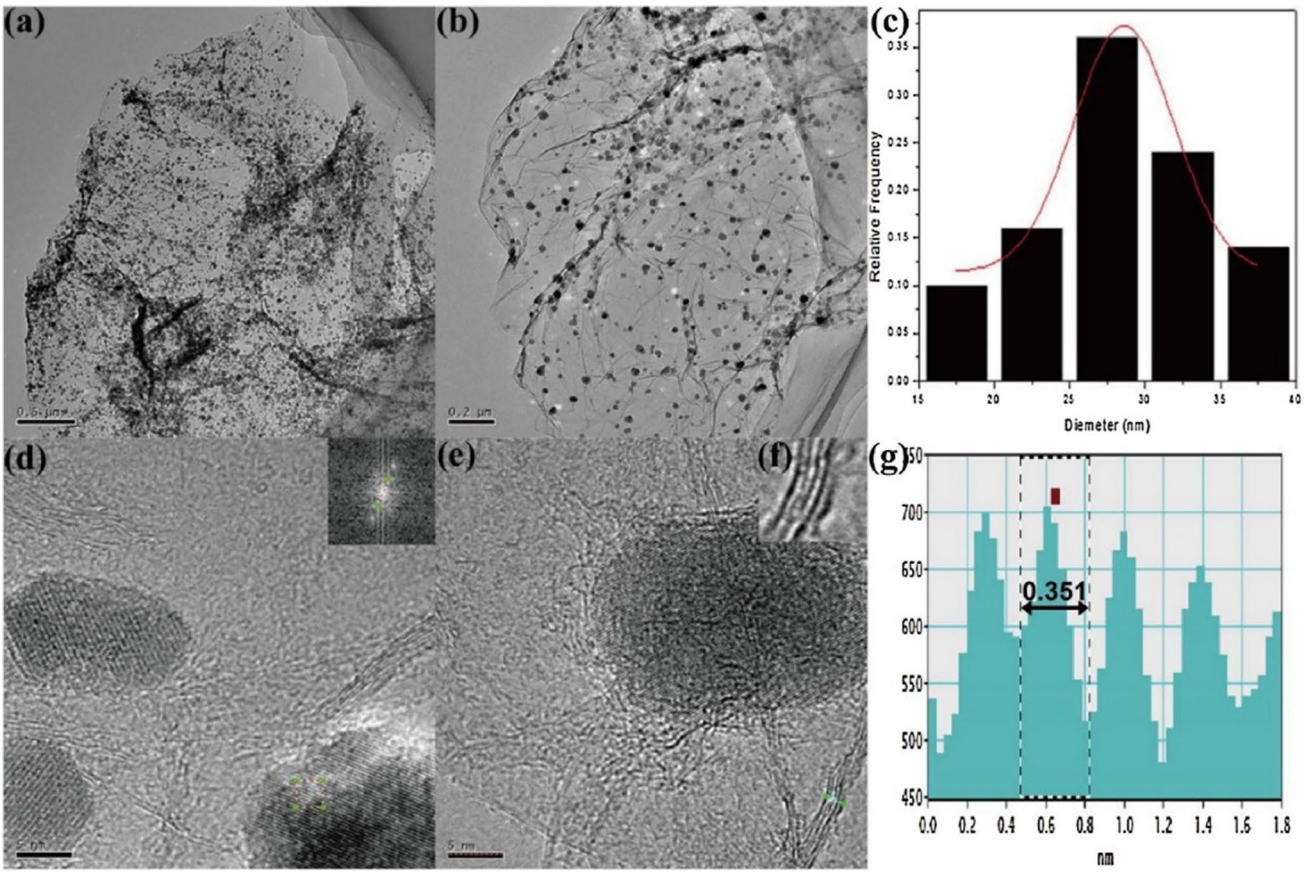

Fig. 7 **a** TEM image of TEA/GO@Fe_3O_4 at 0.5 µm; **b** TEM image of TEA/GO@Fe_3O_4 at 0.2 µm; **c** particle size distribution of TEA/GO@Fe_3O_4 at 0.5 µm; **d** distance between two lattice fringes examined by Digital Micrograph; **e** the short green line appearing in the lower right corner indicates the edge of TEA/GO@Fe_3O_4; **f** as an inset in (**e**): **f** is the enlarged view of the edge displayed by the green line; and **g** is the profile image examined by Digital Micrograph (Cao et al. 2018) (for more details with regard to the interpretation of colours used in this figure and images therein, the online version of this article can be consulted at https://doi.org/10.1016/j.colsurfa.2018.04.009); based on **a** through to **d**, the Fe_3O_4 nanostructures have been depicted as having characteristic spherical shapes and as being dispersed on the graphene oxide surface, and especially on the edge (Cao et al. 2018). This figure has been reproduced from Cao et al. (2018) with the permission of Elsevier (© 2018 Elsevier B.V. All rights reserved) under licence number 4855160414566 (for both print and electronic formats)

the use of this composite support to grow ZnO nanoflowers. Similarly, use of carbon nanotubes was also found useful in improving the photocatalytic ability of ZnO due to improvement in surface area, charge transport and light absorption (Bagheri et al. 2020). They reported that removal of dye (reactive blue 203) was highest (99%) in case of ZnO stabilized on MWCNTs as compared to the 85% and 19% by ZnO and bare MWCNTs, respectively. It is worth to mention that most of the carbon-based photocatalysts require post-process filtration for their reuse. The reusability of materials can be facilitated by finding suitable strategies that can offer quick, easy and effective recovery of photocatalysts from the reaction medium. In this regard, the development of magnetic materials is gaining significant attention as illustrated recently in Bomila et al. (2018), Kayani et al. (2018), Kalam et al. (2018), Eskandari et al. (2019), Patil et al. (2020), Ciocarlan et al. (2020) and Ebrahimzadeh et al. (2020).

Akkari et al. (2017) used sepiolite clay immobilized with magnetite (Fe_3O_4) and ZnO to develop an efficient magnetic photocatalyst that completely removed the methylene blue dye in aqueous solution (under UV irradiation for 2 h). Though ZnO/magnetite/sepiolite exhibited similar catalytic ability to ZnO/sepiolite, its use was advantageous as it magnetic nature offered an ease in its recovery after treatment. The presence of magnetite, a mixed valent Fe mineral, introduces the magnetic character in the photocatalyst that ensures a convenient recovery (with an external magnetic field) for reuse in repeated photocatalysis cycles (Usman et al. 2018). Owing to this desirable feature, use of magnetite with ZnO has also been suggested elsewhere (Wang et al. 2018a; Atla et al. 2018). For example, Atla et al. (2018) developed different photocatalysts using ZnO and magnetite including ZnO/Fe_3O_4 (M1), ZnO/SiO_2/Fe_3O_4 (M2) and ZnO/APTS–SiO_2/Fe_3O_4 (M3). All these materials were magnetically separable, but their photocatalytic

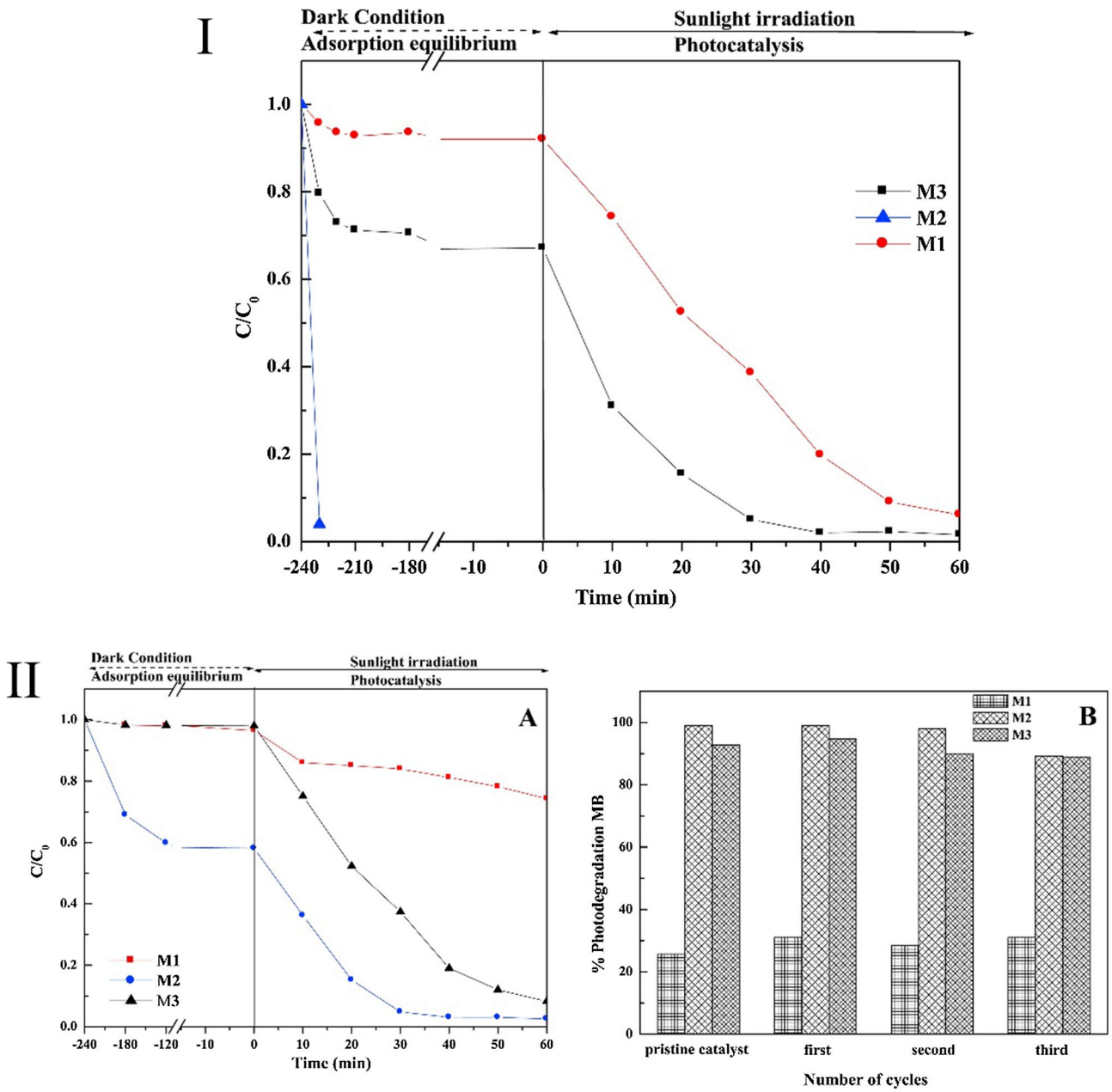

Fig. 8 Photocatalytic degradation of methylene blue by using three photocatalysts ZnO/Fe_3O_4 (M1), ZnO/SiO_2/Fe_3O_4 (M2) and ZnO/APTS–SiO_2/Fe_3O_4 (M3) at a catalyst loading of 500 mg (image **I**) and an optimum dose of 5 mg (image **II**(**A**)) and image **II**(**B**) reporting the results of the reusability studies of M1, M2 and M3 (Atla et al. 2018). Degradation is mentioned as C/C_0 where C represents the concentration of a dye at a given reaction time, whilst C_0 denotes its initial concentration. This figure has been reproduced from Atla et al. (2018) with the permission of Elsevier (© 2018 Elsevier B.V. All rights reserved) under licence number 4855160631579 (for both print and electronic formats)

ability was dependent on the presence of ZnO defects that was the following order: M2 > M3 > M1. At high catalyst loading (500 mg/30 mL), M2 completely removed the methylene blue dye by adsorption, whilst M3 and M1 exhibited both the adsorption and photocatalysis (Fig. 8). When catalyst loading was decreased to 5 mg (suggested as optimum loading), no adsorption was observed for M1 and M3 (dye removal only by photocatalysis), whilst M2 exhibited both the adsorption and photocatalysis (Fig. 8). The presence of silica was linked to the best performance of M2 in terms of adsorption as well as the photocatalytic ability, whilst its absence (as in M1) decreased the treatment ability (Fig. 8). Silica layer protected the magnetic core from oxidation and dissolution (higher stability) and decreased the recombination time (higher photocatalytic

ability). Coating of APTS decreased the adsorption capacity of M3 (by increasing particle size) and photocatalytic ability (by decreasing surface defects in the sample). Similar findings regarding the role of SiO_2 were reported by Wang et al. (2018a) in a ZnO heterostructure composed of Fe_3O_4@SiO_2@ZnO@Au that was developed by a multistep protocol. For this, Fe_3O_4 core surface was coated by SiO_2 interlayer followed by the use of this product to grow ZnO nanorods and functionalization of Au NPs (Wang et al. 2018a). The obtained material was highly efficient to photodegrade rhodamine B (93.54% removal after 80 min of UV irradiation). Moreover, Fe_3O_4@SiO_2@ZnO@Au maintained its core–shell structure, structural stability, magnetic properties and photocatalytic ability for five treatment cycles. Contrary to the negative role of APTS coating (Atla et al. 2018), Au loading increased the photocatalytic efficiency as ZnO/Au heterojunction improved the transfer of electrons which ensures that photogenerated charge carriers are quickly separated (Wang et al. 2018a). However, adequate quantity of Au is an important consideration as, at higher amounts, Au particles are susceptible to aggregation which can inhibit further production of electrons and thus affect the photoinduced behaviour (Wang et al. 2018a).

In recent years, different dopants have been explored to render ZnO particles as more efficient photocatalysts such as aluminium (Sharma et al. 2019), cobalt (Chithira and Theresa John 2020), iodine (Wang et al. 2016), iridium (Dhanalakshmi et al. 2020), magnesium (Adam et al. 2020), nitrogen (Prabakaran and Pillay 2019; Sun et al. 2020), palladium (Pd) (Rodrigues et al. 2020) and silver (El-Bindary et al. 2019; Rodrigues et al. 2020). These materials have been doped by using different synthesis methods such as co-precipitation (Adam et al. 2020; Rodrigues et al. 2020; Chithira and Theresa John 2020), ultrasonic disposition (El-Bindary et al. 2019) and hydrothermal method (Wang et al. 2016; Prabakaran and Pillay 2019; Sun et al. 2020). The choice of these methods is based on the desired properties and methods which are characterized by process simplicity and lower-temperature requirements were advocated such as hydrothermal. Use of all these dopants successfully resulted in a significant efficiency in photocatalytic ability and stability as compared to the bare ZnO (Fig. 9). Studies regarding the use of these doped ZnO-based photocatalysts revealed their strong stability in reusability studies except for iodine-doped ZnO (Wang et al. 2016). However, decorating ZnO with TiO_2 improved its stability as discussed in above paragraphs (Wang et al. 2016). Use of cobalt induced the magnetic properties in the photocatalyst that could be advantageous for a facile recovery (Chithira and Theresa John 2020). Sharma et al. (2019) confirmed by XPS elemental characterization and EDAX mapping that doping of Al on ZnO caused the substitution of Zn by Al but without causing any change in hexagonal structure of ZnO. The presence of Al in lattice structure prevented the electron recombination and holes on catalyst surface which improved the catalytic ability (Sharma et al. 2019). Largely, following observations were noted as a result of doping: (1) substitution at lattice sites induces the surfaces defects and modifies the associated chemistry, (2) a disparity in the ionic radius between the ZnO host and doping agent dictates the defect chemistry, (3) structural disorders arise due to variation in the oxidation state of doping agent and (4) changes in band gap, light absorption properties and ultimately the photocatalytic ability (Sushma and Girish Kumar 2017).

A recent trend has been the development of doped ZnO particles which are further stabilized on carbon materials to further improve the photocatalytic ability (Mohamed and Shawky 2018). For example, photocatalytic degradation

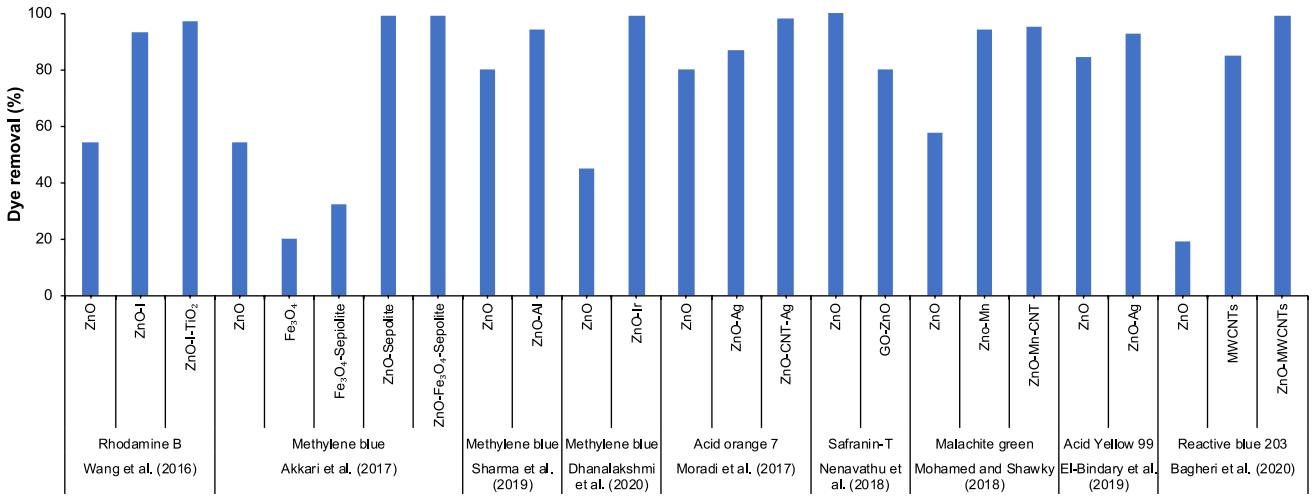

Fig. 9 Photocatalytic removal (%) of various dyes by selected ZnO-based photocatalysts. As reaction conditions vary in these studies, the efficiency of the photocatalysts should not be compared amongst different studies, but rather with the materials tested in the same study for a fair comparison. Data herein have been compiled from Akkari et al. (2017), Bagheri et al. (2020), Dhanalakshmi et al. (2020), El-Bindary et al. (2019), Mohamed and Shawky (2018), Moradi et al. (2017), Nenavathu et al. (2018), Sharma et al. (2019) and (Wang et al. 2016)

of malachite green increased significantly from 57% (with bare ZnO) to 94% (Mn-doped ZnO) (Mohamed and Shawky 2018). Using CNT as a support for Mn-doped ZnO further improved the degradation to 95% in addition to increasing its surface area that varied in the following order: 39.63 $m^2 g^{-1}$ (Mn-doped ZnO@CNT) > 37.99 $m^2 g^{-1}$ (bare ZnO) > 25.56 $m^2 g^{-1}$ (Mn-doped ZnO). Using CNT as a support improves the surface area which could improve the adsorption and ultimately can result in rapid photocatalytic removal. Moreover, separation of electron pairs is effective in the presence of CNT which improves the photocatalytic ability as witnessed during degradation of acid orange by Ag-doped ZnO@CNT by Moradi et al. (2017). They observed that use of CNT improved the surface area of loaded Ag-doped ZnO onto its surface (to 23 $m^2 g^{-1}$ from 18 $m^2 g^{-1}$ Ag-doped ZnO). In addition to the highest photocatalytic ability of Ag-doped ZnO@CNT (98% dye removal as compared to the 87% by Ag-doped ZnO), it was more stable as it retained its photocatalytic ability for four consecutive treatments (3% loss against 13% loss by Ag-doped ZnO). It should be noted that optimum contents of CNT should be chosen for an efficient pollutant removal. Photocatalytic ability of Mn-doped ZnO@CNT (Mohamed and Shawky 2018) and Ag-doped ZnO@CNT (Moradi et al. 2017) was maximum in the presence of 1% and 5% (w/w) of CNT. An increase in concentration beyond that significantly decreased the photocatalytic ability of ZnO as higher contents of clay could intercept the light absorption to the surface of photocatalyst and increase the solution turbidity (Moradi et al. 2017; Mohamed and Shawky 2018).

It is also interesting to point out that biogenic methods have also been employed to synthesize ZnO NPs. They are considered as environmentally friendly alternatives to chemical synthesis methods as they do not involve any hazardous chemicals. Rather, they rely on the use of biological agents (such as plant extracts and microbes) as reductants for the synthesis of ZnO. For this, plant extracts are mixed with Zn at suitable temperature and pH without any external addition of chemicals and stabilizing agents. Plant extracts contain variety of phytochemicals which act as reducing agent to synthesize ZnO. Use of biogenic ZnO exhibited successful results in photodegradation of dyes (Fowsiya et al. 2016; Karnan and Selvakumar 2016; Madhumitha et al. 2019). Owing to the eco-friendly nature and strong environmental implications, development of the biogenic ZnO for different environmental applications has been the subject of different recent reviews (Ahmed et al. 2017; Basnet et al. 2018).

Multiwalled carbon nanotubes-type photocatalysts

Carbon materials at the nanoscale have outstanding thermal and chemical stability, and based such properties carbon nanotubes (CNTs) are being increasingly synthesized using different methods for a number of diverse applications in engineering (Zhao et al. 2016). According to the literature, CNTs have been receiving more and more research attention by reason of their one-dimensional macromolecular configuration, high specific surface area and special chemical structure (Zhao et al. 2016). Moreover, with the high quality of progress in the use of CNTs, multiwalled carbon nanotubes (MWCNTs) have thereafter been fabricated as described, for example, in Sharma et al. (2018), Araga and Sharma (2017), Zada et al. (2017), Lv et al. (2017), Joseph et al. (2019) and Patel et al. (2017). MWCNTs are made up of many nested layers of very well concentrically arranged rolled graphite sheets (Zhao et al. 2016). Chemical functionalization, by the way of a functional group addition (Fiyadh et al. 2019), of the surfaces of MCNTs is also a growing area of research because of the improved properties and capabilities of the resulting structure (Elias et al. 2017; Moradi et al. 2017). The surfaces of the CNTs can be tuned and engineered through the incorporation of specific heteroatoms to enhance the surface wettability and improve adsorption capacities for certain types of compounds (Patiño et al. 2015). According to the discussions in Fiyadh et al. (2019), functionalization of CNTs can be covalent and non-covalent, whereby the former class is when functional groups get attached by covalent forces to the skeletal structure of CNTs through chemical reaction, and the latter type of functionalization occurs when functional groups coat the CNTs walls (Karousis et al. 2010).

Xia et al. (2007), Mamba et al. (2015), Zouzelka et al. (2016), Réti et al. (2016) and Panahian and Arsalani (2017) have indicated that CNTs can be combined with TiO_2 to generate composite structures for subsequent use as photocatalysts. Based on data in the literature, besides providing for a large surface area support to the TiO_2 particles, CNTs equally significantly retard the recombination of electrons and holes (Zouzelka et al. 2016; Karthika and Arumugam 2017; Natarajan et al. 2017). In their study, Hossain et al. (2018) observed a prominent broad peak at ~ 3400 cm^{-1} from the FTIR spectrum of the multiwalled carbon nanotubes they had synthesized and it confirmed the oxidation of some C atoms by nitric acid and sulphuric acid on the surface of multiwalled carbon nanotubes. Iron or silver was doped into the titanium dioxide-multiwalled carbon nanotubes composites, and the subsequent decrease of the energy band gap favoured a more pronounced photocatalytic degradation of methylene blue under visible light conditions. Hossain et al. (2018) attributed the excellent catalytic photodegradation capacity of the Ag–TiO_2–multiwalled carbon nanotubes and Fe–TiO_2–multiwalled carbon nanotubes composites to the following mechanistic processes: (1) adsorption and photoinduced absorption of electrons by the multiwalled carbon nanotubes and (2) trapping of electrons by the iron or silver inside the TiO_2

matrix, in supplement to the usual photocatalytic characteristics of titanium dioxide. In a very recent study by Wei et al. (2019), an N-doped carbon nanotubes–$FePO_4$ composite has been successfully prepared using phosphate residue using surface modification and chemical vapour deposition. Wei et al. (2019) reported that the N-doped carbon nanotubes–$FePO_4$ composite could degrade 98.9% of rhodamine B in 60 min under Fenton-like conditions and that the nanocatalyst was able to conserve high (more than half) its catalytic capacity after six successive cycles of use. Table 4 reports the key features reported in other selected studies with regard to the functionalization and doping methods of novel doped catalyst/MWCNTs composites.

Table 4 Studies reporting the synthesis of doped catalyst/multiwalled carbon nanotubes composites intended for use in the degradation of dyes

Material	Catalyst	Doping ratio	Catalyst/MWCNT (w/w)	Method	Final treatment	Target dye	References
Commercial MWCNT	Pd-doped–ZrO_2	0.5, 1, 2 wt%	1	Co-precipitation	The suspension was dried 100 °C for 12 h, calcined at 400 °C for 5 h and pulverized to obtain the powdered nanocomposite	Acid blue 40	Anku et al. (2016)
Commercial MWCNT	ZnO/NiO	95% ZnO 1% NiO-94% ZnO 3% NiO-92% ZnO	0.05	Co-precipitation	The suspension was dried in oven at 100 °C for 4 h The material was then calcined at 300 °C for 3 h to obtain ZnO/NiO-loaded MWCNTs	Methyl orange	Khan et al. (2018)
Commercial MWCNT	Ce-doped ZnO	0.5% Ce	–	Microwave irradiation	The sample was dried in an oven at 80 °C for 12 h	Methylene blue	Elias et al. (2017)
Commercial MWCNT	Mn–Zn NPs	50%	1	Co-precipitation	The mixture was heated at 60 °C for 2 h with occasionally stirring The mixture was cooled, filtered and then washed the MWNTs/Mn–Zn oxides NPs several times with distilled water in order to remove unreacted chemicals The MWNTs/Mn–Zn oxides NPs were dried and stored for further use	Malachite green	Zada et al. (2017)

Degradation dynamics of dyes by doped photocatalysts

The use of advanced oxidation processes (AOPs) for the degradation of organic compounds has received immense attention in the scientific world over the last few decades (Cheng et al. 2016; Nidheesh et al. 2018; Fernandes et al. 2019; Serna-Galvis et al. 2019; Verma and Samanta 2018; Crini and Lichtfouse 2019; Batista et al. 2010; Bello and Raman 2019). The different AOPs include photocatalysis, ozonation, electrochemical treatments and hydrogen peroxide-mediated oxidation as well as the combination of these processes (Rauf and Ashraf 2009). Amongst them, heterogeneous photocatalysis can be considered as a very promising approach for the removal of dyes under in situ conditions (Rauf and Ashraf 2009), and several NPs have been developed from semiconductors to be used as photocatalysts (Chakrabarti and Dutta 2004; Khan et al. 2012; Yan et al. 2017). The key advantages of using semiconductor NPs as photocatalysts are they are relatively inexpensive, they are easy to produce and they can degrade a wide range of organic molecules under ambient conditions just by utilizing solar energy (Khan et al. 2012). This section summarizes the advances made in the use of photocatalytic NPs for the degradation of dyes with a focus on their mode of action, influence of determining parameters and reusability.

Mode of action photocatalytic NPs

Photocatalysts are made from semiconductors that are characterized by a typical electronic configuration consisting of an empty conduction band and filled valence band separated by an energy gap (Hoffmann et al. 1995). This energy gap (also called 'band gap') is the amount of energy required to excite a valence electron from its ground state in the valence band to a free state in the conduction band. In the case of photocatalysis, if a photon carrying enough energy to neutralize the band gap is incident on an electron present in the valence band, it leads to the excitation of the electron and its promotion into the conduction band (Rauf et al. 2007). As the electron elopes into the conduction band, a positively charged vacancy is generated in the valence band which is termed as a hole. This way, an electron–hole pair is generated in the lattice. These photogenerated charge carriers are also called excitons. The excited electron residing in the conduction band and the hole in the valence band can migrate within the crystal lattice and on diffusing to the surface they can react with the adsorbed dye molecules. They can react either directly or indirectly through the formation of free radicals (Sambur and Chen 2016). Based on their mode of action, the process of photocatalysis can be classified as direct and indirect photocatalysis. In case of direct photocatalysis, electron–hole pairs that are photogenerated within the semiconductor lattice react directly with the dye molecules instead of forming intermediate species in the reaction. The two kinetic models proposed to explain the mechanism of photocatalysis are described in the following.

Langmuir–Hinshelwood model

According to the Langmuir–Hinshelwood model, the photocatalysis reaction occurring on the surface of the photocatalyst can be divided into three steps. In the initial step, the dye molecule gets adsorbed onto the surface of the photocatalyst as depicted in Eq. (1). In the second step, the photogenerated holes travel to the surface where they get trapped by the adsorbed dye molecule to form an unstable intermediate as depicted in Eq. (3). In the next step as depicted in Eq. (4), this intermediate is decomposed on reacting with an electron. The degradants are then desorbed from the surface. Thus, the dye is converted into a less harmful form and the catalyst's surface is restored to its original form at the end of the process (Rauf and Ashraf 2009). The reactions involved in this pathway can be depicted as follows:

$$S + \text{Dye} \rightarrow S \cdot \text{Dye} \tag{1}$$

$$\text{Photocatalyst} + h\nu \rightarrow h^+ + e^- (\text{photogeneration of excitons}) \tag{2}$$

$$S \cdot \text{Dye} + h^+ \rightarrow \text{unstable intermediate} \tag{3}$$

$$\text{Unstable intermediate} + e^- \rightarrow S \cdot \text{Product} \rightarrow S + \text{product} \tag{4}$$

Hence, it can be inferred that the rate of photocatalysis is directly proportional to the number of dye molecules adsorbed onto the surface of the catalyst, which in turn is dependent on the concentration of the dye in the solution. The rate of photocatalysis according to this pathway can be calculated using the equation $v = kK_aC_d/(1 + K_aC_d)$ (or $1/v = 1/k + 1/kK_aC_d$) (Chang 2000). In the latter equation, v denotes the rate of the reaction, K_a denotes the adsorption rate constant, k denotes the photocatalysis rate constant and C_d denotes the concentration of the dye in the solution.

Eley–Rideal's model

This kinetic model was proposed by D.D. Eley and E.K. Rideal in the year 1938. According to this model, only one of the reactants gets trapped on the surface of the photocatalyst, whereas the other reactant remains free in the mobile phase. In our case, the holes are trapped on the surface and the dye remains in a free state in the solution. There are certain

defects (D) present on the catalyst's surface where the holes get trapped on reaching the surface, thus forming the surface-active centre as depicted in Eq. (6). These active centres then react with the dye molecules to form an unstable species which is subsequently decomposed, and the surface defect is restored to its original form as depicted in Eq. (7). Some of the active centres might also undergo decay on recombining with electrons as depicted in Eq. (8) (Rauf and Ashraf 2009).

$$\text{Photocatalyst} + h\nu \rightarrow h^+ + e^- \text{(photogeneration of excitons)} \quad (5)$$

$$D + h^+ \rightarrow D^+ \quad (6)$$

$$D^+ + \text{dye} \rightarrow \text{Unstable Intermediate} \rightarrow \text{Product} + D \quad (7)$$

$$D^+ + e^- \rightarrow D \quad (8)$$

Although direct photocatalysis is thermodynamically feasible, the failure of the photocatalytic materials to carry out degradation efficiently under non-aqueous condition makes it questionable (Rothenberger et al. 1985). Indirect photocatalysis is another approach that explains the process of photocatalysis, in which the excitons formed do not directly react with the dye molecules. Instead, they react with the exciton trapping molecules adsorbed to the surface of the catalyst to form free radicals, which then react with the dye molecules. The primordial exciton trapping molecules are adsorbed water molecules, hydroxide ions and subsurface lattice oxygen (Rothenberger et al. 1985; Turchi and Ollis 1990). The holes react with water molecules to form hydroxyl radicals and hydronium ions as depicted in Eq. (9); the holes may also react with the surface-adsorbed hydroxide ions to form hydroxyl radicals as in Eq. (10). The excited electrons react with oxygen molecules and hydronium ions to form hydrogen peroxide which can further dissociate in the presence of oxygen to form hydroxyl ions as depicted in Eqs. (11) and (12) (Chang 2000).

In the case of TiO_2 photocatalysts, some electrons might also react with Ti^{IV} active centres to form Ti^{III} active centres as in Eq. (13) (Rothenberger et al. 1985). Other reactive radicals such as $HO_2^{\cdot}$and HO_2^- are also formed, but the hydroxyl ions are the primordial reactive species in the case of indirect photocatalysis (Turchi and Ollis 1990). These reactive species oxidize the dye molecules to form an unstable intermediate, which finally disintegrates into smaller, less harmful molecules as depicted in Eq. (14). The different reactions involved in indirect photocatalysis can be depicted as follows:

$$\text{Photocatalyst} + h\nu \rightarrow h^+ + e^- \quad \text{(Photogeneration of excitons)}$$

$$h^+ + H_2O \rightarrow HO^{\cdot} + H^+ \quad (9)$$

$$HO^- + h^+ \rightarrow HO^{\cdot} \quad (10)$$

$$O_2 + 2e^- + 2H^+ \rightarrow H_2O_2 \quad (11)$$

$$H_2O_2 \rightarrow 2HO^{\cdot} \quad (12)$$

$$Ti^{IV} + e^- \rightarrow Ti^{III} \quad (13)$$

$$HO^{\cdot} + \text{Dye} \rightarrow \text{Unstable intermediate} \rightarrow CO_2 + H_2O \quad (14)$$

There are four mechanisms by which the hydroxyl ions are assumed to react with the dye molecules (Turchi and Ollis 1990). According to the first mechanism, the hydroxyl ion and the dye molecule are speculated to react with each other, whilst both adsorb onto the catalyst's surface. The second mechanism states that the reacting dye molecule remains adsorbed to the photocatalyst's surface, whereas the hydroxyl ion remains in a free state before their reaction. According to the third mechanism, the reacting hydroxyl molecule remains bound to the surface, whereas the reacting dye molecules exist in a free state in the solution during the reaction. According to the fourth mechanism, both the dye and the hydroxyl ions react, whilst they are in an unbound state. The rate equation in all the four cases takes a form which is very similar to the Langmuir–Hinshelwood rate equation (Rothenberger et al. 1985). According to the second and the fourth mechanism, the hydroxyl ions are said to be capable of existing in a free state in the reaction mixture for some time until it reacts with a molecule. Whilst in free state, the hydroxyl ion can travel across a very limited distance in the reaction mixture before it ends up reacting with a substrate (S). The theoretical distance travelled by the hydroxyl ion before they end up reacting with a substrate can be estimated using the equation $\Phi' = K_{OH}\,[S]/(D/L^2)$, where L stands for the average distance travelled by the hydroxyl ion until it reacts, $[S]$ denotes the concentration of the substrate in the reaction mixture, Φ' denotes the reaction–diffusion modulus, K_{OH} stands for the reaction rate constant and D denotes the diffusion coefficient (Turchi and Ollis 1990). Dye degradation by free hydroxyl ions is only efficient in case of slurries which offers very low interparticle distance. However, in the case of immobilized photocatalysts, the interparticle distance is high which makes dye degradation using free hydroxyl ions inefficient (Hasnat et al. 2005; Turchi and Ollis 1990). A combined indirect–direct pathway in which both direct and indirect photocatalysis takes place simultaneously has also been proposed by many researchers to explain the mechanism of photocatalysis (Rome'as et al. 1999). Some recent works wherein the photocatalytic degradation of dyes has been modelled using the Langmuir–Hinshelwood model and Eley–Rideal model are grouped in Table 5.

Table 5 Studies reporting an acceptable fit of the Langmuir–Hinshelwood and Eley–Rideal models to the kinetics of photocatalytic degradation of dyes

Dye(s)	Photocatalyst	Kinetic model	Kinetic parameters	Observation(s)/inference(s)	References
Methyl orange and Congo red degrading under visible light irradiation	2%Al–2%Ni–ZnO nanostructure (had the highest catalytic activity)	Langmuir–Hinshelwood	Highest degradation rate constant obtained for photocatalyst (0.014 min^{-1})	100% removal of methyl orange within 30 min; trapping experiments unveiled that $O_2^{\cdot-}$ had a significant role in the catalytic degradation of methyl orange and Congo red	Reddy et al. (2020)
Methylene blue	Y-doped $BiFeO_3$ (in the presence of κ-carrageenan)	Langmuir–Hinshelwood	Rate constant = 0.0170 min^{-1} for an $R^2 = 0.979$	Removal efficiency of 97.6 ± 0.1% at 180 min with 1% Y–$BiFeO_3$ Optimum catalyst dosage for 99% degradation = 0.1 g of 1% Y-doped $BiFeO_3$	Abdul Satar et al. (2019)
Reactive Red 43	Samarium-doped ZnS NPs	Langmuir–Hinshelwood	2°-order kinetic rate constant = 0.1303 (mg L^{-1} min^{-1}) Adsorption equilibrium constant = 1.024 (mg L^{-1})$^{-1}$	$Sm_{0.04}Zn_{0.96}S$ brought about 95.1% decolourization after 120 min of treatment 4% Sm-doped ZnS NPs had the most decolourization Scavengers, namely chloride, carbonate, butanol and isopropyl alcohol decreased efficiency of decolourization	Hanifehpour et al. (2016)
Amaranth and methylene blue	N-doped ZnO visible light active	Langmuir–Hinshelwood	Adsorption coefficients: 0.14 L mg^{-1} for methylene blue and 0.10 L mg^{-1} for amaranth, both under visible light	After sixth run, catalyst retained appreciable photocatalytic activity (this being indicative of its favourable stability and absence of modification of surface structure)	Sudrajat and Babel (2017)
Acid Red 1	Sm-doped CdS NPs	Langmuir–Hinshelwood	Apparent rate constant of pseudo-first-order model = 0.0163 min^{-1}	Activated complex theory of Eyring revealed that photocatalysis was endothermic and non-spontaneous for the range 25–45 °C	Khosroshahi and Mehrizad (2019)

Table 5 (continued)

Dye(s)	Photocatalyst	Kinetic model	Kinetic parameters	Observation(s)/inference(s)	References
Rhodamine B (under visible light irradiation)	Co_3O_4 and Ag–Co_3O_4 composites	Eley–Rideal	Apparent rate constant = 0.0140 min^{-1} at 313 K Activation energy = 19.9 kJ mol^{-1} (based on corresponding Arrhenius plot)	Deposition of silver on Co_3O_4 greatly enhanced photocatalytic activity of Co_3O_4 About 100% photodegradation of 40 ml rhodamine B solution obtained at 313 K in 90 min with 50 mg Ag–Co_3O_4 photocatalyst (for 100 mg L^{-1} initial dye concentration)	Saeed et al. (2018)

Parameter-dependent efficiency of photocatalysts

The efficiency of photocatalyst refers to the rate at which the photocatalyst can mineralize the dye molecules under specific environmental conditions. The efficiency of photocatalysts is modulated by a variety of factors which can be both external and internal. Internal factor refers to parameters such as the physical structure and composition of the photocatalyst. External factors (as exemplified in Table 6) refer to the parameters such as temperature, pH, the concentration of the photocatalyst, irradiation intensity, reaction temperature and the presence of additives and impurities in the reaction mixture (Alaoui et al. 2009; Chung and Chen 2009; Hanifehpour et al. 2016; Nasirian et al. 2017; Bakhtkhosh and Mehrizad 2017; Saeed et al. 2018; Malini and Allen Gnana Raj 2018; Han et al. 2018; Khosroshahi and Mehrizad 2019; Abdul Satar et al. 2019).

Effect of pH

The pH of a reaction mixture can alter the rate of reaction in variegated ways. Changes in the pH of the reaction mixture can lead to the alteration of the surface properties of the photocatalyst. The pH at which the catalyst's surface is neutrally charged is called zero points of catalyst (pH_{zpc}) (Souza et al. 2016). In case of amphoteric photocatalysts, under acidic condition ($pH < pH_{zpc}$) the surface reacts with the excess hydronium ions present in the solution, causing it to be protonated, and thus, it acquires a positive charge. Whereas, under alkaline conditions ($pH > pH_{zpc}$) the surface gets deprotonated on reacting with the excess hydroxide ions, making the surface negatively charged. For instance, in the case of titania, the following reactions take place under different pH conditions (Jawad et al. 2016):

$$TiOH + H^+ \rightarrow TiOH_2^+ \quad \text{(Under acidic condition)}$$

$$TiOH + OH^- \rightarrow TiO^- + H_2O \quad \text{(Under basic condition)}$$

These changes in surface charge can greatly influence the adsorption of the dye onto the surface of the photocatalyst. When the surface is positively charged under acidic conditions, negatively charged anionic dyes are attracted towards it, and as a result, they get more easily adsorbed. Similarly, under basic pH, the efficacy of adsorption of cationic dyes is much higher (Bubacz et al. 2010). This increase in adsorption leads to a higher rate of dye degradation which is evident. For instance, in 2010, Bubacz and co-workers stated that the efficiency of TiO_2-mediated degradation of anionic dye methylene blue increases with an increase in pH of the solution (Bubacz et al. 2010). In an experiment carried out by Kazeminezhad and Sadollahkhani, the photocatalysis rate was compared for cationic dye methylene blue, anionic dyes bromocresol green and Rose Bengal

Table 6 Parameters analysed for their effects on the degradation dynamics of dyes under the action of doped photocatalysts

Photocatalyst	Dye	Influencing parameter(s) investigated	References
Er^{3+}:$YAlO_3$/Fe- and Co-doped TiO_2-coated composites	Azo fuchsine	Time for solar light irradiation, photocatalyst amount, initial concentration of dye, kind of organic dyes	Xu et al. (2010)
C-doped TiO_2	Rhodamine B	Amounts of carbon-doped TiO_2, initial concentration of rhodamine B	Cinelli et al. (2017)
C–N-co-doped TiO_2 nanotube arrays	Methyl orange	pH, bias potential	Chen et al. (2015)
Functionalized ZnS quantum dots and Fe_3O_4 magnetic nanoparticles	Victoria blue R	pH, initial dye concentration, contact time, catalyst dosage	Rajabi et al. (2016)
N–TiO_2/$ZnFe_2O_4$-2	Rhodamine B	Catalyst loading, type of dyes, catalyst stability	Yao et al. (2015)
Pd-doped TiO_2	Methylene blue and methyl orange	pH, catalyst dose, initial dye concentration	Nguyen et al. (2018)
Mn-doped ZnO	Orange G	pH	Barzgari et al. (2016)
Ni-doped, Cr-doped and Mo-doped TiO_2	Methylene blue	pH	Chaudhari et al. (2018)
Ce-, La- and Ho-doped ZnO nanoparticles	Reactive Orange 29	Doping source, pH, sonication temperature and time, mass ratio of doping source to the precursor of ZnO synthesis, calcination temperature and time, pH of solution, light intensity, dosage of catalyst, initial concentrations of inorganic salts	Sheydaei et al. (2019)
Cu-doped ZnO	Direct Blue 71	pH, irradiation time duration, dosage of photocatalyst, initial dye concentration	Thennarasu and Sivasamy (2016)
ZnS and Cd-doped ZnS nanoparticles	Alizarin red S	Photocatalyst concentration, pH, dye concentration	Jabeen et al. (2017)
Bi-doped and Bi–N-co-doped TiO_2 nanocomposites	Acid Red 85	pH of solution, dopant stoichiometry, amount of catalyst, electron acceptors, illumination time and light intensity, dye concentration	Thejaswini et al. (2016)
NiO–ZnO-doped onto nanozeoliteX	Methyl orange and Eriochrome Black T	NiO–ZnO ratio, initial dye concentration, pH, photocatalyst dosage	Karimi-Shamsabadi et al. (2017)
Co- and S-co-doped nano-size TiO_2	Crystal violet, malachite green, Procion Blue MXR, Alizarin Red S	Dye concentration, catalyst dose, pH, dopant contents	Siddiqa et al. (2015)
Ni-doped $ZnFe_2O_4$ nanomaterials	Methylene blue	Catalyst dosage, initial pH	Padmapriya et al. (2016)
Ag_3PO_4/AgBr/Ag-decorated HKUST-1 MOF composite	Auramine-O, methylene blue and erythrosine	Initial dye concentrations, dosage of photocatalyst, flow rate of solution, aeration rate, rotational speed, duration of illumination	Mosleh et al. (2017)
TiO_2 powder in a Pickering emulsion system	Brilliant red X_3B, Congo red, methyl orange, orange G	Preparation parameters: concentration, solid phase/oil phase/water ratio; irradiation time	Li et al. (2019)
Cu-doped TiO_2 NPs	Methylene blue and methyl orange	pH	Nguyen Thi Thu et al. (2016)
Fe-doped TiO_2/rGO	Rhodamine B	pH, catalyst dosage and initial dye concentration	Isari et al. (2018)
N-doped ZrO_2	Amaranth and methylene blue	Dye concentration, catalyst dose, pH, salinity	Sudrajat et al. (2016)
Mn-doped ZnO NPs	Methylene blue	Amount of catalyst, initial pH, initial dye concentration	Anju Chanu et al. (2019)

Table 6 (continued)

Photocatalyst	Dye	Influencing parameter(s) investigated	References
Salicylic acid-surface-modified TiO_2 in a Pickering emulsion-based photocatalytic reaction system	Direct Red 80	Oil–water ratio, pH, temperature, stirring	Nawaz et al. (2017)
WO_3-doped ZnO NPs	Direct Blue 15	Dopant percentage, suspension pH, catalyst concentration, initial dye concentration, light intensity, contact time	Ebrahimi et al. (2019)
Co-doped ZnO	Remazol BB	Initial dye concentration, pH, photocatalyst mass, H_2O_2 concentration	Tanji et al. (2019)
Cr-doped TiO_2	Methylene blue	Sample loading, dopant concentration and irradiation time	Koh et al. (2019)
Ag_2O@Ag-modified $BiVO_4$ composites	Rhodamine B, methylene blue	Initial dye concentration, calcination temperature, initial pH and mineralization ability	Yang et al. (2016)
Silver-doped ZnO thin films	Reactive Red 195, Reactive Yellow 145 and Reactive Orange 122	Catalyst dose, dye concentrations, H_2O_2 addition	Abdelsamad et al. (2018)
Copper-doped TiO_2–Bi_2O_3 nanocomposite	Methyl orange	Amount of catalyst, dye concentration and initial pH of solution (modelling and optimization of influence of factors performed using central composite design based on RSM	Barahimi et al. (2019)
Platinum-decorated cupric oxide–silicon dioxide	Acridine Orange dye	Photocatalyst dose, platinum doping	Gadah and Basaleh (2020)
Ti^{3+}-doped In_2O_3 nanocubes	Methylene blue	Dopant concentration, UV irradiation duration,	Shanmugapriya et al. (2020)
Sm^{3+}/Er^{3+}-co-doped TiO_2 mesoporous monolithic network	Acid Blue 113	pH of solution, stoichiometry of dopant/co-dopant, amount (dosage) of photocatalyst, intensity of light, dye concentration, effect of photooxidizers	Sompalli et al. (2020)

(Kazeminezhad and Sadollahkhani 2016). The anionic dye Rose Bengal in the latter study underwent better adsorption and degradation at pH 4 and pH 8 in comparison to those observed at pH 11. Similarly, for cationic dye methylene blue, the optimum pH for adsorption was found to be in the basic range. Being an anionic dye, bromocresol green was expected to have an optimum pH in the acidic range. However, it was found to be in the basic range between pH 8–11. This could not be explained using the previously mentioned theory.

Under acidic conditions, the concentration of H^+ ions is higher compared to hydroxide ions. Most of the photogenerated electrons are adsorbed by the H^+ ions, and the number of hydroxyl ions formed is very low due to the scarcity of hydroxide ions. Hence, positive holes are the dominant oxidizing species at low pH. Since the movement of the holes is limited to the lattice of the photocatalyst, a low pH might limit the rate of photodegradation. At a higher pH, the number of hydroxide radicals available for the formation of hydroxyl radicals is higher which provides a positive impact on the rate of photocatalysis. This might be an explanation to the previously stated anomaly with bromocresol green. Ahirwar and co-workers studied the degradation of indigo carmine by mesoporous TiO_2 (Ahirwar et al. 2016). Indigo carmine has a positively charged penta-heterocyclic-N group. Hence, in the latter study, it was expected to have an optimum pH for degradation in the basic range. However, it was observed that the reaction was favoured at a lower pH (4), and with an increase in pH (4–11), the reaction rate fell quite considerably, and this was explained by the fact that the rate of adsorption of the dye molecules was so high that it prevented the photons from reaching the catalyst's surface, as a result of which excitons were not produced and photocatalysis did not take place.

The variation in the rate of photocatalysis with alteration in pH is dependent on the type of material being used as the photocatalyst and on the chemical properties of the dye being degraded. The behaviour of a chemical dye under a specific pH can also modulate the efficacy of degradation. Some dyes tend to form intramolecular hydrogen bonds at high pH, which greatly stabilizes their structure leading to a decrease in photocatalysis (Reza et al. 2017). Studies suggest that at acidic pH, the degradation of azo dye Amaranth is greatly reduced, and this is because the excess H^+ ions react with the dye's chromophore, reducing the electron density at –N=N– bond, thus making it less susceptible to electrophilic attack by the radicals (Sudrajat and Babel 2017). Industrial effluents from different industries are released at different pHs. However, if the type of dye present in the effluent is known, then the pH of the effluent can be adjusted to the optimum value based on the data obtained from prior investigations. This method can greatly enhance the efficiency of effluent treatment.

Dosage of photocatalyst

The rate of dye degradation is greatly influenced by the concentration of the photocatalyst being used in the reaction mixture. A higher concentration of photocatalysts provides a greater surface area for the degradation reaction to take place, as a result of which a higher amount of excitons are produced to participate in the reaction (Reza et al. 2017). This greatly increases the rate of photocatalysis. The change in the rate of the photocatalysis with the change in the concentration of the photocatalyst TiO_2 was explained using a power-law model by Hamad et al., assuming that it follows first-order kinetics, in the form of the following equation $\ln K_{app} = \ln K + n \ln [TiO_2]$, where K_{app} is the apparent rate constant, K is the true rate constant, n is an exponent and $[TiO_2]$ refers to the concentration of the photocatalysts in the reaction mixture. A plot of $\ln K_{app}$ versus $\ln [TiO_2]$ will represent a straight line with slope n (Hamad et al. 2016). The increase in efficiency of photocatalysis to increase in photocatalyst concentration is only evident up to a certain threshold value. A very high concentration abates the efficacy of the reaction by increasing the turbidity of the reaction mixture which, in turn, decreases the penetrability and distribution of light required for excitation of the photocatalysts through scattering (Reza et al. 2017). A high concentration of photocatalyst also tends to increase the chance of intraparticle interaction which can cause agglomeration of the catalysts, which in turn reduces the surface area available for the reaction. The decrease in photocatalysis at high photocatalyst concentration might also be because at higher concentration the excited photocatalysts gets deactivated on colliding with a photocatalyst that is at ground state (Hamad et al. 2016). It can be depicted through the equation $TiO_2^* + TiO_2 \rightarrow TiO_2^{\#} + TiO_2$. Here, TiO_2^* and $TiO_2^{\#}$ represent the activated and the deactivated form of the catalyst, respectively. Thus, by knowing the optimal concentration of photocatalyst from the previous researches one can find out the amount of photocatalyst that should be added to a certain volume of effluent to optimize the rate of degradation.

Concentration of dye

Sudrajat and Babel studied the effect of dye concentration on the rate of photocatalysis using Amaranth and methylene blue over N-doped ZnO photocatalysts (Sudrajat and Babel 2017). In the work, it was observed that with an increase in Amaranth concentration from 5 to 25 mg L^{-1} the degradation efficiency fell from 91.3 to 70.1%. Similarly, with an increase in MB concentration from 5 to

25 mg L^{-1} the degradation efficiency dropped from 93.2 to 64.1%. This is because at higher concentration the dye molecules adsorbed on the surface of the photocatalyst are so high that they inhibit the light photons required for photoexcitation from reaching the photocatalyst's surface. Hamad and co-workers studied the rate of degradation of dichlorophenolindophenol using mesoporous TiO_2 (Hamad et al. 2016). It was noted that with an increase in dye concentration, the rate of reaction initially increased linearly up to a certain value and it then decreased with further increase in the concentration of the dye. This can be elucidated by the fact that the amount of photocatalyst is constant and with an increase in dye concentration the amount of dye getting adsorbed to the surface increases which leads to a higher rate of degradation. However, this increase is maintained only up to a certain value as long as enough free photocatalytic surface area and illumination is available to degrade the dye. When the dye concentration surpassed this value, the adsorbed dye molecules on the catalyst's surface become so high that they start to prevent the photons from reaching the catalyst's surface, which in turn inhibits the production of excitons required for photocatalysis. Furthermore, with the increase in dye concentration, there is a competitive effect imposed by the dye molecules on the adsorption of OH^- and O_2 onto the surface; as a result, the formation of O_2^- and $^{\cdot}OH$ radicals is greatly suppressed (Sudrajat and Babel 2017). The degree of surface coverage (θ) by the dye can be given as a function of the dye concentration (C) in the solution by the equation $\theta = KC/(1 + KC)$, where K is a constant (Zhou et al. 2018). Furthermore, a high concentration of dyes makes the solution intensely coloured, which in turn decreases the path length of the light, thus preventing it from reaching the photocatalyst (Ahirwar et al. 2016). Photocatalysis causes the dye molecules to be mineralized into inorganic ions such as sulphates and phosphates. With the increase in dye concentration, these inorganic ions formed as a result of which degradation also increases. These inorganic ions then compete with the dye molecules for the oxidizing radicals, which reduces the number of the oxidizing radicals available for dye degradation. This greatly reduces the rate of photocatalysis. This is an alternate approach to explain the decrease in efficiency of photocatalysis with an increase in the concentration of inorganic dyes (Jia et al. 2016).

Influence of additives and impurities

Effluents are filled with many types of ions and molecules which greatly modulate the rate of dye degradation (Senthilraja et al. 2016). Ions such as Fe^{2+}, Ca^{2+}, Mg^{2+}, Al^{3+}, Na^+, K^+, NH_4^+, Cl^-, PO_4^{3-}, SO_4^{2-}, HCO_3^- and NO_3^- are generally present in wastewater (Alahiane et al. 2014; Azzaz et al. 2018; Isari et al. 2018). Many of these are $HO^{\cdot}$ and electron scavenging in nature, i.e. they readily react with the hydroxyl radicals, which greatly reduces the amount of $HO^{\cdot}$ available to react with the dye molecules. As a result, the rate of the reaction is greatly attenuated. Alahiane and co-workers studied the effect of various inorganic ions on the rate of TiO_2 mediated photocatalysis of Reactive Yellow 145 (Alahiane et al. 2014). Thereafter, it was observed that the presence of SO_4^{2-} and Cl^- ions can enhance the rate of photodegradation. SO_4^{2-} and Cl^- react with the hydroxyl radicals to form strong oxidizing intermediates $Cl^{\cdot}$ and $SO_4^{\cdot-}$ which can readily degrade the dye molecules. HCO_3^- and HPO_4^{2-} are competitively adsorbed onto the active centres present on the surface which prevents the dye molecules from getting adsorbed. Furthermore, they act as hydroxyl scavengers which greatly attenuates the process. CH_3COO^- ions react with the holes to form methyl radicals and carbon dioxide. Thus, reducing the numbers of holes available to produce hydroxyl radicals. Sudrajat and Babel studied the influence of sodium chloride salts in the degradation of Amaranth dye (Sudrajat and Babel 2017). It was observed that with an increase in NaCl concentration from 0.3 to 1.2 g L^{-1}, the degradation efficiency increased from 90.9 to 93.1%. However, a further increase to 9.6 g L^{-1} caused the degradation efficiency to fall. In the latter study, the initial increase in efficiency was attributed to the fact that the Cl^- ions reacted with the photocatalyst to form $Cl^{\cdot}$ ions which have an oxidation potential (2.47 V) and can easily degrade the dye molecules. Furthermore, the Cl^- ions react with the holes, thus preventing it from recombining with the electrons. However, with further increasing the Cl^- molecules start competing with the dye molecules for reacting with the catalyst's surface which greatly reduces the rate of the reaction. Studies also suggest that the carbonate radicals ($CO_3^{\cdot-}$) formed as a result of the reaction between carbonate ions and hydroxyl ions, have a high oxidizing potential and can degrade a wide range of molecules (Ye et al. 2018). Besides, they are more stable and mobile compared to the hydroxyl radicals which gives them the ability to react with the dye molecules present in the bulk of the solution (Ye et al. 2018). Furthermore, they can also act as quenchers and help in charge separation, thus preventing recombination (Ye et al. 2018). Similarly, bicarbonate ions in low concentration have also been depicted to enhance the rate of photocatalysis (Dalhatou et al. 2015).

Oxidizing agents are often added to the reaction mixture to increase the photocatalytic activity. Khataee and co-workers reported that with increasing the concentration of H_2O_2 in the reaction mixture a higher number of free radicals are produced which boosts up the process of dye degradation (Khataee et al. 2016). However, beyond a certain concentration, the H_2O_2 molecules start acting as hydroxyl radical

scavengers which greatly reduces the rate of the reaction (Khataee et al. 2016). Also, at a high concentration, the H_2O_2 gets adsorbed onto the surface of the photocatalyst, thus blocking the sites for the reaction to take place (Alahiane et al. 2014). The presence of natural organic matters (NOMs) can also interfere with the rate of reaction. This can be attributed to the fact that NOMs compete with the dye molecules for the active site (Ye et al. 2018). Furthermore, they can also absorb the light being supplied for the catalysis reaction to take place (Ye et al. 2018). Both of these factors can attenuate the rate of photocatalysis.

Effect of temperature and irradiation intensity

Hu and co-workers studied the role of temperature on TiO_2-mediated degradation of methyl orange (Hu et al. 2010). Sixfold increase in the value of the rate constant from 3.52×10^{-4} to 2.17×10^{-3} min^{-1} was observed on increasing the reaction temperature from 38 to 100 °C. Karimi and co-workers studied the photocatalytic degradation of azo dyes using nano strontium titanate (Karimi et al. 2014). On increasing the temperature from 30 to 50 °C, a gradual increase in the rate of photocatalysis was observed. This can be attributed to the fact that on increasing the temperature the production of photoexcitons and the rate of oxidation increase. Priyanka and Srivastava (2013) studied the effect of increasing temperature on iron-doped ZnO-mediated photodegradation of azophloxine dye for the range 30 to 60 °C, and it was reported that with the increase in temperature up to 50 °C the efficiency of photocatalysis increased (Priyanka and Srivastava 2013). However, at 60 °C, the efficiency of the reaction was found to be lower. This was due to the self-scavenging effect of the hydroxyl radicals at high temperature.

The role of irradiation intensity on the rate of photocatalysis of various organic compounds was initially studied by Ollis et al. (1991) who reported that at lower irradiation intensity the rate of the reaction follows the first-order kinetics, and there exists a linear relationship between the irradiation intensity and photocatalytic activity. On further increasing the irradiation intensity beyond a certain value, the rate of photocatalysis becomes dependent on the square root of irradiation intensity. However, at a very high irradiation intensity, the rate of the reaction becomes constant as all the active sites become saturated, and no more exposed active sites remain available for the exploiting the extra energy. Similar results were reported by Wu and co-workers whilst studying the degradation of HF6 coral pink in a photocatalytic slurry reactor using TiO_2 (Wu et al. 2006). An increase in photocatalytic activity was obtained by increasing the intensity up to 64 W, beyond which no further changes were noticed.

Reusability of photocatalysts

One of the major challenges is to overcome the difficulties by which the photocatalysts can be recovered from the reaction mixture for further reuse (Li et al. 2018) (Table 7). The small size of the photocatalytic NPs makes it difficult to separate them from the reaction mixture. Hence, in view to overcome the latter shortcoming, the photocatalyst is often immobilized onto various materials having a significant size. Immobilization of photocatalysts also addressed the process engineering issues related to photocatalytic particle washout (Zhu et al. 2018; Goutham et al. 2019), especially in continuous-flow systems and aggregation of the particles observed particularly at high concentrations (Dong et al. 2015; Shet and Vidya 2016; Vaiano et al. 2017a; Argurio et al. 2018). This makes it easier to separate the photocatalysts from the reaction mixture for reuse. The different substances used for immobilizing photocatalysts are, for example, pumice (Shao et al. 2019), stainless steel wire-mesh (Chang et al. 2019), glass (Pickering et al. 2017; Xing et al. 2018; Pirinejad et al. 2019), cellulose acetate film (Boruah et al. 2019), cellulosic fibres (Jouali et al. 2019), polyethersulfone matrix (Hir et al. 2017), activated charcoal, zeolite, polymers, cement and clay (Hofstadler et al. 1994; Ao and Lee 2005; Mohamed and Mohamed 2008; Meng et al. 2008; Jafari et al. 2016; Pan et al. 2019) (Table 8). The physiochemical properties of the support being used play a major role in modulating the rate of photocatalysis, and they are (Pozzo et al. 1997): high porosity, low manufacturing cost, high stability, non-toxicity, high transparency, chemical inertness, strong surface binding with the photocatalyst and separability. In a comprehensive review, Srikanth et al. (2017) have concluded that ease of availability, high durability, chemical inertness, low density and mechanical stability are principal factors which have to be considered when selecting appropriate supports for photocatalysts. The use of activated charcoal offers a very high porosity which makes it possible to adsorb a high amount of dyes and provides a large surface area for the reaction to take place (de Brites-Nóbrega et al. 2013). Similarly, glass is used to overcome the problem with low permeability of light as in most of the supports used. This is because glass being transparent facilitates uniform illumination (Pozzo et al. 1997). One of the major drawbacks of this method of immobilization is that the catalyst-carrying carriers get settled down at the bottom which greatly reduces the active surface for the reaction. To overcome this, the carriers should be uniformly suspended in the solution, and accomplishing this can be quite resource-consuming.

In recent years, the use of a photocatalytic membrane made by fabricating photocatalysts onto a membrane matrix using the phase inversion technique has shown to be quite promising in overcoming the problem of reusability (Li et al. 2018). The advantage of using this technique is that it

Table 7 Reusability performances of selected photocatalysts for the photocatalytic degradation of dyes

Dye	Photocatalyst	Reusability performance	References
Methylene Blue	Fabricated Carbon nanotubes/TiO_2/Ag NPs-doped/surfactant C10 nanocomposites	Reusability performance of photocatalyst was tested by reusing it for five consecutive cycles Efficiency decreased from 100 to 92% after the first three cycles. At the end of the fifth cycle, photocatalytic activity declined to 77%	Azzam et al. (2019)
Reactive Red 43	Sm-doped ZnS NPs	Reusability of photocatalyst $Sm_{0.04}Zn_{0.96}S$ was tested by subject it to ten cycles of reuse; up to five cycles of reuse, its efficiency was maintained above 80%; however, by the end of the tenth cycle, it fell to around 75%	Hanifehpour et al. (2016)
Rhodamine B	Fe-doped TiO_2 incorporated onto reduced graphene oxide	After five cycles of reuse, there were about 12% decrease in efficiency of dye removal and no significant modification in structure of photocatalyst	Isari et al. (2018)
Rhodamine B	CeO_2/Y_2O_3 nanocomposites	After three consecutive cycles of reuse, only 5% decrease in the photocatalytic efficiency recorded	Magdalane et al. (2017)
Naphthol Blue Black	Gd, N and S-tridoped TiO_2 embedded on multiwalled carbon nanotubes	After five cycles of reuse, 91.8% photocatalytic efficiency was reported	Mamba et al. (2015)
Methylene Blue	N-doped reduced graphene oxide/$CoWO_4/Fe_2O_3$ ternary nanocomposite	2.5% of loss in activity was reported after five successive cycles of reuse	Mohamed et al. (2018)
Congo red and methyl red	Sulphated TiO_2/WO_3 nanocomposites	Photocatalyst was subjected to five cycles of dye degradation; a degradation efficiency greater than 90% was observed for both dyes	Patil et al. (2019)
Methyl Orange	Al,Ni-co-doped ZnO nanostructures	Negligible drop in performance was reported after reusing it for five times	Reddy et al. (2020)
Acid Red 18	Sn-loaded Au–ZnO	Catalyst was subjected to four successive cycles of reuse; at the end of the fourth cycle, an efficiency of 91.3% was reported	Senthilraja et al. (2016)
Congo red	Polyaniline/Fe^0-doped bismuth oxychloride	About 9% decrease in the photocatalytic activity was reported after three cycles of reuse	Tanwar et al. (2017)
Acid Red 85	Bi-doped and B-N-co-doped TiO_2	Reusability studies were carried out for a total of four cycles; complete degradation of dye was reported during the first two cycles, and during the last two cycles, a degradation efficiency of 97.5% was achieved	Thejaswini et al. (2016)
Methylene blue and methyl orange mixed dye	Ag–CeO_2	Photocatalyst was reused up to five successive cycles; at the end of the fifth cycle, a degradation rate of 88.94% and 85.62% was reported at 664 nm and 463 nm, respectively	Ayodhya and Veerabhadram (2020)
Methylene Blue	Undoped and Y-doped $BiFeO_3$	Reusability performance of the doped and undoped photocatalyst was tested by reusing them for five consecutive cycles; the removal efficiencies of the nanomaterials prepared were maintained above 90% up to four consecutive cycles; however, it decreased to about 60% during the fifth cycle	Abdul Satar et al. (2019)

Table 7 (continued)

Dye	Photocatalyst	Reusability performance	References
Brilliant smart green	N-doped ZnO/graphene oxide (NZGO-1)	NZGO-1 gave a 100% degradation and 80% mineralization of Brilliant smart green within 90 min of irradiation After three cycles of reuse, the photocatalytic efficiency was 94%	Peter et al. (2019)

combines the process of filtration and photocatalysis into a single unit (Li et al. 2018). It also reduces the rate of electron–hole recombination which then greatly increases the efficacy of the reaction (Juntrapirom et al. 2017). The most commonly used supporting membrane matrices are apparently polyvinylidene fluoride, polysulfone and cellulose acetate (Wang et al. 2017; Melvin Ng et al. 2017; Kuvarega et al. 2018; Li et al. 2018). The major limitation of this technique is that with usage time the reacting surface of the supporting matrix gets clogged due to the accumulation of products, thus decreasing the efficiency of the processes (Mozia 2010). In an attempt to overcome this limitation, various photocatalysts are being developed so that they can be easily separated from the reaction mixture just by applying an external magnetic field. According to Sreelekha et al. (2016), a photocatalyst having good magnetic properties at the nanoscale enables for the possibility to have magnetic separation of the used photocatalyst particles, which happens to be a relatively very simple and efficient strategy to remove suspended solids from aqueous solutions or effluents with no need for further separation. For example, Mohanta et al. (2013) evaluated the photocatalytic performance of magnetic $SrFe_{12}O_{19}$ and $SrFe_{11.4}Al_{0.6}O_{19}$ under visible light and sunlight for the degradation of Congo red and reported that appreciably magnetization values of around ~ 52 emu/g at 300 K had been obtained, and this magnetic property of the photocatalyst was helpful for its separation from the reaction cell when a low strength magnetic field was applied after the reaction. Later, Sreelekha et al. (2016) have prepared virgin and co-doped covellite copper (II) sulphide NPs (to be thereafter assessed for the sunlight photocatalytic degradation of rhodamine B) whereby the pristine CuS was found to be endowed with diamagnetic property and the co-doped NPs had increasing room-temperature ferromagnetism with higher doping precursor concentrations. Last but not least, Sanjeev Kumar et al. (2019) recently synthesized undoped and gadolinium-doped ZnS NPs to be assessed for their photocatalytic degradation capacity for methyl orange and methylene blue dyes and an industrial effluent and reported, *inter alia*, that room-temperature magnetic studies of gadolinium-doped ZnS NPs indicated that this material exhibited magnetic hysteresis.

Photocatalytic degradation in mixed-dye systems

Textile effluents have been reported to be recalcitrant with regard to their complete amenability for remediation by conventional biological and physico-chemical methods. Their refractory characteristic has been strongly associated with the various species (namely many types of dyes like acid, basic, dispersed, direct, reactive, sulphurous and azoic

Table 8 Studies revisiting the main properties of immobilization material used, the essentials of the immobilization approach, the dye(s) and photocatalyst used and observations made and inference(s) drawn in the respective study

Material used for immobilization	Immobilization approach	Dye and photocatalyst	Observations	Inference(s)	References
Graphene oxide-fabricated carbon electrodes	Graphene NPs deposited on carbon electrode using an electrochemical deposition approach for subsequent use as catalyst bed; TiO_2 NPs incorporated on bed by a thermal process	Acid Red 14 and TiO_2 NPs immobilized on graphene oxide catalyst bed	Acid Red 14 easily removed using graphene oxide–carbon electrode–TiO_2 composite in photocatalytic reaction under ultraviolet light irradiation	Stability tests demonstrated that the fabricated graphene oxide could enhance durability of immobilized TiO_2 NPs significantly	Akerdi et al. (2016)
Fused silica substrates	RF magnetron sputtering approach	Rhodamine 6G and $Ca_{1-x}Ln_xMnO_3$ (Ln = Sm, Ho; $0.1 \leq x \leq 0.4$) films over fused silica substrates	Pure characteristics perovskite phase for all fabricated films (with the exception of $Ca_{0.9}Ho_{0.1}MnO_3$) Decrease in crystallite size when amount of ion substituted was increased Some the fabricated $Ca_{1-x}Ho_xMnO_3$ and $Ca_{1-x}Sm_xMnO_3$ films gave higher photocatalytic activities for Rhodamine 6G degradation when compared to titania For same value of x, Ho-type films had higher photocatalytic activity	Ho-type films are more efficient photocatalysts than Sm-based ones under the visible light photodegradation of Rhodamine 6G Enhanced photocatalytic activity of Ho-type films attributed principally to larger structure distortion, smaller mean crystallite size and band gap energy	Barrocas et al. (2016)
Polyvinylidene fluoride (PVDF) pellets	Zinc sulphide NPs fabricated by low-temperature precipitation; zinc sulphide NPs incorporated onto pellets by phase inversion	Methylene blue and PVDF–zinc sulphide pellets	Zinc sulphide NPs had been compactly immobilized onto the surface of PVDF surface (were not being released) and had experienced no loss of photocatalytic activity Findings showed that PVDF matrix had no adverse influence on optical properties of zinc sulphide NPs By reason their large size (5 mm) and very good mechanical stability, PVDF–ZnS pellets had been easily dispersed in photocatalytic reactor	Removal efficiency of methylene blue with PVDF–zinc sulphide pellets (> 95%) was more than that obtained with the control PVDF pellets or zinc sulphide NPs examined	Guo et al. (2019)

Table 8 (continued)

Material used for immobilization	Immobilization approach	Dye and photocatalyst	Observations	Inference(s)	References
Polystyrene	Nitrogen-doped TiO_2 synthesized by sol–gel method; deposition of different amounts of nitrogen-doped TiO_2 particles onto polystyrene by solvent casting	Methylene blue and nitrogen-doped TiO_2 on polystyrene support	For N-doped TiO_2 amount augmented from 0.05 to 0.3 g: under visible light irradiation, 0.015 nitrogen-doped TiO_2/polystyrene, 0.05 nitrogen-doped TiO_2/polystyrene, 0.1 nitrogen-doped TiO_2/polystyrene, 0.2 nitrogen-doped TiO_2/polystyrene and 0.3 nitrogen-doped TiO_2/polystyrene catalysts gave significant photocatalytic activities with the decolourization efficiency of methylene blue reaching up to 77% for the 0.3 g nitrogen-doped TiO_2 (after 90-min irradiation)	Optimal amount of immobilized photocatalyst = 0.2 g for total visible light photocatalytic decolourization methylene blue solution after 180 min	Ata et al. (2017)
Immobilization in the form of thin films	Films fabricated by spray pyrolysis method	Methyl orange and pure WO_3 and Yb-doped WO_3 thin films	3 at% Yb:WO_3 film had good PEC response (1.72 times more than with pure WO_3 film) For greater doping percentage, photocurrent decreased because of more defects in film which act as recombination centres/sites to impede photocurrent generation 96% degradation of methyl orange in 320 min using 3 at% Yb:WO_3 photoelectrode	3 at% Yb:WO_3 photoelectrode produced higher degradation efficiency of methyl orange than pure WO_3 photoelectrode through photoelectrocatalytic degradation reaction	Mohite et al. (2017)

Table 8 (continued)

Material used for immobilization	Immobilization approach	Dye and photocatalyst	Observations	Inference(s)	References
Cotton fabrics	Silica–titanium sols prepared using sol–gel method; procedures for preparation of photocatalysts explained in Landi et al. (2017)	Rhodamine B and immobilized N-doped TiO_2nano-SiO_2–HY nanocomposites	TiO_2 nano, TiO_2nano-SiO_2 and TiO_2nano-SiO_2–0.25HY photocatalysts were differently dispersed on cotton fabrics With HY zeolite in nanocomposites, no change observed in decolourization of rhodamine B after 5 h of photocatalytic experiments; yet, degradation of N-de-ethylated intermediates was favoured (excluding situation when large quantity of zeolite was used in nanocomposites fabrication) Overall, photodegradation of rhodamine B-containing solutions with cotton fabrics functionalized with TiO_2nano-, TiO_2nano-SiO_2 and TiO_2nano-SiO_2–0.25HY led to the formation of degradation products not much more cytotoxic than that obtained from original rhodamine B solution Yet, 26% decolourization was observed in rhodamine B-containing solution consisting of pristine cotton fabric (plausibly because of OH groups present on cellulose fibres and by reason of oxygen trapped within fibres)	Fabrics coated with composite materials had lower concentration of N-de-ethylated intermediates those treated with cotton fabric coated by the TiO_2 only	Landi et al. (2019)

having intricate but specific molecular structures, oxidants such as hydrogen peroxide, surfactants, sulphate, different salts such as NaCl and Na_2CO_3, waxes and organic matter), and they may variably contain (Manenti et al. 2015; Chong et al. 2015; Gajera et al. 2015; Amaral et al. 2017). So, when taking into account the mutual influences and extents of competition amongst organic dyes and other organic and inorganic species which are present in real (textile) wastewater remediation systems, it becomes of significant relevance and importance to also investigate and understand thoroughly the different aspects of process dynamics of photocatalytic degradation of the mixed dyes. Amongst the several parameter influences existing within the reaction milieu and amidst the specific process parameter sensitivities which can be exerted on the different stages of the overall process of mixed-dye photocatalytic degradation, the adsorption of the individual-dye molecule from bulk of the mixture and the photocatalytic activity of the catalyst *vis-à-vis* the dyes are grow really complex. An analysis of the literature scoped for this review has indicated that relatively very few studies have studied the photocatalytic degradation of dyes in mixed-dye systems. Even fewer studies have investigated four-dye systems. Given the paucity of empirical data in this specific branch of mixed-dye photocatalytic degradation, the following discussions attempt to capture some recent assorted findings and very interesting features thereof in view to highlight the extent of complexity and possibilities associated with such mixed-dye systems.

In comparison with single-dye systems whereby a very wide variety and number of dyes have been analysed, mixed-dye systems have been much less studied under the photocatalysis research banner and appear much to have used mostly different combinations of rhodamine B, methyl orange and methylene blue as the test dyes. As Tomei et al. (2016) have rightly argued, a large portion of the research investigations on the decolourization of textile wastewaters have been carried out on synthetic solutions of single dyes, and such individual-dye systems may barely be representative of the real situation. In another work, Rodrigues et al. (2020) fabricated silver- and palladium-impregnated ZnO-based catalysts to be examined for the photocatalytic degradation of Reactive Blue 19 and Reactive Blue 21 found in textile wastewaters using an annular low-power ultraviolet photoreactor. In Rodrigues et al. (2020), besides examining the photocatalytic degradation reactions, the concentration profiles developed in the photocatalytic reactor were mathematically modelled using the mass balance conservation law, and it was found that the best photocatalytic degradation of dyes predicted by the model could be achieved when using lower initial dye concentration, smaller catalyst size, and higher length/diameter of the reactor. Some interesting notes made by Rodrigues et al. (2020) were that their analysis demonstrated that many catalysts assessed for the photodegradation of pure dyes do not function as expected in real wastewaters, and most studies reported in the literature have probed the photodegradation of pure dyes using high-power radiation for obtaining high degradation rates. Whilst it might arguably be feasible to 'mimic' effectively the range and composition of textile effluents to some extent, dyes having similar spectra can be expected to respond in a different way during treatment. The latter complex behaviour is indeed both a real limitation and challenge when it comes to assessing potent dye-removing materials because certain limitations on performance may then be observed already in the toned-down mixed-dye system under examination. In the end, the inherent complexity of real dye-laden effluents and the search for highly effective dye-removing schemes with debatably representative (or rather, debatably non-representative) synthetic dye solutions impede the applicability and scalability of the garnered investigational data to the formulation of real effluent remediation routes, which otherwise commonly contain several competing chemical species.

The following sections revisit studies which have dealt with the photocatalytic degradation of dyes in mixed-dye systems. A few years back, Huo et al. (2014) have reported that the degradation yields for both rhodamine B and methylene blue had decreased when during the photocatalytic degradation dynamics of their corresponding binary system when compared to those yields recorded when the dyes were analysed singly. Huo et al. (2014) explained that the dyes had occupied the same active sites inclusive of the photogenerated holes and $^{\cdot}OH$ radicals. Nevertheless, in the mixed methylene blue–methyl orange photocatalytic degradation process, degradation of methylene blue had been considerably reduced, whilst that of methyl orange had been significantly enhanced when compared with those degradation performances recorded with single methylene blue or methyl orange. Huo et al. (2014) explained the latter results on basis of the reaction chemistries involved such that the presence of methylene blue had facilitated methyl orange degradation because that of methylene blue had consumed photoinduced holes and thence decreased their recombination with photoelectrons consumed for triggering the degradation of methyl orange. As a result, the degradation of methyl orange was enhanced, and the degradation yield of methylene blue decreased due to methyl orange because the degradation of the latter was also using the photoinduced holes. A little later, from their findings, Arab Chamjangali et al. (2015) observed that the simultaneous degradation/decolourization of methyl orange and methylene blue under the action of Ag–ZnO multipods was influenced by the Ag–ZnO multipods dosage, pH of the reaction solution, initial dye concentration and silver doping. Veldurthi et al. (2015) have analysed the photocatalytic activity of $LiMg_{0.5}Mn_{0.5}O_2$ on mixed aqueous solutions comprising methyl orange and methylene blue under visible light illumination. Veldurthi

et al. (2015) reported that the $LiMg_{0.5}Mn_{0.5}O_2$ photocatalyst had a preferential decomposition for methyl orange. Further analysis with isopropyl alcohol, benzoquinone and ammonium oxalate indicated that the isopropyl alcohol at 2 mmol L^{-1} and ammonium oxalate at the same concentration had largely slowed down the degradation of the mixed dye, whilst 2 mmol L^{-1} of benzoquinone had little effect in decreasing the degradation rate. Veldurthi et al. (2015) then inferred that $^{\cdot}OH$ radicals and holes, rather than superoxide radicals, had a crucial part at play in the photocatalytic degradation dynamics of mixed. On basis of their findings, Veldurthi et al. (2015) have put forward the following mechanism for the mixed-dye photocatalytic degradation process:

$$LiMg_{0.5}Mn_{0.5}O_2 + h\nu\left(\geq E_g\right) \rightarrow e^-_{CB} + h^+_{VB}$$
$$O_2 + e^-_{CB} \rightarrow O_2^{\cdot-}$$
$$H_2O + h^+_{VB} \rightarrow OH^{\cdot} + H^+$$
$$O_2^{\cdot-} + H^+ \rightarrow HO_2^{\cdot}$$
$$2HO_2^{\cdot} \rightarrow H_2O_2 + O_2$$
$$H_2O_2 \rightarrow 2OH^{\cdot}$$
$$h^+_{VB}/OH^{\cdot} + \text{dye} \rightarrow \text{By-products.}$$

Fig. 11 FTIR spectra of **a** Degussa P25, **b** Au/InBi-3D and **c** InBi-3D obtained as a result of the degradation of aqueous solution of methylene blue + rhodamine B at different irradiation times as the reaction progressed; **d** FTIR spectra of original samples; and **e** FTIR peak relative intensity versus irradiation time of the degradation reaction of aqueous solutions of methylene blue, rhodamine B and rhodamine B + methylene blue over the samples under the influence of 0.6 mL hydrogen peroxide (Ji et al. 2015). This figure has been reproduced from Ji et al. (2015) with the permission of Elsevier (Copyright © 2014 Elsevier B.V. All rights reserved) under licence number 4855160932810 (for both print and electronic formats)

In an extensive and comprehensive study, Ji et al. (2015) reported that the *x*M/InBi-3D materials had produced high visible light photocatalytic activities for the degradation of rhodamine B, methylene blue and mixed rhodamine B and methylene blue under the influence of a small quantity of hydrogen peroxide. Moreover, amongst the several materials that had been synthesized, Ji et al. (2015) found that the 0.08%Au/InBi-3D had brought about a complete degradation of rhodamine B, methylene blue and mixed rhodamine B and methylene blue within 50, 90 and 120 min, respectively (Fig. 10 and Fig. 11).

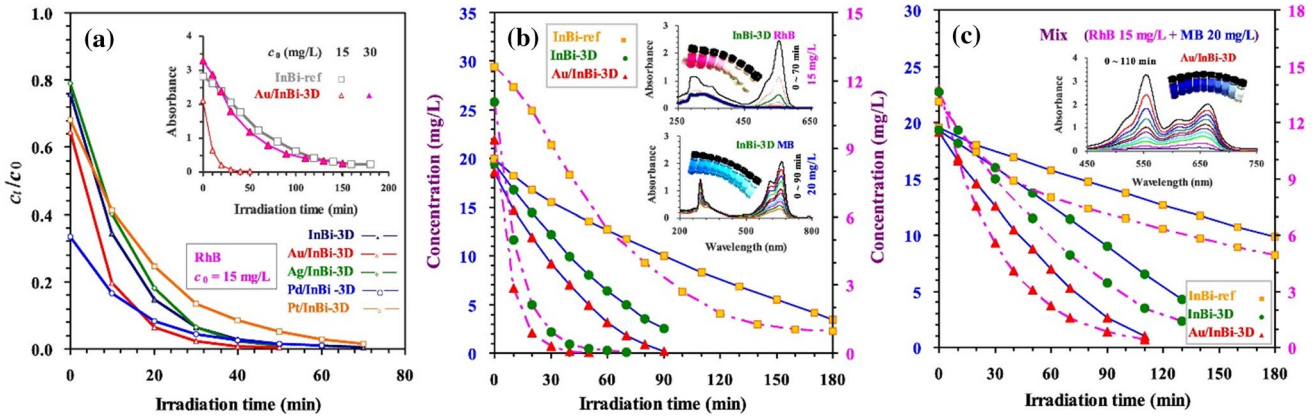

Fig. 10 **a** Rhodamine B concentration versus irradiation time for photocatalytic degradation of rhodamine B aqueous solution (initial concentration of 15 mg L^{-1}) over InBi-3D and M/InBi along with that of rhodamine B aqueous solution (initial concentration of 15 mg L^{-1}) over InBi-ref, and of rhodamine B aqueous solution (initial concentration of 15 mg L^{-1} and 30 mg L^{-1}) over Au/InBi-3D (inset in top half of this image) under the influence of 0.6 mL hydrogen peroxide under visible light ($\lambda \geq 400$ nm) illumination; **b** methylene blue (shown in solid lines) and rhodamine B (depicted in dotted lines) concentrations versus irradiation time over InBi-ref, InBi-3D and Au/InBi-3D for photocatalytic degradation of methylene blue (initial concentration of 20 mg L^{-1}) and rhodamine B (initial concentration of 15 mg L^{-1}) aqueous solution under the influence of 0.6 mL hydrogen peroxide under visible light ($\lambda \geq 400$ nm) illumination; and **c** rhodamine B (depicted in dotted lines) plus methylene blue (shown in solid lines) concentration versus irradiation time for photocatalytic degradation of mixed rhodamine B and methylene blue aqueous solution over InBi-ref, InBi-3D and Au/InBi-3D under same conditions of hydrogen peroxide treatment and under visible light ($\lambda \geq 400$ nm) illumination (all three images and conditions reported by Ji et al. (2015)). In image (C), after 110 min of photocatalytic degradation reaction, the concentrations of methylene blue and rhodamine B in the mixed rhodamine B and methylene blue had reached ca. 1.0 mg L^{-1} and 0.44 mg L^{-1} over the Au/InBi-3D catalyst, ca. 14.1 mg L^{-1} and 7.2 mg L^{-1} over the InBi-ref catalyst, ca. 6.5 mg L^{-1} and 2.1 mg L^{-1} over the InBi-3D catalyst, and ca. 3.5 mg L^{-1} and 10.4 mg L^{-1} over Degussa P25, respectively (Ji et al. 2015). Also, despite that the concentration of methylene blue was lower for the scenario with Degussa P25, the observed '*tile blue*' colour of the final titanium dioxide powders indicated that methylene blue had probably been adsorbed onto the titanium dioxide surface [the latter observation being eventually inferred based on the changes of the FTIR bands recorded for different degradation time (Fig. 11) (Ji et al. 2015)]. This figure has been reproduced from Ji et al. (2015) with the permission of Elsevier (Copyright © 2014 Elsevier B.V. All rights reserved) under licence number 4855160932810 (for both print and electronic formats)

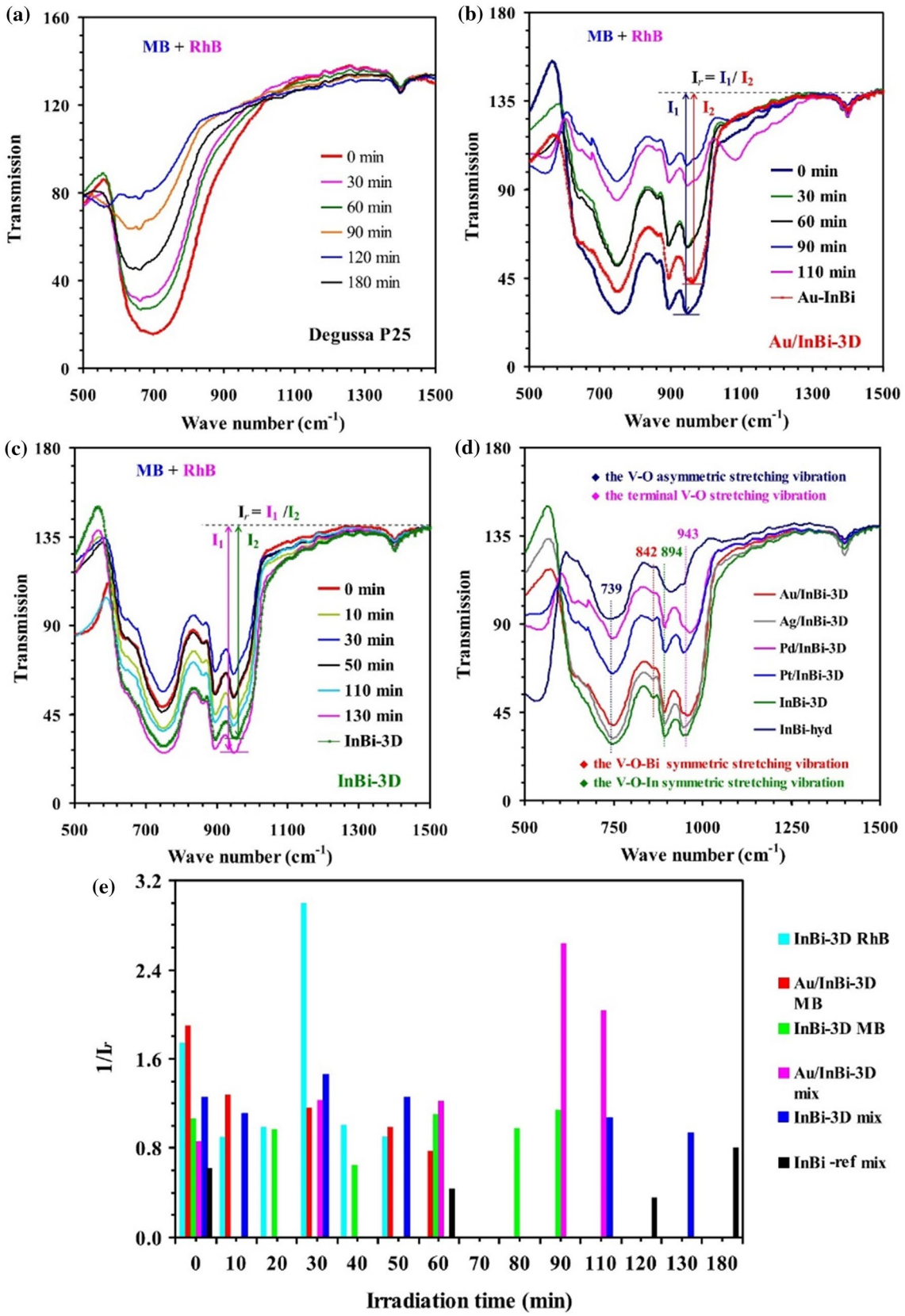
(a)
MB + RhB
Transmission
Wave number (cm-1)
0 min
30 min
60 min
90 min
120 min
180 min
Degussa P25
(b)
MB + RhB
Ir = I1/ I2
I1
I2
0 min
30 min
60 min
90 min
110 min
Au-InBi
Au/InBi-3D
(c)
MB + RhB
Ir = I1 /I2
0 min
10 min
30 min
50 min
110 min
130 min
InBi-3D
InBi-3D
(d)
the V-O asymmetric stretching vibration
the terminal V-O stretching vibration
739
842 894
943
Au/InBi-3D
Ag/InBi-3D
Pd/InBi-3D
Pt/InBi-3D
InBi-3D
InBi-hyd
the V-O-Bi symmetric stretching vibration
the V-O-In symmetric stretching vibration
(e)
1/Ir
Irradiation time (min)
InBi-3D RhB
Au/InBi-3D MB
InBi-3D MB
Au/InBi-3D mix
InBi-3D mix
InBi -ref mix

In their study, Nipane et al. (2015) analysed the photocatalytic degradation performance of a ZnO nanorod-reduced graphene oxide (ZnONR-RGO) composite for a methylene blue and methyl orange mix. Thereinafter, it was observed that absorption at 664 nm, by reason of methylene blue, had decreased fast when compared to unmixed methylene blue. Nipane et al. (2015) inferred that in a methylene blue–methyl orange mixture, methylene blue gets degraded faster under the action of the ZnONR and ZnONR–RGO composite. Interestingly, one unexpected result obtained by Nipane et al. (2015) was that the degradation of methyl orange still took place to an appreciable extent of 77% within 90 min in the mix although no catalyst had been used. Nipane et al. (2015) put forward a explanation to the observations made whereby it was argued that because the zeta potential of the ZnONR–RGO composite is − 23.7 mV, the absorption of methylene blue (which is a cationic dye) was more pronounced in effect when compared to that of methyl orange which is anionic. Here, use of the term 'absorption' seems somewhat confusing since it is more likely that the methylene blue molecules, being effectively cationic, had adsorbed onto the surface of the ZnONR–RGO composite most plausibly as a result of electrostatic interactions. In their work wherein a dyeing effluent was simulated by a binary dye mixture, Han et al. (2016a) reported that the as-fabricated 2% Er^{3+}-doped BiOI porous microspheres had yielded outstanding performance in the removal of unmixed and mixed methyl orange, rhodamine B and methylene blue under visible light irradiation. Han et al. (2016a) noted that the photodegradation efficiency of rhodamine B in the methyl orange + rhodamine B binary dye system had risen up to almost 95%, whereas that of methyl orange reached 93%, 88% and 76% for initial concentrations of 20 mg L^{-1}, 30 mg L^{-1} and 40 mg L^{-1}, respectively. Furthermore, in the other binary dye mixture with methyl orange and methylene blue, the photodegradation efficiency of methyl orange had reduced significantly from 83 to 67% when initial concentration of methyl orange was increased from 20 to 30 mg L^{-1}, whilst the photodegradation efficiency of methylene blue experienced a small rise of 5% from 90%. Based on the specific dye total removal data, Han et al. (2016a) reported that total dye removal quantities had increased when their initial concentrations were increased in the aqueous solutions.

In Han et al. (2016b), the time variation of spectral changes occurring during the photodegradation of mixed dyes (rhodamine B and mixed-dye effluent (Orange IV, methyl orange and malachite green)) solution over a Sn-doped BiOCl photocatalytic material synthesized in a solution of pH 6 was analysed. A number of interesting results were reported in Han et al. (2016b), and they are: mixed rhodamine B and methyl orange solution could be easily degraded after 8 h; maximum absorption of a rhodamine B and Orange IV mixture had a decreasing profile with the band for rhodamine B shifted from 553 to 500 nm and the peak absorption of Orange IV reduced after 8 h of irradiation; for the rhodamine B–malachite green mix, the latter could be entirely degraded within 8 h, and that this excellent photodegradation performance had been set on account of the similarity in chemical structure of the latter two dyes. Han et al. (2016b) also conducted some innovative analysis for the photocatalytic degradation of a mix of all the dyes involved in the study. Based on the notion that rhodamine B and malachite green have similar chemical structures and can apparently exhibit such a similarity in a positively charged state, whereas methyl orange and Orange IV share some structural similarity in a negatively charged state, Han et al. (2016b) have argued that the latter specificities in chemical structural could be possible reasons explaining why rhodamine B–malachite green mix is likely to be degraded 'in preference' to the methyl orange–Orange IV mix.

Li et al. (2016) simulated a wastewater as an aqueous solution containing 10 mg L^{-1} methyl orange, rhodamine B and methylene blue, respectively. Based on UV–Vis absorption spectra data, Li et al. (2016) inferred that mixed dyes could not be entirely completely removed using the $Bi_2O_2CO_3$ and Ag_2CO_3 synthesized catalysts after 180 min under visible light irradiation. Still, these the latter observed that all peaks had steadily diminished and eventually disappeared after 180 min using $Ag_2CO_3/Bi_2O_2CO_3$ as catalyst (with no fresh peaks depicted in the UV and visible light region). In this study, Li et al. (2016) eventually demonstrated that a priority can develop for the catalyst used (herein, being a $Ag_2CO_3/Bi_2O_2CO_3$ composite [(having molar ratio of $Ag^+/Bi^{3+} = 1/1$)]) *vis-à-vis* its individual component in regard to dye effluent remediation. Moreover, in view to elucidate the plausible reaction mechanism(s) operating, Li et al. (2016) tested benzoquinone (1.0 mmol L^{-1}), tertiary butanol (1.0 mmol L^{-1}) and ethylene diamine tetraacetic acid (1.0 mmol L^{-1}) as potential scavengers of radicals and holes. Li et al. (2016) made a series of interesting observations which shed some light on the involvement of radicals and holes in the dye degradation mechanistic pathways. First, Li et al. (2016) noted that photocatalytic degradation of rhodamine B over one of the $Ag_2CO_3/Bi_2O_2CO_3$ composite (with a molar ratio of Ag^+/Bi^{3+} of 1/1) was only little influenced by tertiary butanol addition, thus indicating that hydroxyl radicals had a minimal involvement in this dye's degradation; conversely, the photocatalytic degradation efficiency of rhodamine B diminished when benzoquinone was added and this bore testimony that superoxide radicals played an important role her; and finally, the photocatalytic activity of $Ag_2CO_3/Bi_2O_2CO_3$ (Ag^+/Bi^{3+} of 1/1) composite had been totally suppressed by the addition of ethylene diamine tetraacetic acid, thus indicating that holes could have also been part of the mechanism leading to rhodamine B degradation.

Using a facile pH-mediated chemical precipitation procedure along with a self-built Z-scheme heterojunction under visible light illumination, Yang et al. (2016) prepared new Ag_2O@Ag-modified $BiVO_4$ composites. In Yang et al. (2016), it was observed that in comparison with pure Ag_2O and $BiVO_4$, AgAgBV had yielded an elevated photocatalytic activity as a result of the favourable separation of electron–hole pairs in the heterojunction construction. Moreover, the Ag_2O@Ag-modified $BiVO_4$ composite having an initial $BiVO_4/Ag_2O$ mass ratio of 10:1 produced the most significant degradation efficiency for dye under test whereby empirical findings indicated that individual rhodamine B or methylene blue system could undergo complete photodegradation within a relatively short irradiation time (48 min for 20 mg L^{-1} methylene blue and 15 min for 10 mg L^{-1} rhodamine B. However, it also becomes apparent that the dye molecules and the intermediates produced during the degradation process competed with each other for initial absorption and catalytic sites on the surface of $Ag_2O/BiVO_4$ composite material such that direct competition with the active species led to a lowering in the degradation rate for rhodamine B and methylene blue. Yet, irrespective of the observed mutual suppression (i.e. understandable in the form of an inhibition to reaction) phenomenon, an appreciably higher photocatalytic performance was recorded for the dye mixture. Based on the time-based absorption spectrum changes of rhodamine B, methylene blue and rhodamine B + methylene blue aqueous solutions, and the photodegradation of rhodamine B + methylene mixture under the effect of $Ag_2O/BiVO_4$ (1:10) composite under visible light illumination from Yang et al. (2016), a number of important observations and inferences could be made. These were: (i) rhodamine B and methylene blue had been fully photodegraded in 20 and 48 min, respectively, whereas methylene blue had attained a high decomposition rate in both mixed-dye solutions but that of rhodamine B was considerably inhibited (particularly at elevated starting dye concentrations) and (ii) the degradation rate of methylene blue was significantly faster than that of rhodamine B and this could be set on account of methylene blue having a more pronounced affinity to the catalyst composite than rhodamine B had, and hence, favourable absorption led to better dye photodegradation. Moreover, based on the total organic carbon removal profiles, it was observed that TOC removal in individual-dye and mixed-dye degradation varied appreciably, whereby in the degradation process of the single rhodamine B and methylene blue, TOC removal reached 90.2% and 93.2%, respectively (Yang et al. 2016). Moreover, the corresponding TOC removals for the mixed-dye scenarios were significantly lower wherein TOC removal for the 10 mg L^{-1} rhodamine B + 20 mg L^{-1} methylene blue was only at 32.5% (Yang et al. 2016). On the whole, it was deduced that although the overall degradation time in a 5 mg L^{-1} rhodamine B + 10 mg L^{-1} methylene blue mixed-dye solution was longer than for any of the individual dye, the final TOC removal reached an acceptably high 88.2%, and this performance was indicative of the $Ag_2O/BiVO_4$ heterojunction having a desirable capacity for mineralization (Yang et al. 2016). More experiments indicated that degradation efficiencies of rhodamine B significantly diminished from 99.80% to a very low 26.55% and even lower 3.12% when benzoquinone and triethanolamine were added to the dye system, respectively (Yang et al. 2016). A similar degradation behaviour was observed with methylene blue when treated with benzoquinone and triethanolamine. Yang et al. (2016) eventually deduced that superoxide and h^+ were the principal active photogenerated species accountable for much enhanced photocatalytic performance for dye degradation.

Choi et al. (2016) fabricated nano-assembled TiO_2/BiOX hybrid microspheres wherein X was Cl, Br or I, and then extensively analysed these microspheres for their respective photocatalytic activities with individual (tartrazine and orange G), mixed dyes (methyl orange + rhodamine B + methylene blue), natural dyes extracted from grapes and cabbages and a commercially available drink in the presence and absence of hydrogen peroxide under visible light illumination. Based on their findings, Choi et al. (2016) observed that for the mixed dyes, TiO_2/BiOI had the greatest adsorption capacity whilst TiO_2/BiOCl exhibited the highest photocatalytic activity. Moreover, methyl orange in the mixed-dye systems had been the fastest to be photodegraded for all photocatalysts analysed (Fig. 12).

Lee et al. (2016b) examined the effectiveness of photocatalysts for a mixed-dye system of methyl orange, rhodamine B and methylene blue under visible light prior to and after AgX-loading (X being Cl, Br and I). The concentration used for each dye here was kept at 10 mg L^{-1} for X = Cl and Br, whilst for X = I, the concentrations were all 20 mg/L, and an adsorption run was undertaken over the mixed dye for 60 min under dark conditions and then applied visible light irradiation. Amongst the several new findings, it was thereafter found that the photocatalytic activity was in the order of BiOCl ≤ BiOBr < BiOI microspheres, and photodegradation rate was in the order methylene blue < rhodamine B < methyl orange (Lee et al. 2016b). Quite of a surprise, loading of AgX led to a decrease in photocatalytic activities but still AgCl/BiOCl composite had been endowed with an enhanced photocatalytic activity for methylene blue degradation. Moreover, the dye degradation rate was in the order of methylene blue ≈ rhodamine B < methyl orange for AgCl/BiOCl and AgBr/BiOBr microspheres, whereas the corresponding dye degradation rate order was methylene blue < rhodamine B ≈ methyl orange for AgI/BiOI microspheres (Lee et al. 2016b). With the nanoplate format of BiOX and AgX/BiOX, results were particularly more interesting wherein now the dye degradation rate had the order

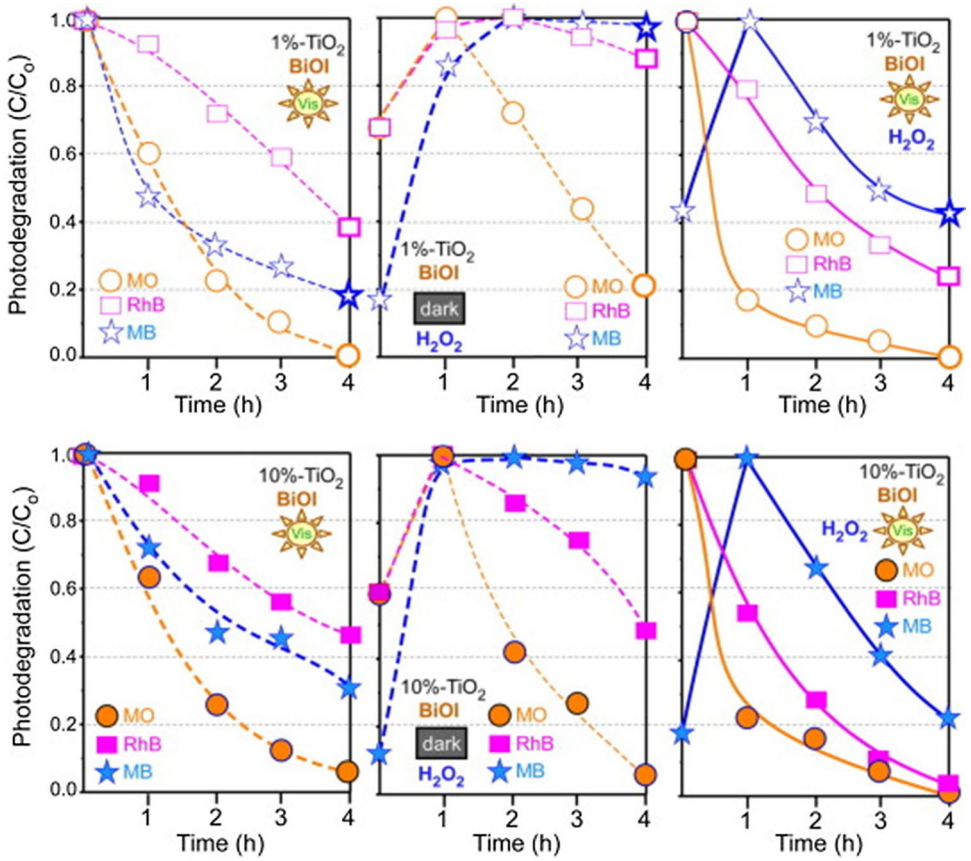

Fig. 12 Photodegradation (C/C_o) of the mixed dyes in the presence of (right column) and in the absence of (left column) hydrogen peroxide over the fabricated 1 mol% (top row) and 10 mol% (bottom row) TiO_2/BiOI microspheres (in the amount of 10 mg), and with photodegradation data with hydrogen peroxide in dark conditions shown in images located in the middle column, reported in Choi et al. (2016). Some of the highlights of this set of results primarily discussed in Choi et al. (2016) are: (i) after a 1-h adsorption under dark conditions and hydrogen peroxide addition, under visible light irradiation thereafter for 4 h, the TiO_2 (1 mol%)/BiOI microspheres led to the total degradation of methyl orange, but less degradation for methylene blue (80%) and rhodamine B (60%); under a similar treatment, for the TiO_2 (10 mol%)/BiOI, dye degradation performance was somewhat different with 98% for methyl orange, 64% for methylene blue and 54% for rhodamine B; for the TiO_2 (1 mol%)/BiOI used under dark conditions with hydrogen peroxide, no degradation was noted for methylene blue but methyl orange had undergone 80% degradation; with TiO_2 (10 mol%)/BiOI, dye degradation had been improved (almost total degradation for methyl orange, 98% for rhodamine B and 80% for methylene blue after 4 h; quite of an interest, adsorbed dyes had desorbed upon hydrogen peroxide except in the case where TiO_2 (1 and 10 mol%)/BiOCl and TiO_2 (1 and 10 mol%)/BiOBr microspheres were examined; hence, for the case TiO_2 (1 mol%)/BiOI was examined under visible light irradiation with hydrogen peroxide, methyl orange had been totally degraded, whilst the degradation for rhodamine B was 78% and 59% for methylene blue (after 4 h). This figure has been reproduced from Choi et al. (2016) with the permission of Elsevier (Copyright © 2016 Elsevier B.V. All rights reserved) under licence number 4855161215967 (for both print and electronic formats)

of rhodamine B < methylene blue ≪ methyl orange. Lee et al. (2016b) also observed that methyl orange was degraded the fastest and rhodamine B had the slowest rate of degradation. In the case of nanoplates, and unlike the microspherical format of the composites, the photocatalytic activities of BiOX did not decrease following loading with AgX, and AgBr/BiOBr nanoplates had an enhanced photocatalytic activity (Lee et al. 2016b). In the case of BiOX nanoplates, photocatalytic activity was in an order of BiOI < BiOBr ≤ BiOCl. Upon AgX loadings, the change in catalytic activity could be attributed to freshly aligned energy levels and interfacial wavefunction mixing (Lee et al. 2016b). For rhodamine B and methylene blue, the order changed to BiOBr < BiOI ≈ BiOCl whereas for methyl orange, catalytic activity was ordered as follows: BiOBr ≈ BiOI ≈ BiOCl.

In more recent studies, other diverse photodegradation performances have been reported. For example, Wang et al. (2018b) reported that 4-I/C-TiO_2 had exhibited good photocatalytic activity for methyl orange and rhodamine B mixed degradation and that the photocatalyst could equally fulfil photocatalytic degradation (manifestly higher than that with commercial P25) in mixed system under a 60-min lasting natural sunlight irradiation. Other than the findings of dark catalytic tests, I/C-codoping was also observed

to have effectively speeded hydroxyl radical production from the generated hydrogen peroxide, which was formed for enhanced photocatalytic dye degradation (Wang et al. 2018b). Along with the weakening in the intensities of the distinguishing absorption peaks for methyl orange and rhodamine B under the effect of the 4-I/C-TiO_2 upon xenon lamp irradiation (which thus hinted to the remarkable photocatalytic activity of the latter material for mixed-dye degradation), the XRD and XPS results indicated no apparent change in the crystal structure and chemical composition of 4-I/C-TiO_2, and this led to the inference that the latter photocatalyst had acceptably good catalytic stability.

In yet another interesting study not using rhodamine B, methyl orange and/or methylene blue this time, Abdelsamad et al. (2018) examined the photodegradation of a synthetic textile wastewater consisting of three reactive azo dyes, namely Reactive Red 195, Reactive Orange 122 and Reactive Yellow 145 under the effect of Ag-doped ZnO thin films. Abdelsamad et al. (2018) reported the difference in decolourization between single and mixed dyes followed the order: Reactive Yellow > Reactive Red 195 > Reactive Orange 122. Recently, Palanivel et al. (2019) observed that in the mixed-dye system, the degradation range of methylene blue was quite higher than that with rhodamine B under sunlight illumination under the presence of hydrogen peroxide and that the methylene blue photodegradation reached 100% under sunlight irradiation within 35 min, whereas the photodegradation of rhodamine B attained 92% after the same duration in the presence of hydrogen peroxide. Lastly, Lebedev et al. (2019) examined the photocatalytic degradation of mixed basic and acidic dyes by a single catalyst, Ag/Ag_2O/$BiNbO_4$. Whilst the mixed system comprising rhodamine B and Acid Red 1 was not examined due to their overlap of absorption spectra observed in the 500–550 nm, complete photodegradation of methylene blue and Acid Red 1 in methylene blue–Acid Red 1 mixed systems of 1:1, 2:1 and 1:2 (on a volume basis) was observed with treatment by 0.015 g of 7 wt% Ag-loaded $BiNbO_4$ (Lebedev et al. 2019). Moreover, Lebedev et al. (2019) reported that the net degradation of Acid Red 1 (attaining 85%) was independent of volume ratio, whilst the degradation of methylene blue was influenced by the volume ratio; degradation behaviours which were set on account of the different *p*-type and *n*-type materials taking part in the reactions during the degradation process.

Biocompatibility and ecotoxicological implications

Biocompatibility refers to the property of a material to be compatible with living tissues. The photocatalytic NPs to be used for decontaminating the environment from harmful dyes will eventually enter the environment even after its use. These NPs deposited into the environment have high chances of being in contact with living tissues in the future, through direct or indirect means. Hence, the NPs to be used in the natural environment should be, in principle, highly biocompatible. Otherwise, they might cause immense damage to nature. Although photocatalytic NPs are reported to be biocompatible to some extent, some recent studies suggest that they can be cytotoxic to a certain degree (Khan et al. 2015b).

Several studies suggest that NPs can be harmful to the cells in a variety of ways. They can give rise to reactive oxygen species which may lead to oxidative stress (Ng et al. 2017; Gallo et al. 2018), can also interact with the proteins (Bourgeault et al. 2017; Cao et al. 2019) or can also enter the cell and cause damage to the DNA and the organelles (Wagner et al. 2011; Abudayyak et al. 2017; Sayed and Soliman 2017). Horie and co-workers studied the cytotoxicity of TiO_2 NPs on Human keratinocyte HaCaT cells (Horie et al. 2016). Under non-illuminated condition, the anatase TiO_2 NPs did not show any cytotoxicity. However, it was observed that the rutile TiO_2 NPs inhibited cell proliferation and induced the expression of HO-1 gene expression. Under UVA irradiation, no cytotoxicity was observed for the anatase NPs. However, the rutile NPs were observed to cause cell damage due to poration of the cell membrane, induction of oxidative stress and a decrease in mitochondrial activity. The cytotoxicity of TiO_2 NPs on human skin was also tested using EPI-200, consisting of epidermal keratinocytes as the human 3D skin model. LDH leakage, IL-8 secretion and skin irritation were not observed under irradiated and non-irradiated condition. Hence, it was inferred that they are non-toxic to human skin, which may be due to the presence of *stratum corneum* that prevented the NPs from entering the cell. Cui and co-workers studied the cytotoxicity of TiO_2-based nanofibres on macrophages, human liver cells and kidney cells and observed no cytotoxicity up to a concentration of 220 μg mL^{-1} (Cui et al. 2015). The cytotoxicity of six commercially available TiO_2 NPs against *Escherichia coli* in an aquatic environment was studied by Tong et al. (2013). In the latter work, cytotoxicity was observed for P25, Pigment White 6 (Cat. 4162-01), anatase powder (Cat. 232033) and anatase nanopowder (Cat. 637254) under stimulated solar irradiation. Rutile powder (Cat. 204757) and rutile nanopowder (Cat. 637262) were found to be non-toxic. Sai Saraswathi and Santhakumar studied that zirconium oxide used for the remediation of azo dyes was cytotoxic to breast cancer cells (MCF 7) only beyond a high concentration of 500 μg mL^{-1} (Sai Saraswathi and Santhakumar 2017). Hence, its use is safe and environment friendly. Fakhri and Nejad studied the antimicrobial, antifungal and cytotoxic properties of molybdenum trioxide (MoO_3) nanoparticles and came to observe that these NPs inhibited the growth of *E. Coli*, *Bacillus subtilis*, *Candida albicans* and *Aspergillus*

niger (Fakhri and Nejad 2016). Furthermore, the cytotoxicity of the MoO_3 nanoparticles was tested on MCF-7 and Hep G2 cells by MTT assay, and it was observed that with an increase in the concentration of the NPs the viability of the cells decreased. Owing to its biocompatibility, ZnO is widely used in a variety of cosmetic products. However, many recent pieces of research suggest that ZnO is cytotoxic to some extent (Singh 2019). Baek et al. reported that the cytotoxicity of ZnO NPs is related to their size and surface charge (Baek et al. 2011). Smaller-sized NPs were found to be more cytotoxic than larger particles. This may be because a larger size makes it more difficult for the nanoparticles to enter into the cell. Furthermore, positively charged NPs were found to be more cytotoxic than negatively charged ZnO NPs as they were more efficient in producing reactive oxygen species. Punnoose and co-workers reported that the cytotoxicity of ZnO can be altered by modulating the chemical groups bound to its surface (Punnoose et al. 2014).

For ecological safety, the degradants and by-products formed as a result of photocatalysis should be non-toxic. In one study, the cytotoxicity of the reaction mixture formed as a result of the degradation of MB by H-TiO_2 was studied by MTT method on HeLa, HaCaT and MCF-7 cells (An et al. 2016). The reaction mixture showing a high degree of dye degradation (up to 90%) was found to be non-toxic to the cells in that study. In the case of immobilized photocatalysts, the carrier to be used should also be biocompatible and non-toxic. Several carbon derivatives such as lignin, wood, chitosan, cellulose and biochar are used for immobilization because of their high biocompatible and biodegradable nature (Colmenares et al. 2016). Similarly, cellulose acetate is being used to produce photocatalytic membranes because of its biodegradable and non-toxic nature (Li et al. 2018). Moreover, nanotoxicology is an emerging field and it lacks standardized tests which make it difficult to find out the complete toxicity profile of the photocatalytic NPs (Wagner et al. 2011). The introduction of standardized cytotoxicity tests aided by the advances in nanotechnology will make it easier to develop highly efficient and environmentally friendly photocatalysts soon.

Delving deeper in the analysis for this section, a very large proportion of the doped photocatalysts described in the literature and discussed in this review achieve high efficiencies in the removal of several dyes, and constitute a potential avenue for developing a promising technology for the control of release of contaminants of emerging concern (CEC) in the actual environment. However, there appears to be a significant paucity of comprehensive studies which have investigated the detailed potential ecotoxicological impacts and their respective implications related to the release of these overwhelmingly nanostructured doped photocatalysts into the environment. Nanocatalysts, and expectedly nanostructured doped photocatalysts, released into the aquatic ecosystems may interact with the biota inducing potentially adverse effects at different levels of biological organization making up the food chains and biodiversity (Saggioro et al. 2015) resulting, in the end, in fast growing and critical environmental and human health concerns. Once released into the environment, it is expected that nanostructured doped photocatalytic materials will interact amongst themselves and also with the surrounding components of the environment. The rate of aggregation/agglomeration and sedimentation of ENMs is controlled by the concentration, surface area and forces involved in collision; however, the fate of these ENMs might be also determined by parameters such as osmolarity, pH and natural organic matter content, which will eventually have an influence on the uptake and toxicity levels in exposed organisms (Corsi et al. 2014). In Fig. 13,

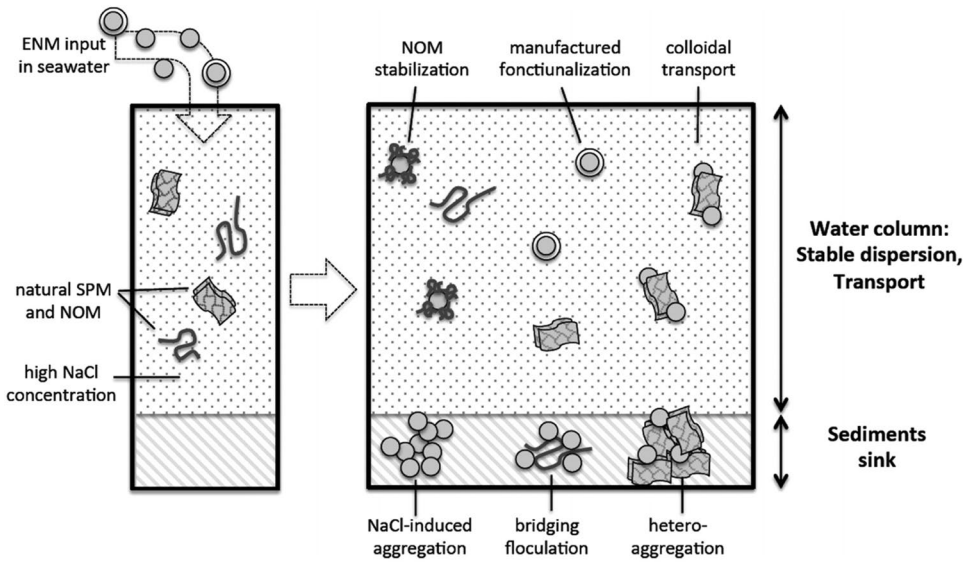

Fig. 13 Potential fate of engineered nanomaterials in seawater (Corsi et al. 2014). This figure has been reproduced from Corsi et al. (2014) with the permission of American Chemical Society (Copyright © 2014)

the potential fate of ENMs once released into seawater is depicted.

There is much apparently a very scarce pool of data in the literature on the assessment of the toxicity levels associated with the use of nanostructured doped photocatalyts for dye degradation. The very few studies which were shortlisted in this regard for the present analysis are discussed briefly below. It is observed that such studies have dealt with the toxicity assessment of the undoped and doped photocatalytic nanomaterials before the dye degradation, the dye alone and the photodegradation products on different plants, aquatic and human cellular entities normally used in the specific context. The variations and paucity of results reported in these few studies do not allow in reaching a definite inference with respect to the types and degrees of toxicity expected in the real milieus of potential release or contamination by the nanomaterials and other species generated during the photodegradation of the dye. This is because each study is 'unique' in itself with respect to the scale of the assessment, the dye tested, the photocatalytic dye degradation conditions, the extents of degradation of the dye and degree of mineralization reached, the test subject(s) used to assess the toxicity levels and the specific architecture and chemical composition of the photocatalytic materials used (de Sousa Filho et al. 2020; Serrà et al. 2020). For example, recently, Ozmen et al. (2018) reported several interesting findings when studying the photodegradation of disperse red 65 using core@shell nano-TiO_2 particles. Amongst the complete set of observations made in Ozmen et al. (2018), the highlights comprised the following: (1) even at the maximum test concentration of core@shell NPs of 250 mg L^{-1}, there was little mortality in comparison with the control groups in *Danio rerio* and *Xenopus laevis* embryos, (2) the lower concentrations of NPs had not caused lethality to the embryos of the *D. rerio* and *X. laevis* species, (3) the prepared core@shell NPs had not brought about developmental abnormalities in the embryos, (4) however, an exposure to the photocatalytic degradation products of disperse red 65 obtained after 1 h of photodegradation led to 100% mortality in both test species after a 96-h exposure, (5) a photocatalytic degradation reaction lasting 2 h could partially lessen the lethal effect for *X. laevis* embryos, (6) 3 h of photocatalytic degradation of disperse red 65 had not led to mortality in the *X. laevis* embryos, viand in the case of *D. rerio* embryos, a 3-h photocatalytic degradation of disperse red 65 using the synthesized TiO_2 and SiO_2@TiO_2 catalysts had eliminated the lethal effects of disperse red 65 on the zebrafish embryos. Serrà et al. (2020) recently reported a significant enhancement in algal viability when using supported ZnO@ZnS core@shell micro/nanoferns after noting that the corresponding ecotoxicity after a 96-h light exposure was considerably lower in comparison with the ZnO films, ZnO NPs, ZnO micro/nanoferns or ZnO@ZnS NPs at concentrations ranging from 25 to 400 mg L^{-1}.

In the study of Khataee et al. (2015), it was found that 5 mg L^{-1} of malachite green dye had given rise to an appreciable degree of toxicity after a week and that had induced a significant decrease of the total carotenoids and total chlorophyll in fully grown fronds of *Spirodela polyrhiza*. Conversely, in the latter study itself, in the cases of exposure to undoped and a 4% Er-doped PbSe NPs, the total chlorophyll content was not significantly reduced when compared to the behaviour observed for the control test scenario. Balbi et al. (2017) reported both different and common particle behaviours in the different media used for the screening of cellular toxicity. The latter workers observed a number of biological effects brought about by different Fe-doped n-TiO_2 particles examined in the different cellular systems, and those effects were indicative of a certain degree of cytotoxicity. It is also important to highlight that an increased production of nitric oxide was observed in some cases and this behaviour was indicative of a propensity for the onset of pro-inflammatory processes in the cell models studied at concentrations that had not induced any cytotoxicity in human vascular endothelial cells or had induced a low cytotoxicity in immune cells (Balbi et al. 2017). Notwithstanding the removal of lethal effects in certain tests, the latter studies still transpire to some appreciable extent that the overall dynamics involved in dye degradation using photocatalytic nanomaterials eventually do induce certain ecotoxicological and environmental risks which can persist and may not therefore be downplayed. Therefore, the development of new nanostructured doped photocatalytic materials and their commercialization must be imperatively accompanied by thorough studies for elucidating the ecotoxicological aspects and environmental risk levels and also for examining the modes of action and impacts of potential residues to non-target organisms (Almeida et al. 2019). Hence, comprehensive ecotoxicological studies are strongly required in the real milieus of potential release points of nanostructured doped photocatalytic materials. The results of such studies will most expectedly lead to garner a whole assessment and ecotoxicity profile of the potential applications of these engineered nanomaterials (ENMs) and thence determine the selection of the eco-friendly and sustainable ENMs for environmental remediation programs (Corsi et al. 2018).

Developments in the design of photocatalytic reactor processes

Besides the operational concerns of separation, recovery and particle agglomeration, the use of photocatalysts in the powdered state has also been associated with potential damage to recirculation pumps (Vaiano et al. 2017b). In view

of addressing the latter issues, the immobilization of the catalyst in one way or the other to a specific support material has brought a number of advantages. These advantages have been revisited earlier in this review but are associated with findings based on batch-type laboratory-scale experimental systems having small reaction volumes. Given that the core requirement is to remediate real dye-laden waters which vary significantly in their environmental conditions, characteristics and flows, it becomes primordial to formulate and examine the performances of larger and novel reactor-type systems employing immobilized photocatalysts, which come out being the better performing ones on the whole. Yet, additional studies and optimization analysis are needed to probe the behaviour of slurry-type reactor systems having suspended particles. The aim of this section is not to make an elaborate review (which might otherwise be viewed as redundant) of all the recent types of photocatalytic reactors employed in the remediation of organic pollutants such as dyes or pharmaceuticals, but rather to take stock of some of the salient reactor design parameters, operational process variations and key findings of recently designed and assessed photocatalytic reactors using photocatalysts (both dispersed and immobilized) for dye degradation. At this stage, the reader is welcomed to browse the following excellent reviews (amongst others) which have been published recently on photocatalytic reactors and given a broad range of useful information on the topic: Argurio et al. (2018) whereby the use and numerous characteristics of photocatalytic membranes in photocatalytic membrane reactors have been extensively discussed; Zheng et al. (2017) wherein a very large number of photocatalytic membrane reactor configurations and the related influencing factors for operations have been discussed; Abdel-Maksoud et al. (2016) whereby the selection criteria of reactor design for scale-up purposes and potential commercialization of titania-based solar photocatalytic reactor systems have been analytically reviewed; Mazierski et al. (2016) who classified and described a number of photoreactors used for gas phase and liquid phase reactions; Iglesias et al. (2016) who performed a critical review and comparison of photocatalytic processes which include membranes, photocatalysis and membrane filtration and photocatalytic membrane reactors, identified the related process intensification indices and reflected on the future trends; Zhang et al. (2016) who reviewed the research and development advances achieved in membrane fouling mechanisms of photocatalytic membrane reactors, the influences and interactions of photocatalytic processes on membrane fouling, and various fouling control approaches; Molinari et al. (2017) whereby the different application of various photocatalytic membrane reactor configurations in water treatment for the degradation of organic pollutants and in the preparation of synthesis of organic compounds have been critically reviewed; Sundar and Kanmani (2020) who have recently extensively reviewed 24 photocatalytic reactor designs and compared them using the following benchmarks: apparent reaction rate constant, photocatalytic space–time yield, space–time yield, specific removal rate and electrical energy consumption, and then inferred that the design of a photocatalytic reactor requires the careful consideration of reactor throughput, performance of reactor system, energy efficiency of system and the cost; and last but not least, Kumari et al. (2020) who have compared photocatalytic membrane reactors on account of the degradation rate of some common POPs found in wastewater.

An analysis of the recent literature shows a number of positive developments in the design of novel photocatalytic reactors and the attempts made to 'process intensify' the reactor systems intended for potential scale-up and industrial application under stable steady-state regimes. Das and Mahalingam (2020) have indicated that when it comes to the use of immobilized photocatalysts intended to service large-scale systems, a paucity of adequate light irradiation on the catalyst surface can be a major drawback encountered in conventional reactors. Das and Mahalingam (2020) have also indicated that airlift reactor configurations can offer favourable mixing or agitation between the different phases involved without the need to have a standalone or separate mechanical agitation unit, hence allowing for better mass transfers.

There are also microreactors (microfluidic reactors) which have been gaining research attention in the design of pollutant remediation systems in contrast to the conventional macroscale reactors (CoMRs) (Hamaloğlu et al. 2017; Zhao et al. 2017c; de Sá et al. 2018; Yusuf et al. 2018; Rashmi Pradhan et al. 2019). Unlike the case of CoMRs which are impeded in their performance because of mass transfer limitations and poor photon management (Jayamohan et al. 2016; Zhao et al. 2017c), microfluidic reactors are characterized by the presence of a thin liquid layer on the surface of the catalyst which limits the loss of photons (Jayamohan et al. 2016). There are key advantages which are associated with microfluidic reactors, namely that they offer more interaction of species involved with the catalysts because of greater surface-to-volume ratio, they have shorter diffusion distance, better mass transport, higher photocatalytic efficiency (Meng et al. 2013; Jayamohan et al. 2015), low consumption of reagents, decreased generation of waste materials and reduced energy consumption. For example, Jayamohan et al. (2015) examined the photocatalytic degradation methylene blue in a microfluidic system using 12 µm titania nanotubular arrays photocatalyst under simulated AM 1.5 irradiation (Fig. 14) and observed that (1) the latter catalyst yielded enhanced degradation for the flow rates studied, (2) it could function under diffusion-limited conditions for all the flow rates applied, whilst P25 photocatalyst film could operate under reaction-limited conditions at higher flows.

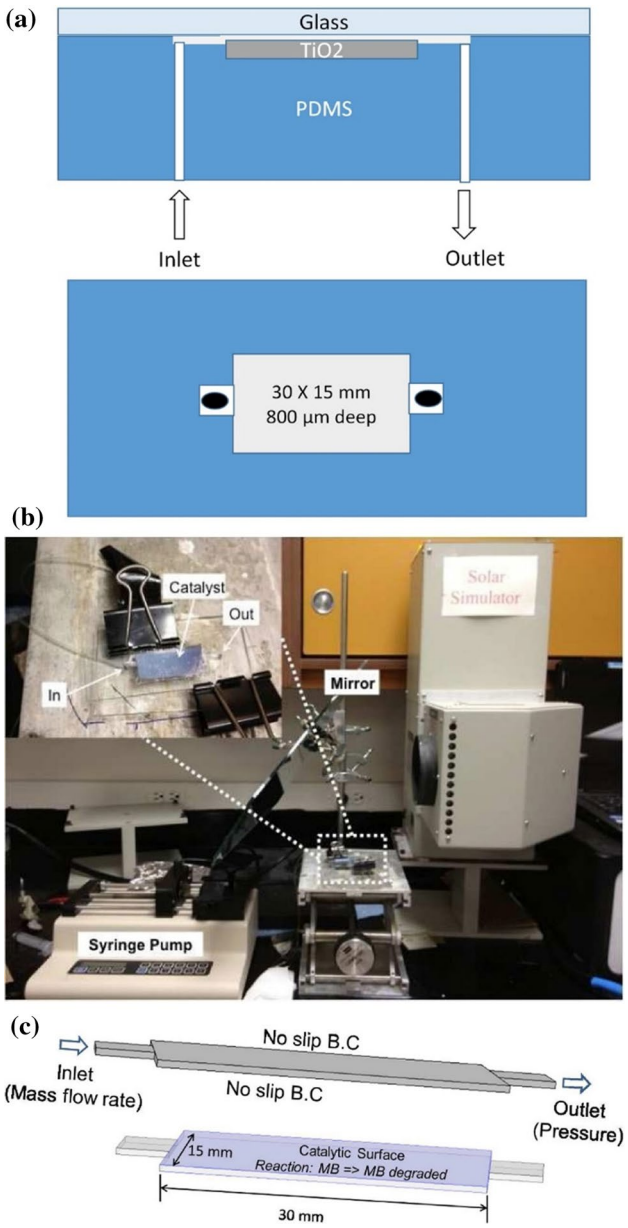

Fig. 14 **a** Top and side views of the microfluidic reactor device developed by Jayamohan et al. (2015) for studying the photodegradation of methylene blue, **b** experimental set-up designed for carrying out the photodegradation of methylene blue in the microfluidic device with the inset in the top left corner showing the actual microfluidic reactor with titania nanotubular arrays photocatalyst embedded thereon and **c** boundary conditions applied in the simulation of the three-dimensional model by Jayamohan et al. (2015) whereby it was assumed that methylene blue molecules need to diffuse to photocatalyst surface for being degraded threat. This figure has been reproduced from Jayamohan et al. (2015) with the permission of Elsevier (Copyright © 2015 Elsevier B.V. All rights reserved) under licence number 4855170131604 (for both print and electronic formats)

Subsequently, the enhanced performance of the titania nanotubular arrays photocatalyst over P25 had been associated with a better diffusion of the reacting species involved and better charge separation. Jayamohan et al. (2015) equally developed a model to simulate methylene blue degradation in the microfluidic channel using COMSOL Multiphysics (Fig. 14), and based on the outcome of the simulations, it was reported that the effect of the diffusion coefficient on the fractional conversion turned out being more sensitive than that obtained from the rate constant. Although Jayamohan et al. (2015) brought forward that the model was amenable to modifications for accommodating pollutants having different diffusion coefficients, different channel geometries or different rate constants, it remained rather challenging to compare the performance of the titania nanotubular arrays photocatalyst with other similar systems because of the variability in flow rates which can exist, variations in channel geometries, differences in concentration of pollutant species and actual surface area of photocatalyst involved in the reaction. Yet, Jayamohan et al. (2015) could eventually use the dimensionless Péclet number to interpret the results. More recently, Liu et al. (2018) have constructed an on-column TiO_2 photocatalytic microreactor in microchannel to study the photocatalytic degradation of rhodamine B and thereafter reported that the photocatalysis kinetics as per the Langmuir–Hinshelwood model in the confined microsystem turned out being tenfold greater than that obtained in macrosystem which had a pseudo-first-order rate constant of 0.033 min^{-1}. Liu et al. (2018) also reported that the photocatalytic activity of the immobilized TiO_2 photocatalyst in the microreactor had good stability under flowing conditions.

However, microfluidic reactor scale-up, which is more of significance when having to remediate larger volumes of contaminated water, is particularly demanding since the working dimensions of the microfluidic devices have to be kept in their appropriate range so that favourable flows and transport regimes are preserved and the same excellent performances are maintained (Yusuf et al. 2018). Notwithstanding the progress achieved in microfluidic reactor design and operation over the recent years, there still remain some hurdles before the robust scale-up of microfluidic reactors becomes fully mastered. One of them is the need to accommodate large processing throughputs with sufficient residence time. This, in turn, will require many microfluidic reactor units to be installed in a most optimal configuration after implementing the best suited numbering-up strategy (Su et al. 2016; Rossetti and Compagnoni 2016; de Sá et al. 2018, 2019; Yusuf et al. 2018). The requirements to still have a uniform enough distribution of fluid and incident light in every microfluidic reactor then also become rather complex to achieve. Moreover, potential scale-up using microreactors added up in parallel might also not be sustainably feasible because of the additional auxiliary equipment then needed at increased costs (Rossetti and Compagnoni 2016).

Hence, there has always been the need to continually develop more novel photocatalytic reactor configurations

which are optimized in their performance and photodegradation efficiency for dyes and other pollutants. Hereinafter, some recent innovative photocatalytic reactor configurations are briefly revisited in Table 9 and other specific configuration and various process operation-related novelties are discussed in more depth below. One interesting feature of these studies is that many of the experimental methods were tailored (as far as practicable) to perform the laboratory-scale and/or bench-scale photocatalytic processes reactions in a way which would give an acceptable 'ground plan' for considering potential scale-up routes eventually leading to potential industrial-scale application. Indeed, in these studies and others, many of the process parameters likely to influence the photocatalytic degradation of the pollutant have been examined. Amongst other, the parameters have included extent of reusability and regeneration, adherence of particles on support material during immobilization process and actual flow-controlled processes, contact angle analysis, influence of type of membranes, interactions of differently synthesized nanophotocatalytic materials in the specific reactor configuration and flow regimes, mass analysis of intermediates and final expected degradation products, mass transport and resistances to mass flow, holes scavenger formation analysis, effects of recirculating mode, condensate flow channel and film thickness, modelling approach of photocatalytic degradation process and reactor configuration modelling, energy consumption, costs involved (e.g. costs for reactants/chemicals like solvents and costs for construction, installation and operation), and last but not least, effects of irradiation intensity, irradiation duration, sonication temperature and time.

Athanasiou et al. (2016) have developed a comprehensive design of an upgraded photocatalytic membrane water purification reactor using advanced titania nanomaterials which comprised, in its final configuration, the following main components and features (Fig. 15): 30 monolithic multichannel ultrafiltration membranes with each membrane counting 19 channels; fibre optics (31 optical fibres) in view of obtaining energy autonomy and cater for uniform lighting provision throughout the reactor interiors; reactor shell enclosing the totality of the fibre optics and multichannel monolithic membranes; recirculation tank; clean water tank; a reactor cover; and optimized pressure drop profiles along membranes. Furthermore, Athanasiou et al. (2016) enhanced the photodegradation capability of the novel photoreactor by minimizing the static volumes of raw and intermediate flow channels, and in doing so, the photocatalyst mass-to-the fluid mass ratio prevalent within the static reactor volume could be expected to augment and promote photocatalytic reactions. Summing up, Athanasiou et al. (2016) concluded that the innovative design formulated was in line with the ultimate goal of scale-up for an eventual treatment of a relatively large flow of 50 m^3 daily of contaminated water. In another interesting work, Colombo and Ashokkumar (2017) indicated that the CSTR configuration for process operations tends to be limited to the use of fixed-bed reactors, and this leads to significant decrease in the efficiency of the process. In an attempt to address the latter concern, these workers have developed combined dispersed photocatalyst–CSTR system for continuous operation using two dyes (rhodamine B and metanil yellow) and a C-doped TiO_2 micron-sized catalyst. Colombo and Ashokkumar (2017) reported some very encouraging features of their system in that it could give an increase in degradation reaching as high as 110% in comparison with the batch mode of operation, and also to more prolonged (> 42 h) of continuous operation with no blockage of the filter material and no catalyst deactivation. Additionally, the incorporation of short and periodic sonication was found to be effective in inhibiting catalyst accumulation on the filter surface and hence leading to stable flow regimes (Colombo and Ashokkumar 2017). From reactor optimization studies involving differently combined Ag, Pd and/or TiO_2 nanoparticulate photocatalyst assessed for the degradation of methyl orange and Rose Bengal, Pickering et al. (2017) have demonstrated the significance of configurational effects of the plasmonic phenomena occurring in photocatalytic reactors. Specifically, Pickering et al. (2017) showed that a layered configuration of plasmonic and photocatalytic phases in a recirculating thin film photoreactor makes an optimal use of plasmonic enhancement (twofold improvement in comparison with a much lower 10% improvement obtained in control experimental runs) towards photocatalysis and that, on the whole, geometric arrangement is a crucial aspect to be considered in such systems. According to the latter workers, the use of the layered configuration improves process efficacy through lesser blockage of the active TiO_2 surface sites, minimized inhibition of light absorption and less oxidation of silver when in contact with TiO_2. Consequently, the cascading benefits to the photocatalytic reaction environment are (1) higher available area of photocatalyst per illuminated area and absorption area of photocatalyst in metal-modified photocatalysts and (2) a more realistic configuration of the reactor sustaining flow experiments.

Mosleh et al. (2018) have fabricated $CuO/CuO_2/Cu$ NPs which were assessed for their photocatalytic performance in degrading safranin O and methylene blue in an innovative rotating packed bed reactor (RPBR) comprising blue light-emitting diode as the irradiation source (Fig. 16). (Mosleh et al. 2018) reported a number of interesting results and enhanced features of the RPBR which led to having better degradation efficiencies and relatively less irradiation time in comparison with conventional reactor systems. Moreover, the high centrifugal field and the use of a distributor in the reactor system for the dispersion of solution led to the formation of thin layers and small droplets from the thick

Table 9 Main design and process operation features incorporated in recent novel photocatalytic reactors developed to enhance dye degradation capability

Dye(s)	Photocatalyst(s)	Type of reactor(s) studied	Innovative feature(s) in study	Main observations	References
Acid violet 7	ZnO/polypyrrole composite	Continuous annular reactor using immobilized photocatalyst	Light-emitting diodes lamp arranged centrally to provide visible light irradiation Effect of mass transfer assessed using a modelling approach based on a full 3-D convection–diffusion–reaction model	Photocatalytic degradation of acid violet 7 was kinetically controlled Using visible light arranged centrally in continuous annular photocatalytic reactor is a feasible design configuration	González-Casamachin et al. (2019)
Methylene blue, Direct Blue-15, malachite green and amaranth	TiO_2 immobilized on mosquito net	Photocatalytic reactor providing for UV light-emitting diodes (LEDs)	Use of different light exposures (6, 12, 18, 24 and 30 UVLEDs) in experiments	Augmenting exposed surface area of TiO_2-coated on mosquito net support with more and more UVLEDs brings enhanced photodegradation	Jo and Tayade (2016)
Real industrial dye wastewater	Zinc oxide/polyethylene glycol (PEG) NPs	Membrane photocatalytic reactor	Reactor performance examined using four different membranes	Zinc oxide-PEG NPs and ultrafiltration-polypiperazine-amide (UF-PPA) had significant potential in improving fouling mitigation from occurring in reactor UF-PPA membrane outsmarted in performance because of higher amount of normalized flux in comparison with other membranes	Desa et al. (2019)
Brilliant blue and tartrazine yellow	UV-C/H_2O_2/TiO_2	Photocatalytic flow reactor using PET bottles	Bottoms of two water bottles were linked horizontally in modified system view to avoid junction of tops present in initial reactor design	Modified reactor configuration gave only removal rates of dyes of 99% after 240 min, whereas first design gave similar rates in 180 min (plausibly because altered volumes of sample in chamber and treatment and mixing regimes of phases)	Do Nascimento et al. (2019)

Table 9 (continued)

Dye(s)	Photocatalyst(s)	Type of reactor(s) studied	Innovative feature(s) in study	Main observations	References
Methyl orange	Hematoporphyrin/nitrogen-doped TiO_2 nanohybrid (both in suspended and immobilized states) Immobilization done onto quartz Raschig ring (qRasR) random packing and wire gauze structured packing (WGSP)	Visible light helical flow photoreactor	Experimental runs conducted under three process configurations, namely slurry reactor with suspended nanohybrids powders, nanohybrids coated on WGSP immobilized in region between tubes photoreactor and a reactor configuration with the active space of the reactor randomly filled with nanohybrids-coated qRasR	89.4% MO was degraded during 60 min using mild hematoporphyrin grafted of 3HP/N-TiO_2 nanohybrid coated on quartz Raschig rings (3 layers thick) Random packing gave the highest efficiency and had the lowest energy consumption	Mesgari and Saien (2017)
Acid orange 7	Immobilized undoped, N-doped and B-doped TiO_2 composite filter membranes (quartz fibre filters as support material)	Photocatalytic membrane reactor	Reactor incorporated combined photocatalytic degradation and dead-end filtration as dye removal processes Operation under dark and ultraviolet irradiation	Optimization of doping parameters, namely type of dopant and the respective concentrations on TiO_2 filters affects removal of Acid orange 7 under UVA irradiation Elevated doping concentrations normally observed to give enhanced membrane removal in comparison with lower lowest dopant concentration Further analysis needed to probe the influence of visible light or sunlight on efficacy of doped membranes in photocatalytic membrane reactor	Hatat-Fraile et al. (2017)

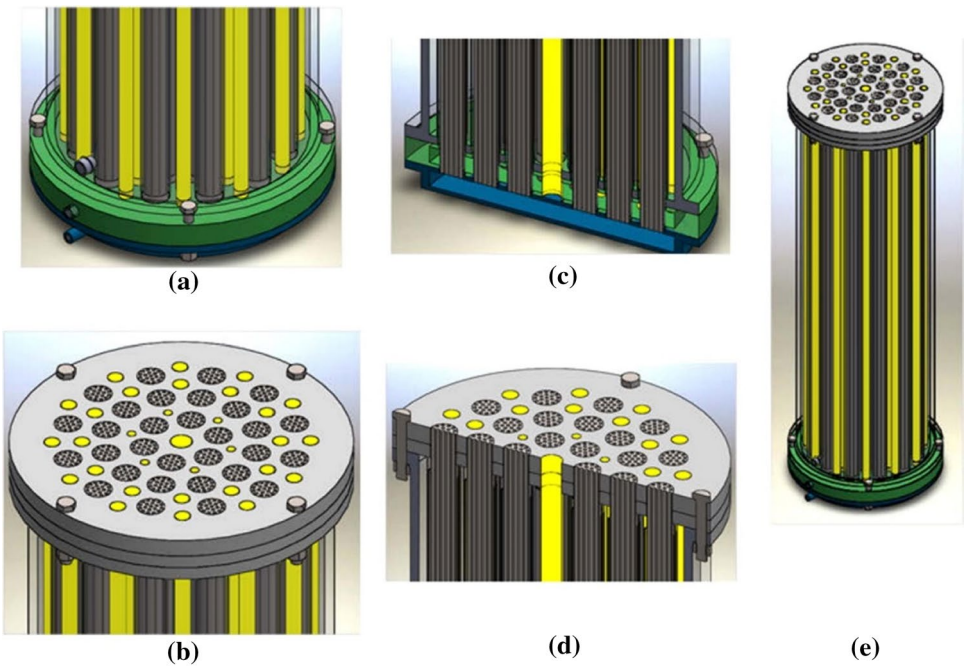

Fig. 15 Images of **a** the lower base, **b** the upper base of the assembled photocatalytic reactor, **c**, **d** the corresponding cross sections and **e** the finally assembled upgraded continuous-flow photocatalytic reactor comprising monolithic multichannel ultrafiltration membranes and optic fibres developed by Athanasiou et al. (2016). The essential features comprise: (1) 30 monolith multichannel ultrafiltration membranes each of diameter 29 mm and 1.23 m long and each membrane consisting of nineteen 3.5-mm-diameter channels and (2) 31 optical fibres (each 1.18 m long) whereby one optical fibre of diameter 23.5 mm is placed in the centre and six optical fibres of diameter 9.5 mm and 24 optical fibres of diameter 17 mm have been placed cyclically in the photocatalytic reactor. This figure has been reproduced from Athanasiou et al. (2016) with the permission of Elsevier (© 2015 Elsevier B.V. All rights reserved) under licence number 4855170331342 (for both print and electronic formats)

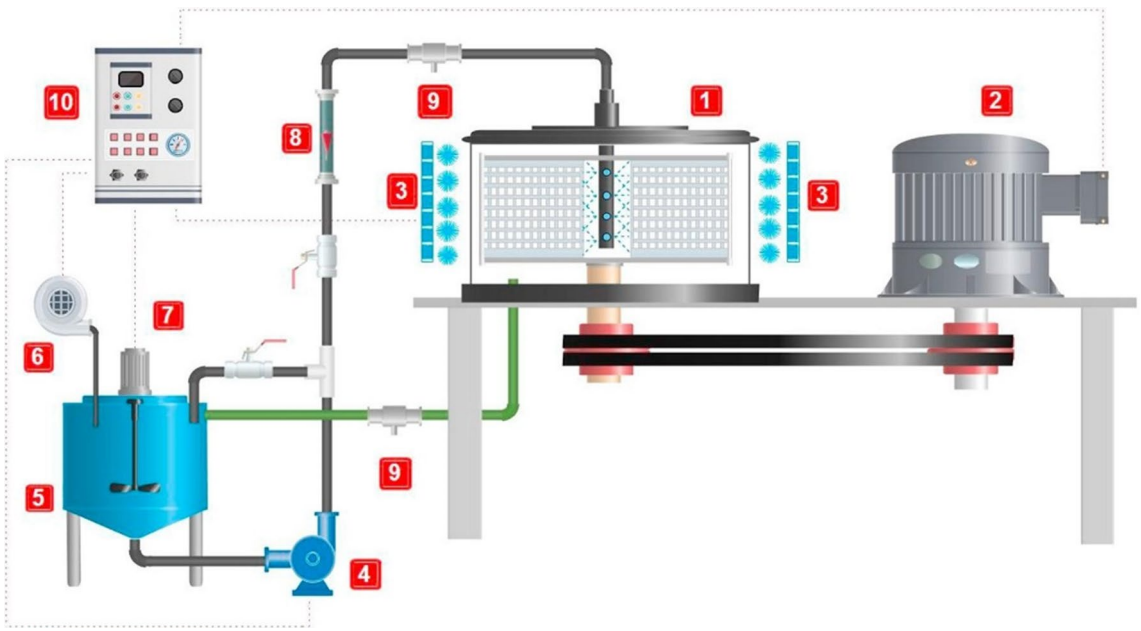

Fig. 16 Rotating packed bed reactor developed by Mosleh et al. (2018) which comprises a rotating porous packed bed of porosity 0.85, bed height 40 mm, inside diameter of 30 mm and rotation speed ranging from 400 to 1200 rpm (1), motor (2), stripe LED (3), pump (4), storage tank (5), air pump (6), stirrer (7), flow meter (8), sampling point (9) and a control box to control the rotational speed of the motor (10). This figure has been reproduced from Mosleh et al. (2018) with the permission of Elsevier (© 2017 Elsevier B.V. All rights reserved) under licence number 4855170487624 (for both print and electronic formats)

films, as a result of which the liquid–solid interfacial area was considerably increased (Mosleh et al. 2018). Besides the enhancement of mass transport, the reactor developed by Mosleh et al. (2018) also allowed for a proper distribution of light which was suitable to sustain adequate photocatalytic activity. Recently, Das and Mahalingam (2020) have developed a novel reactor which contained an immobilized photocatalytic film within an internal loop airlift reactor (Fig. 17). On basis of their findings, Das and Mahalingam (2020) discussed the merits of the novel reactor developed and indicated that only 2 h had been sufficient to achieve a near total mineralization of the very recalcitrant remazol turquoise blue under ultraviolet irradiation, and the design was relatively simple and could be amenable to scale-up. Still, Das and Mahalingam (2020) reported that use of doped photocatalysts and waste polystyrene as a potential substrate under sunlight could bring more advantages to the system in its being then cost-efficient and eco-friendly. In an earlier study, Sheydaei et al. (2019) synthesized Ce-, La- and Ho-doped ZnO photocatalyst to be used in a continuous-flow sono-photocatalysis/membrane separation reactor for the visible light sono-photocatalytic removal of Reactive Orange 29. This study was particularly interesting in its scope to taken into account a large number of process parameters and undertake a Taguchi optimization of the photocatalysis process run in the sono-photocatalysis/membrane separation. The removal of the RO29 dye by the Ce-ZnO photocatalyst via the sono-photocatalysis process was observed to be significantly higher than those obtained via photocatalysis, sonocatalysis and sonolysis, and under optimized operational conditions of photocatalyst concentration at 1.5 g L^{-1}, initial pH 10, a hydraulic retention time of 50 min, the RO29 removal efficiency was very high at 97.84% via the sono-photocatalysis/membrane separation reactor process (Fig. 18). In addition, Fig. 19 and Fig. 20 give two examples of innovative flow-type photoreactor systems.

Still more on innovative photocatalytic reactor systems, there is indeed quite a number of recent patents in the literature (https://patents.google.com/) which compile reports demonstrating prowess in the development of novel designs for photoreactor systems intended to house configurational conditions which are conducive for highly efficient photochemical reactions and processes leading to the degradation of different pollutants and/or purification of contaminated liquids. Some of the configurational conditions encountered during the writing of this review can be lumped into those related to enhancing fluid exchange and fluid flows using structural components like blades and baffles, adjustable configurations of optical components and variable/optimized extents of illumination, or still variable operating

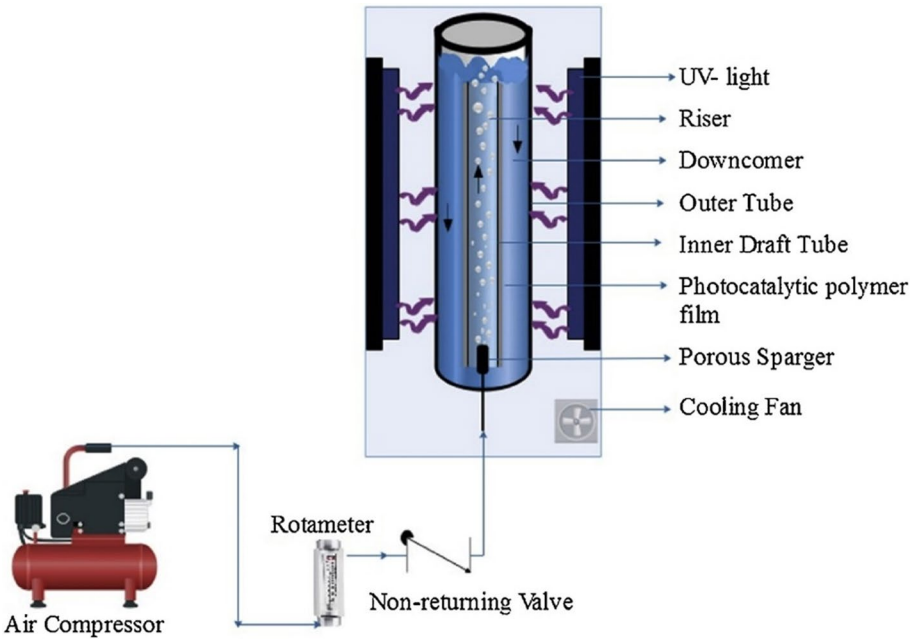

Fig. 17 Internal loop airlift photocatalytic reactor developed by Das and Mahalingam (2020). As per the descriptions in Das and Mahalingam (2020), this new design comprised an internal loop airlift photocatalytic reactor constructed of quartz glass column 8 cm ID and 0.3 m long (volume = 1.5 L) housing an inner draft tube of 2/4/6 cm OD (22 cm in length); the reactor is installed in a 60 cm × 50 cm wooden chamber with vertically fixed ultraviolet lights of intensity 1.97 Klux on the walls; and having a mixing or liquid circulation brought about through air bubbling using a sintered porous sparger located at the bottom of the reactor through an inner draft tube. This figure has been reproduced from Das and Mahalingam (2020) with the permission of Elsevier (© 2019 Elsevier B.V. All rights reserved) under licence number 4855170706370 (for both print and electronic formats)

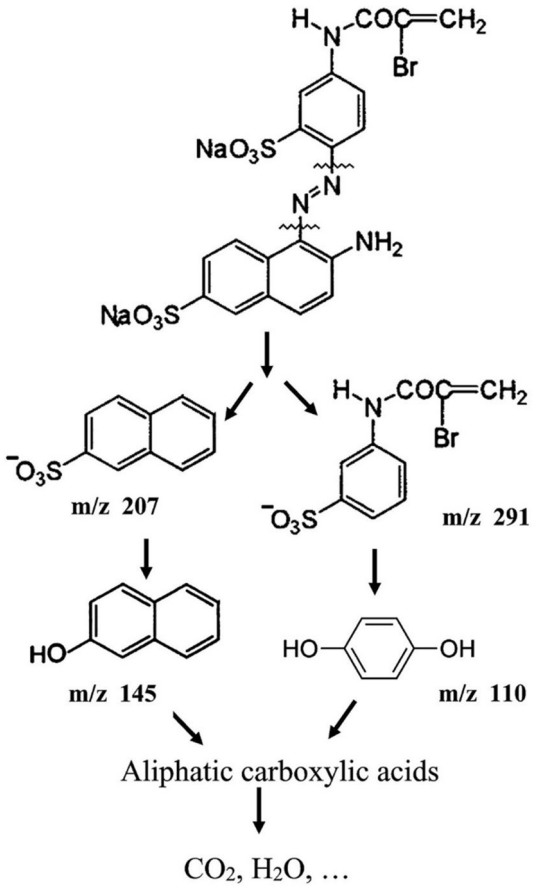

Fig. 18 Mechanism for the degradation of Reactive Orange 29 via the sono-photocatalysis process (based on GC–MS data) proposed by Sheydaei et al. (2019). According to the latter workers, the sono-photocatalytic degradation of RO29 under optimized conditions brought a 50% removal of chemical oxygen demand, and a total organic carbon removal of 45% (under the best operational conditions) which was considered a relatively high degree of mineralization. This figure has been reproduced from Sheydaei et al. (2019) with the permission of Elsevier (© 2019 Elsevier B.V. All rights reserved) under licence number 4855170883735 (for both print and electronic formats)

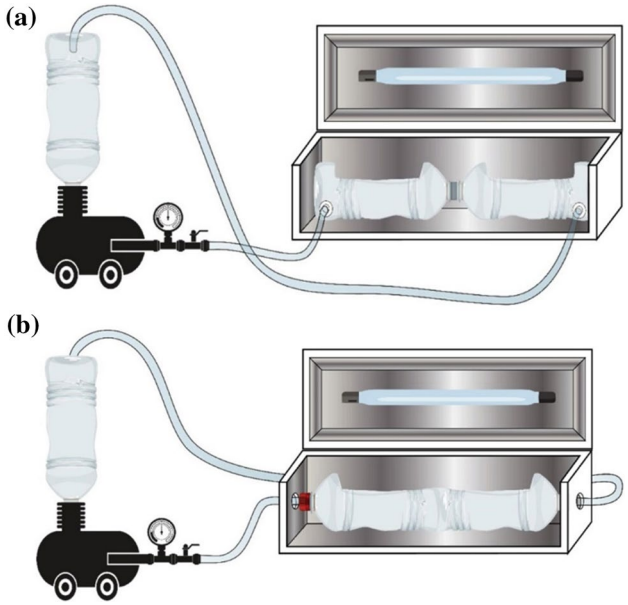

Fig. 19 **a** Arrangement of PET bottles in PET flow reactor with about 160 cm^2 of PET area removed from the side of every of the two PET bottles horizontally aligned so as to enable direct light harvesting in solution and **b** modified PET flow reactor configuration whereby bottoms of both PET bottles have been joined horizontally in view of avoiding junction of tops in design shown in **a** (a zone whereat no reaction is expected because of a paucity in light penetration) developed by Do Nascimento et al. (2019). This figure has been reproduced from Do Nascimento et al. (2019) with the permission of Elsevier (© 2019 Published by Elsevier Ltd.) under licence number 4855171052085 (for both print and electronic formats)

photodegradation modes which can be either standalone, combined or hybridized with other degradation processes such as ozonation. The innovative design features originate from diverse areas of system improvement and optimization and eventually contribute in significantly better photochemical performances. For example, Lin and Huang (2017) (Source: Lin K and Huang YJ, 2017. *Photocatalyst apparatus and system.* U.S. Patent Application 15/607,567; https://patents.google.com/patent/US20170259254A1/en) reported that the fine-array porous materials present in the photocatalyst equipment could efficiently reflect the ultraviolet light emitted by the optical pump and that the resulting illumination had led to considerably higher photocatalytic activity of the photocatalyst system and also lowered the impairment to living organisms caused by the ultraviolet light. In an invention coming later, Keith (2018) (Source: Keith J, Uvairx Inc, 2018. *Reaction Core System for Photocatalytic Purifiers*. U.S. Patent Application 15/740,322; https://patents.google.com/patent/US20180185539A1/en) also explored the interplay of system components (frame housing the source of light, blades and coating of material) and their mutual angular arrangements in a photocatalytic reactor to induce reflection of part of the light emitted by the source of light onto certain parts of the exterior surface of an adjacent blade. Still on the relative interplay of system components, Barreto (2019) (Source: Barreto RD, Purdue Research Foundation, 2019. *Continuous-flow photo-reactor for the photocatalytic destruction of water-soluble ethers*. U.S. Patent 10,364,167; https://patents.google.com/patent/US10364167B2/en) invented different photocatalytic systems whereby one comprised a series of photoreactors operating on a continuous-flow mode, and another system which consisted of at least 2 photoreactors in parallel connection and operating in continuous flow too with glass materials coated with the catalyst. In another example of an interesting invention coming earlier, Schuetz (2018) (Source: Schuetz R, 2018. *UV Light Reactor for Contaminated Fluids*. U.S. Patent Application 15/924,255; https://patents.google.com/patent/US20180265382A1/en) developed a system for

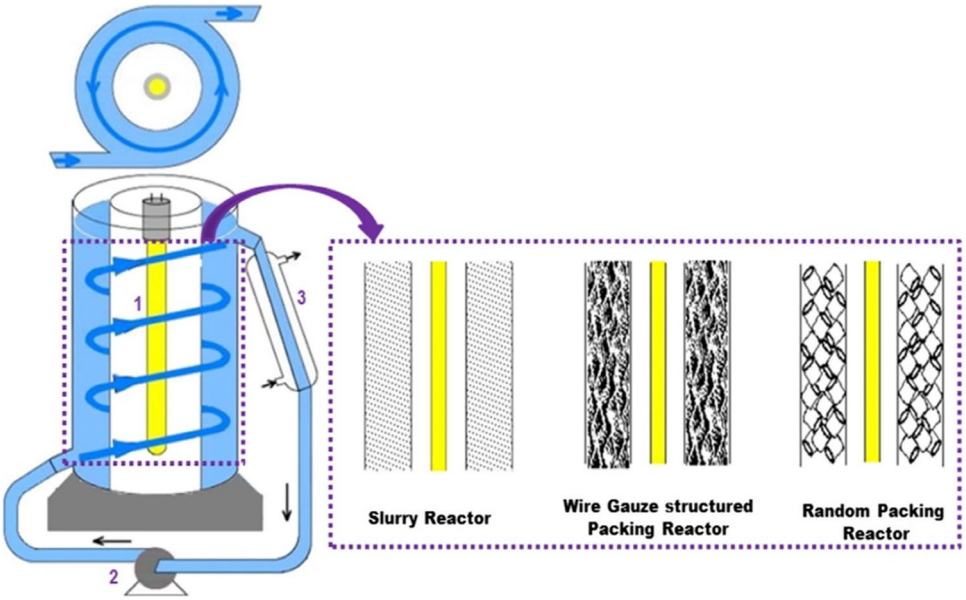

Fig. 20 Schematic diagram of the helical flow photoreactor developed and operated in the random packing reactor, wire gauze structured packing reactor and slurry reactor configurations by Mesgari and Saien (2017). Labels are metal halide visible lamp indicated by 1, circulating pump denoted by 2 and water flow condenser indicated by 3. Based on the descriptions of Mesgari and Saien (2017), the operation of the annular photoreactor occurs in a closed circuit configuration with recirculation of contents at 45 mL s^{-1} of flow rate; the reactor is irradiated with visible light from an Osram 150 W lamp located in the axis of annulus, and the tangential inclined inlet allows material flow in the reactor to follow a precise upward helical path around the source of light until the contents reach the top tangential downward exit. This figure has been reproduced from Mesgari and Saien (2017) with the permission of Elsevier (© 2017 Elsevier B.V. All rights reserved) under licence number 4855171221234 (for both print and electronic formats)

treating a contaminated fluid using UV light. The latter system comprised several removable baffles (loaded with photocatalytic coatings) arranged at pre-set radial distance within the system boundaries which gave rise to meandering pathways running parallel to the light source for exposing the fluid to the ultraviolet light over the full length of the pathways. In the invention of Allcroft (2017) (Source: Allcroft I, CatalySystems Ltd, 2017. *Photocatalytic reactor stator and method of use*. U.S. Patent Application 15/501,672; https://patents.google.com/patent/US20170225139A1/en), a photocatalytic reactor stator was designed with a specific arrangement of surfaces which enabled fluid flows that eventually contributed in enhancing the performance of the system as a photocatalytic reactor. In this invention, the arrangement of surfaces and fluid flow regimes had increased the movement of the photocatalyst which induced larger catalyst surface areas being exposed to the reacting species and source of ultraviolet light. In their disclosure, Yongbing et al. (2017) (Source: Yongbing XIE, Cao H, Sheng Y and Li Y, Chinese Academy of Sciences Institute of Process Engineering, 2017. *Ozone-photocatalysis reactor and water treatment method*. U.S. Patent Application 15/544,460; https://patents.google.com/patent/US20170369346A1/en) give the details of an integrated water treatment system combining ozonation and ozone (O_3) photocatalysis housed within one reactor whereby the strong oxidizing influence of O_3 on unsaturated bond-containing pollutants and the pronounced removal effect of O_3-photocatalysis and photocatalysis on carboxylic acid pollutants are harnessed. The latter design improved the matching degree between O_3 and UV and also overcame the limitations associated with poor efficiency of sewage treatment and high equipment cost. Other interesting inventions which embody novel and more effective photocatalytic reactor systems harnessing the positive influences of tunable/controllable fluid flow regimes, hydrodynamic behaviours, degree of illumination and/or radiation patterns are described in the following patents:

- *Development of a photochemical reactor incorporating a fluid flow-through device* in 'Usami H, Kuroda Y and Imaizumi M, Showa Denko KK and Shinshu University NUC, 2017. *Fluid flow vessel and photochemical reactor*. U.S. Patent Application 15/325,605' (https://patents.google.com/patent/US20170136438A1/en)
- *Flow reactors and flow processes developed to obtain modular, flexible, high-efficiency and high-throughput photochemical flow reactor system* in 'El Jami F, Gremetz SMF, Horn CR, Lobet O and Maury A, Corning Inc, 2020. *Flow reactor for photochemical reactions*. U.S. Patent Application 16/491,041' (https://patents.google.com/patent/US20200016568A1/en)

- *UV-LED reactor concept housing UV-photoreactions or UV-photoinduced reactions and with a reactor design endowed with precise control of both fluidic and optical milieus* in 'Taghipour F, University of British Columbia, 2018. *UV-LED collimated radiation photoreactor*. U.S. Patent 9,938,165' (https://patents.google.com/patent/US9938165B2/en)

Limitations and research directions

The remediation of dye-laden waters is indeed a serious and still challenging environmental issue which is garnering significant and sustained research efforts worldwide. In particular, the area of research dealing with the various aspects of heterogeneous photocatalysis for dye remediation has been propagating very fast. More research is to follow since certain techno-economic issues still persist and limit full-fledged process operation. Based on the above analysis and discussions made within the scope of research articles scouted and examined, it becomes pretty evident that the synthesis and assessment of doped photocatalytic materials for dye degradation is, first of all, a very fertile research discipline. *Fertile* in a number of ways, viz. with respect to the number and very wide variety of heteroatoms which can be incorporated into a semiconductor material or combination of such materials, with respect to the extremely high number of types and adaptations of the synthetic procedures of fabrication and functionalization of the doped photocatalysts, with regard to the very large panoply of dye molecules which have been assessed as model dye molecule, with respect to the breadth and depth of analysis conducted in view of elucidating the influences of a series of environmental factors expected to play a certain determining role in a specific photocatalytic degradation reaction, with regard to the analytical techniques and data processing tools (e.g. empirical modelling, mathematical analysis and modelling, and statistical analysis) employed to present and interpret primary datasets, with regard to monitoring and proposing realistic reaction mechanisms of dye photocatalytic degradation at the atomic and molecular levels, and last but not least, with regard to the multifarious efforts (such as immobilization, membrane development, reactor design and process scale-up) rather recently started in view of dealing with issues related to photocatalytic process design and optimization in relation to dye degradation.

Indeed, following the above analysis, it becomes quasi-undisputable to infer that painstaking research efforts are here being made fast and consistently in several regions of the world by different research groups to design and examine the dye degradation performance of doped photocatalysts. The resulting findings are all, in their own respective context, bringing some form of novel information plausibly important to advance the understanding and potential application of photocatalytic dye degradation processes. It has been interesting and encouraging to note that many different dyes (different in chemical and physical properties) have been assessed in their photocatalytic degradation process by an even larger number of photocatalysts under variable light illumination regimes comprising UV light, visible light and sunlight. This specific trend of considering dye and photocatalyst variability is interesting because it somehow implies that there is not a general combination of these species which can be held as a representative model. This being most ostensibly the case, further work is hence extensively needed in making fair attempts to standardize such heavily complex interactions of chemical species in variable conditions. Notwithstanding the progress achieved so far, there are still a number of limitations which will require earnest consideration in the area of photocatalytic degradation of dyes by doped photocatalysts. When viewed as scientific and engineering challenges, these limitations are expected to foster further research and development in developing more potent photocatalysts (which is, for the least, being green in their synthesis, stable, reusable and cheap in use) and more efficient photocatalytic reactor configurations for treating more and more complex dye-laden waters.

Right at the outset, it is crucial to understanding and stressing that the limitations discussed below cannot not be (so) readily downplayed (for some possible gain in simplification of the underlying photocatalytic process dynamics) when it comes to finding much more comprehensive ways for developing such doped photocatalytic dye-degrading systems which will bring a definite and measurable restorative effect to the issue of dye-laden pollution which continues to pervade in many real locations. Making a start onto some of the major limitations and research avenues, it is observed that the efficiency of photocatalyst recovery and the costs associated thereof remain as process bottlenecks for large-scale implementation of photocatalytic water treatment processes using doped photocatalyst. It is imperative to encourage the development of suitable methods for recovering spent doped photocatalysts in an economic and cost-effective way given such processes are expected to be expensive because of their inherent complexity, and the sought purity of raw materials involved and production costs of doped photocatalysts. Attached to an effective and efficiency post-separation and recovery of nanoscale doped photocatalysts at large-scale operation is also the need to ensure that immobilization of these nanomaterials be feasible on relatively larger supports or immobilizing substrates. In this same line of thinking with regard to sustaining threshold photocatalytic efficiencies in large-scale doped immobilized photocatalytic reactor units, other considerations which then become relevant and of high significance for analysis are the possible rate of erosion of immobilized doped, any rate

of substrates corrosion, any such fluctuations in mechanical strength, structural integrity, shear behaviour, creep and failure behaviour of the composite-doped nanophotocatalyst-supported ensemble. Indeed, as Sharon et al. (2016) have rightly proposed, there is a need to investigate the stability of nanosized photocatalytic composites using Tafel plots in view to probe into their corrosion current and corrosion potential. Additionally, the latter workers also suggested that thermodynamic analyses be also made to quantify parameters such as the free energy of corrosion and enthalpy of corrosion before the nanosized photocatalytic composites may qualify for commercial use.

Delving deeper in the analysis, one of the most noteworthy observations made when preparing this review has been that there is an overwhelmingly large number of studies which have examined the photocatalytic degradation of a synthesized doped photocatalyst material using one single-dye molecule species as the model pollutant. Gratifyingly, the number of patents which have been filed on the synthesis of photocatalyst materials capable of dye degradation has also been increasing since a decade or more. (Some recent examples of such patents are listed in Table 10.) Whilst it is believed that these studies are all *original* in their respective results and interpretations and have hence progressively been contributing to an *incremental* understanding of the photocatalytic degradation of dye molecules under a whole range of variable environmental factors, it still remains a major challenge to come up with some *general* and widely applicable *model dye wastewater* that could be used as a benchmark to assess and compare the performances of several doped photocatalysts at a time and under quasi-similar operational constraints. At present, the wide variations in reaction conditions and characteristics of the photocatalyst material(s) and dye(s) examined in the uncountable photocatalyst–dye systems does not make ample room for an *objective* comparison of the performances. In the event such objective comparisons were possible, the development of standard photocatalyst assessment kits could have been probably envisaged. Moreover, it also remains a major challenge to couple the formulation of one benchmark model dye wastewater with one representative photocatalytic process or photocatalytic reactor design which in turn will (have to) embody sufficient resilience in performance after different modes of operation are selected to accommodate changes in process parameters. Hence, the state of affairs with regard to representativeness of results and their reliable transferability to industrial application in doped photocatalytic dye degradation processes remain pretty complex and highly demanding in terms of further research, analysis and process intensification when designing large-scale photoreactors. In the same breath, elucidating the precise range of intermediates and final photodegradation products, their respective characteristics, fate and set of interactions in the ultimate receiving environments remain collectively a pretty 'grey area' which requires significant research work.

As at present, and equally in this review, it was difficult to make an objective comparison of the dye degradation dynamics of the hundreds of dye-doped photocatalyst(s) pairs tested. It was, however, encouraging to note that since some years, appreciable research efforts have been devoted in studying binary-, ternary- and four-dye systems. The corresponding results have shed some new insights with regard to the complexity in degradation behaviour of such multicomponent dye systems in comparison with single dye-single doped photocatalyst systems. Yet, an extrapolation of such multicomponent dye systems to robust full-scale photocatalytic reactor systems seems to be limited as they do not match the highly variable compositions and complexity of real dye-laden effluents. In corollary, it then becomes very crucial to develop multifunctional doped photocatalysts which could be endowed with such environmental factor-dependent *self-modulated* properties which reduce their selectivity towards one, two or three specific dyes, but instead allows them to interact with and degrade many more dyes in a highly competitive milieu which could be justifiably expected to prevail in real textile effluents. Such tailor-made requirements in one doped photocatalyst will still require substantial research and development ahead.

Another area of research which can be further expanded for enhancing the photocatalytic degradation of dyes using doped photocatalysts is working out such schemes which integrate optimized Pickering emulsions (Mohaghegh et al. 2015; Nawaz et al. 2017; Fessi et al. 2019; Li et al. 2019) within the photocatalytic reactor system design. There are few studies (though not restricted to dye degradation processes) which have made gratifying efforts in using Pickering emulsions to prepare novel materials which had finally contributed in enhancing efficiencies and performance of a specific system. In another study, Shi et al. (2019b) reported that a Pickering emulsion stabilized by TiO_2 Janus particles (fabricated using toposelective surface modification approach) had given the best photocatalytic performance and very good degradation efficiencies in regard to the degradation of high-concentration kerosene and nitrobenzene wastewaters. Hence, it will be an interesting set of further work wherein the knowledge acquired and relatively facile techniques devised in other similar systems can be borrowed to polish the effectiveness of doped photocatalyst synthesis in view of reaching enhanced efficiencies of photocatalytic dye degradation systems.

When analysing the literature scoped for this review, it has been observed that a relatively large number of possible mechanisms have been composed for rationalizing the different photocatalytic degradation processes of dyes. Whilst these mechanisms sound pretty logical and acceptable at the

Table 10 Recent patents on the synthesis and testing of doped-type catalyst materials for their potential to degrade dyes under photocatalytic conditions. These data have been compiled in a very concise format based on the results returned by the search engine 'Google Scholar' (https://scholar.google.com/) from a search using the keywords 'patents doped photocatalytic dye degradation' for the year 2016 and onwards. More elaborate details of each example can be obtained from the corresponding source

Catalyst material(s)	Dye(s)	Highlights of characteristics of catalyst material(s)	Source
Fe-doped TiO_2 photocatalytic porous magnetic microspheres	Methylene blue	Efficient catalyst recovery Porous structures of catalyst (having large specific surface area and more reactive sites) enable diffusion and mass transport of macromolecular reactants between surface and bulk phase of catalyst	Jiang H, Yiqun DENG, Yang H, Liang T, Xiaopeng QI, Zhuowu ZHEN, Rigang NIE, Yucheng LV and Wenyu SHEN, Jiangxi University of Science and Technology, 2019. *Method of preparing large-size high-porosity Fe-doped photocatalytic porous magnetic microspheres and uses thereof*. U.S. Patent Application 16/395,218 (https://patents.google.com/patent/US20190344245A1/en)
I-doped $Bi_2O_2CO_3$ nanosheets and molybdenum disulphide nanoflakes modified nanocarbon fibre membrane	Rhodamine B	High surface area High efficiency for light absorption efficiency Stable catalytic performance Reusable with high photocatalytic efficiency for rhodamine B degradation	Lu J and Chen D, Soochow University (Suzhou Univ), 2019. *Iodine-doped bismuthyl carbonate nanosheet and molybdenum disulphide-modified carbon nanofibre composites, preparation method and application thereof*. U.S. Patent Application 16/171,317 (https://patents.google.com/patent/US20190127883A1/en)
Pucherite and N-doped graphene quantum dot (visible light catalyst)	Methylene blue	Improved visible light catalytic performance and degradation of methylene blue significantly enhanced	Granted paper for invention: CN106964389B More details at https://patents.google.com/patent/CN106964389B/en
Au-doped TiO_2	Methyl orange	Particle size in range of 85-90 nm Fast photodegradation of methyl orange under visible light irradiation Codoping of gold and silver (less gold being used) can lower cost of gold-doped TiO_2 without compromising with corresponding photocatalytic activity	Maparu AK and Rai B, Tata Consultancy Services Ltd, 2016. *Visible light responsive doped titania photocatalytic nanoparticles and process for their synthesis*. U.S. Patent 9,352,302 (https://patents.google.com/patent/US9352302B2/en)
Zinc-doped TiO_2	Methylene blue	Nanocoatings induced a decrease in optical density that resulted because of the photocatalytic degradation of methylene blue Coatings with higher dopants dosage could cause the fastest declines (this behaviour being in line with greater absorbance of UV range light (354 nm) from illumination source used	Averett SB and Averett DR, WELL Shield LLC, 2017. *Titanium dioxide photocatalytic compositions and uses thereof*. U.S. Patent 9,833,003 (https://patents.google.com/patent/US9833003B2/en)
Pd-TiO_2 catalyst	Rhodamine B	Decolourization of rhodamine B (which was used as a measure of its degradation) by Pd-TiO_2 without light filter had the most activity when compared to any other experiments conducted	Guerrero IL, Dunn SC and Neto AML, Queen Mary University of London, 2016. *Photocatalysts*. U.S. Patent Application 15/031,738 (https://patents.google.com/patent/US20160367968A1/en)
Hollow fibre membrane coated with MoO_3 NPs (dope solution was prepared using dry polyphenylsulfone polymer as the core polymer and with different compositions of the molybdenum trioxide)	Methylene blue	Membranes with 2% MoO_3 removed methylene blue (with methylene blue removals of 34.8% and 66.3% under dark and ultraviolet irradiation, respectively) Removal of methylene blue was explained to have occurred because of its cationic molecules getting adsorbed onto the negatively charged surface of the hollow fibre membranes as a result of electrostatic interactions	Al-Ahmed A and Isloor AM, King Fahd University of Petroleum, 2019. *Hollow fibre membrane modified with molybdenum trioxide nanoparticles*. U.S. Patent Application 15/722,450 (https://patents.google.com/patent/US20190099719A1/en)

Table 10 (continued)

Catalyst material(s)	Dye(s)	Highlights of characteristics of catalyst material(s)	Source
C- and/or N-doped TiO_2	Methylene blue, rhodamine B	C- and N-doped TiO_2 could photodegrade methylene blue to levels under the detection level of apparatus used	Thulin LM, Nanoptek Corp, 2016. *Visible light titania photocatalyst, method for making same, and processes for use thereof*. U.S. Patent 9,278,337 (https://patents.google.com/patent/US9278337B2/en)

scale they were investigated and for the exceptionally high photocatalytic activities they explain, there is no clear-cut indication as to the same sequence of reactions happening in actual large-scale photocatalytic reactors comprising doped photocatalysts either in slurry (suspended) or immobilized forms. Bearing in mind that actual large-scale photocatalytic reactors will impose significantly harsher and more dynamic environmental conditions to the doped photocatalysts systems, in corollary, it is therefore a real challenge to design such reactor units which will encompass all the expected process irreversibilities of large-scale operation and still be reproducing the same performance reaped at laboratory-scale testing. A priori, *how* the mechanisms (otherwise making sense for laboratory-scale systems) will be influenced or altered under the real constraints of large-scale doped photocatalyst reactors will demand more extensive experimentation, and especially so, by using advanced modelling and simulation approaches combining chemical sciences, engineering sciences, computational fluid dynamic tools and cost estimation. The implementation of statistically sound 'Design of Experiments (DoE)' at all successive scales (pot or laboratory scale, pilot scale and eventually large scale) of process investigation, analysis and iterative optimization will also be crucial when considering scale-up of the selected (optimal) doped photocatalytic dye degradation systems (Fig. 21). Moreover, in the way towards scale-up, it will be crucial to designing such systems which limit opacity of the substrate(s), enhance the penetration and optimal distribution of irradiation, and harness the hydrodynamic regimes prevailing within the reactor. The latter conditions become more complex to optimize if an additional stimulus such as sonication or microwave irradiation is imposed on the system. Hence, the need to make elaborate enough mathematical analysis and computationally feasible simulation of such extremely complex systems remains widely pertinent.

Conclusion

In the last decade and more, a vast body of literature has been accumulated dealing with the synthesis and examination of several types of doped photocatalysts. The above descriptions and discussions provide a comprehensive analysis of the research trends and development in regard to the fabrication and functionalization of a broad range of novel doped photocatalysts and of their respective capabilities and overall performance for the degradation and mineralization of selected model dyes in mostly single-dye single doped photocatalyst systems and multi-dye single doped photocatalyst reaction environments. In specific, the present review has discussed the upgrading routes of pristine semiconductor photocatalysts using doping and heterostructuring approaches, the mode of action of a large number

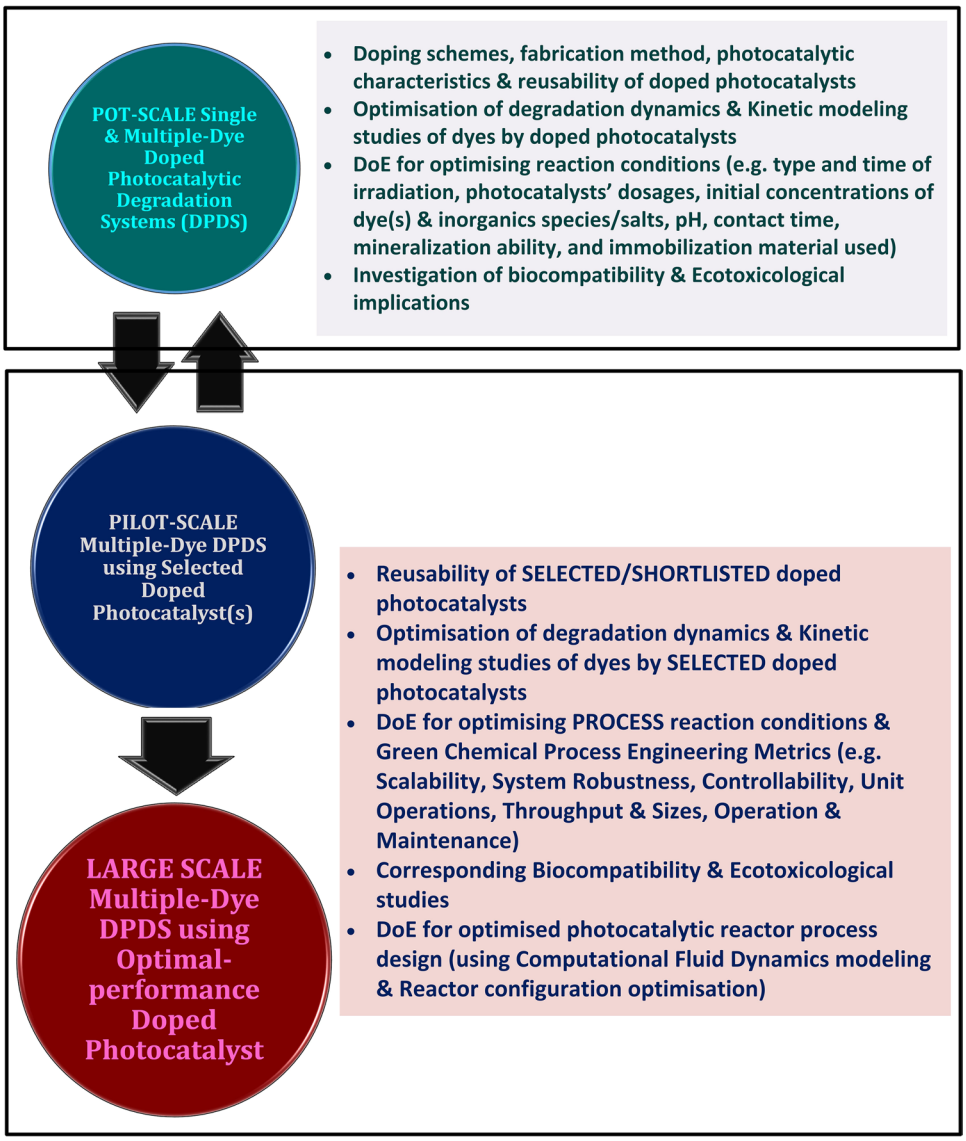

Fig. 21 Flow of reaction and process development links and important considerations for each major stage involved in the formulation of an effective and optimized doped photocatalytic reactor for multiple-dye degradation

of photocatalytic NPs, the parameter-dependent dye degradation/mineralization efficiency and reusability of doped photocatalysts, the photocatalytic degradation behaviours of doped photocatalysts in mixed-dye systems, the biocompatibility and ecotoxicological implications associated with the use of doped photocatalytic materials, the recent progress made in photocatalytic reactor process design and finally the limitations and research directions.

Based on the major observations garnered from this review, it is very encouraging to apprise that significant efforts are being deployed by several research groups in designing and preparing doped photocatalysts which are superior in those properties sought after to enhance the degradation dynamics of many dyes. The application of nanoscience and Green Chemistry Principles are inherent to the fabrication and functionalization methods of the novel doped photocatalysts, and do eventually produce exceptionally potent photocatalytic materials which exhibit a certain versatility in their dye-degrading performance within the reaction conditions they are examined in. Yet, the very fact that most of the performance analysis of the novel doped photocatalysts has been conducted in single-dye systems seems to limit the further use of these materials in much more complex dye-laden aqueous milieus. Such more complex dye-laden aqueous milieus being the ones expected in real dye-contaminated systems, it now becomes almost imperative to gear up and intensify research efforts in the analysis of the doped photocatalysts in multiple-dye systems. Alongside, the development of *process-optimized* pilot-scale and plausibly large-scale photocatalytic dye degradation and mineralization reactor units should also be major branches of research, innovation and development in this area of environmental pollution control and remediation. Equally important, all the associated costs and cash flows involved during

the developing, commissioning, operation and maintenance of eventual large-scale doped photocatalytic dye-degrading systems have to be comprehensively surveyed and optimized both from the technical and financial feasibility perspectives.

The above analysis also transpires that it is important to assess the ecotoxicological characteristics of doped photocatalysts on a case-to-case basis because of the high specificity of their toxic properties emanating from their respective elemental components and the relative coatings. Moreover, the main limitation associated with the current ecotoxicological studies appears much to be that only one (or one specific set of) species is employed to investigate the toxicity properties (i.e. the species used in one study differ(s) from those used in another work). Hence, there is a paucity of a battery of toxicity tests and integrated toxicity data. Consequently, the results are then quite very difficult to interpret comprehensively and be of use in environmental impact assessment procedures thereafter. It will also be crucial to conducting comprehensive ecotoxicological studies in real environments where the nanostructured doped photocatalytic materials are most likely to enter the natural ecosystem and downstream so that a whole risk-related assessment of the potential applications of these nanomaterials be made.

Acknowledgements The authors wish to thank the anonymous reviewers for their constructive comments and suggestions. The authors also wish to put on record our appreciation for the immense efforts deployed by all those who have contributed and continue in doing so to bring novel data in the fields and topics of research and development discussed in this review. The permissions and licences for reuse and inclusion of the figures in this review (for both the print and online versions) have been obtained through the RightsLink® service of the Copyright Clearance Center (https://www.copyright.com/publishers/rightslink-permissions/). The contents of this article have been cross-checked for similarity in suitable platforms and amendments were made accordingly during its writing. This work did not receive any funding.

References

Abdel-Maksoud Y, Imam E, Ramadan A (2016) TiO_2 solar photocatalytic reactor systems: selection of reactor design for scale-up and commercialization—analytical review. Catalysts 6:138. https://doi.org/10.3390/catal6090138

Abdelsamad AMA, Gad-Allah TA, Mahmoud FA, Badawy MI (2018) Enhanced photocatalytic degradation of textile wastewater using Ag/ZnO thin films. J Water Process Eng 25:88–95. https://doi.org/10.1016/j.jwpe.2018.07.002

Abdul Satar NS, Adnan R, Lee HL et al (2019) Facile green synthesis of ytrium-doped $BiFeO_3$ with highly efficient photocatalytic degradation towards methylene blue. Ceram Int 45:15964–15973. https://doi.org/10.1016/j.ceramint.2019.05.105

Abudayyak M, Guzel E, Özhan G (2017) Nickel oxide nanoparticles induce oxidative DNA damage and apoptosis in kidney cell line (NRK-52E). Biol Trace Elem Res 178:98–104. https://doi.org/10.1007/s12011-016-0892-z

Adam RE, Alnoor H, Pozina G et al (2020) Synthesis of Mg-doped ZnO NPs via a chemical low-temperature method and investigation of the efficient photocatalytic activity for the degradation of dyes under solar light. Solid State Sci 99:106053. https://doi.org/10.1016/j.solidstatesciences.2019.106053

Adyani SM, Ghorbani M (2018) A comparative study of physicochemical and photocatalytic properties of visible light responsive Fe, Gd and P single and tri-doped TiO_2 nanomaterials. J Rare Earths 36:72–85. https://doi.org/10.1016/j.jre.2017.06.012

Aggelopoulos CA, Dimitropoulos M, Govatsi A et al (2017) Influence of the surface-to-bulk defects ratio of ZnO and TiO_2 on their UV-mediated photocatalytic activity. Appl Catal B Environ 205:292–301. https://doi.org/10.1016/j.apcatb.2016.12.023

Ahirwar D, Bano M, Khan F (2016) Synthesis of mesoporous TiO_2 and its role as a photocatalyst in degradation of indigo carmine dye. J Sol-Gel Sci Technol 79:228–237. https://doi.org/10.1007/s10971-016-4039-7

Ahmad I (2019) Inexpensive and quick photocatalytic activity of rare earth (Er, Yb) co-doped ZnO nanoparticles for degradation of methyl orange dye. Sep Purif Technol 227:115726. https://doi.org/10.1016/j.seppur.2019.115726

Ahmed S, Annu Chaudhry SA, Ikram S (2017) A review on biogenic synthesis of ZnO nanoparticles using plant extracts and microbes: a prospect towards green chemistry. J Photochem Photobiol B Biol 166:272–284. https://doi.org/10.1016/j.jphotobiol.2016.12.011

Ajmal A, Majeed I, Malik RN et al (2016) Photocatalytic degradation of textile dyes on Cu_2O–CuO/TiO_2 anatase powders. J Environ Chem Eng 4:2138–2146. https://doi.org/10.1016/j.jece.2016.03.041

Akerdi AG, Bahrami SH, Arami M, Pajootan E (2016) Photocatalytic discoloration of Acid Red 14 aqueous solution using titania nanoparticles immobilized on graphene oxide fabricated plate. Chemosphere 159:293–299. https://doi.org/10.1016/j.chemosphere.2016.06.020

Akhundi A, Habibi-Yangjeh A (2016) Novel g-C_3N_4/Ag_2SO_4 nanocomposites: fast microwave-assisted preparation and enhanced photocatalytic performance towards degradation of organic pollutants under visible light. J Colloid Interface Sci 482:165–174. https://doi.org/10.1016/j.jcis.2016.08.002

Akkari M, Aranda P, Mayoral A et al (2017) Sepiolite nanoplatform for the simultaneous assembly of magnetite and zinc oxide nanoparticles as photocatalyst for improving removal of organic pollutants. J Hazard Mater 340:281–290. https://doi.org/10.1016/j.jhazmat.2017.06.067

Alahiane S, Qourzal S, El Ouardi M et al (2014) Factors influencing the photocatalytic degradation of reactive yellow 145 by TiO_2-coated non-woven fibers. Am J Anal Chem 05:445–454. https://doi.org/10.4236/ajac.2014.58053

Alaoui OT, Nguyen QT, Rhlalou T (2009) Preparation and characterization of a new TiO_2/SiO_2 composite catalyst for photocatalytic degradation of indigo carmin. Environ Chem Lett 7:175–181. https://doi.org/10.1007/s10311-008-0154-1

Al-Kahtani AA, Abou Taleb MF (2016) Photocatalytic degradation of Maxilon C.I. basic dye using CS/$CoFe_2O_4$/GONCs as a heterogeneous photo-Fenton catalyst prepared by gamma irradiation. J Hazard Mater 309:10–19. https://doi.org/10.1016/j.jhazmat.2016.01.071

Almeida AR, Salimian M, Ferro M et al (2019) Biochemical and behavioral responses of zebrafish embryos to magnetic graphene/nickel nanocomposites. Ecotoxicol Environ Saf 186:109760. https://doi.org/10.1016/j.ecoenv.2019.109760

Amaral FM, Florêncio L, Kato MT et al (2017) Hydraulic retention time influence on azo dye and sulfate removal during the sequential anaerobic–aerobic treatment of real textile wastewater. Water Sci Technol 76:3319–3327. https://doi.org/10.2166/wst.2017.378

Amaranatha Reddy D, Ma R, Choi MY, Kim TK (2015) Reduced graphene oxide wrapped ZnS–Ag_2S ternary composites synthesized via hydrothermal method: applications in photocatalyst

degradation of organic pollutants. Appl Surf Sci 324:725–735. https://doi.org/10.1016/j.apsusc.2014.11.026

An H-R, Park SY, Kim H et al (2016) Advanced nanoporous TiO_2 photocatalysts by hydrogen plasma for efficient solar-light photocatalytic application. Sci Rep 6:29683. https://doi.org/10.1038/srep29683

An H, Wang H, Huang J et al (2019) TiO_2 nanosheets with exposed 001 facets co-modified by Ag_xAu_{1-x}NPs and 3D $ZnIn_2S_4$ microsphere for enhanced visible light absorption and photocatalytic H_2 production. Appl Surf Sci 484:1168–1175. https://doi.org/10.1016/j.apsusc.2019.04.180

Anastas P, Eghbali N (2010) Green chemistry: principles and practice. Chem Soc Rev 39:301–312. https://doi.org/10.1039/B918763B

Andrade Neto NF, Nascimento LE, Correa M et al (2020) Characterization and photocatalytic application of Ce^{4+}, Co^{2+}, Mn^{2+} and Ni^{2+} doped Fe_3O_4 magnetic nanoparticles obtained by the co-precipitation method. Mater Chem Phys 242:122489. https://doi.org/10.1016/j.matchemphys.2019.122489

Anju Chanu L, Joychandra Singh W, Jugeshwar Singh K, Nomita Devi K (2019) Effect of operational parameters on the photocatalytic degradation of methylene blue dye solution using manganese doped ZnO nanoparticles. Results Phys 12:1230–1237. https://doi.org/10.1016/j.rinp.2018.12.089

Anku WW, Oppong SO-B, Shukla SK et al (2016) Palladium-doped–ZrO_2–multiwalled carbon nanotubes nanocomposite: an advanced photocatalyst for water treatment. Appl Phys A 122:579. https://doi.org/10.1007/s00339-016-0086-8

Ao CH, Lee SC (2005) Indoor air purification by photocatalyst TiO_2 immobilized on an activated carbon filter installed in an air cleaner. Chem Eng Sci 60:103–109. https://doi.org/10.1016/j.ces.2004.01.073

Arab Chamjangali M, Bagherian G, Javid A et al (2015) Synthesis of Ag–ZnO with multiple rods (multipods) morphology and its application in the simultaneous photo-catalytic degradation of methyl orange and methylene blue. Spectrochim Acta Part A Mol Biomol Spectrosc 150:230–237. https://doi.org/10.1016/j.saa.2015.05.067

Araga R, Sharma CS (2017) One step direct synthesis of multiwalled carbon nanotubes from coconut shell derived charcoal. Mater Lett 188:205–207. https://doi.org/10.1016/j.matlet.2016.11.014

Argurio P, Fontananova E, Molinari R, Drioli E (2018) Photocatalytic membranes in photocatalytic membrane reactors. Processes 6:162. https://doi.org/10.3390/pr6090162

Ata R, Sacco O, Vaiano V et al (2017) Visible light active N-doped TiO_2 immobilized on polystyrene as efficient system for wastewater treatment. J Photochem Photobiol A Chem 348:255–262. https://doi.org/10.1016/j.jphotochem.2017.08.054

Athanasiou DA, Romanos GE, Falaras P (2016) Design and optimization of a photocatalytic reactor for water purification combining optical fiber and membrane technologies. Chem Eng J 305:92–103. https://doi.org/10.1016/j.cej.2015.11.080

Atla SB, Lin W-R, Chien T-C et al (2018) Fabrication of Fe_3O_4/ZnO magnetite core shell and its application in photocatalysis using sunlight. Mater Chem Phys 216:380–386. https://doi.org/10.1016/j.matchemphys.2018.06.020

Ayodhya D, Veerabhadram G (2020) Green synthesis of garlic extract stabilized Ag@CeO_2 composites for photocatalytic and sonocatalytic degradation of mixed dyes and antimicrobial studies. J Mol Struct 1205:127611. https://doi.org/10.1016/j.molstruc.2019.127611

Azadi M, Habibi-Yangjeh A (2015) Microwave-assisted facile one-pot method for preparation of BiOI–ZnO nanocomposites as novel dye adsorbents by synergistic collaboration. J Iran Chem Soc 12:909–919. https://doi.org/10.1007/s13738-014-0555-y

Azzam EMS, Fathy NA, El-Khouly SM, Sami RM (2019) Enhancement the photocatalytic degradation of methylene blue dye using fabricated CNTs/TiO_2/AgNPs/Surfactant nanocomposites. J Water Process Eng 28:311–321. https://doi.org/10.1016/j.jwpe.2019.02.016

Azzaz AA, Assadi AA, Jellali S et al (2018) Discoloration of simulated textile effluent in continuous photoreactor using immobilized titanium dioxide: effect of zinc and sodium chloride. J Photochem Photobiol A Chem 358:111–120. https://doi.org/10.1016/j.jphotochem.2018.01.032

Baek M, Kim MK, Cho HJ et al (2011) Factors influencing the cytotoxicity of zinc oxide nanoparticles: particle size and surface charge. J Phys: Conf Ser 304:012044. https://doi.org/10.1088/1742-6596/304/1/012044

Bagheri M, Najafabadi NR, Borna E (2020) Removal of reactive blue 203 dye photocatalytic using ZnO nanoparticles stabilized on functionalized MWCNTs. J King Saud Univ Sci 32:799–804. https://doi.org/10.1016/j.jksus.2019.02.012

Bai S, Shen X, Zhong X et al (2012) One-pot solvothermal preparation of magnetic reduced graphene oxide-ferrite hybrids for organic dye removal. Carbon N Y 50:2337–2346. https://doi.org/10.1016/j.carbon.2012.01.057

Bakar SA, Ribeiro C (2016) A comparative run for visible-light-driven photocatalytic activity of anionic and cationic S-doped TiO_2 photocatalysts: a case study of possible sulfur doping through chemical protocol. J Mol Catal A: Chem 421:1–15. https://doi.org/10.1016/j.molcata.2016.05.003

Bakhtkhosh P, Mehrizad A (2017) Sonochemical synthesis of Sm-doped ZnS nanoparticles for photocatalytic degradation of Direct Blue 14: experimental design by response surface methodology and development of a kinetics model. J Mol Liq 240:65–73. https://doi.org/10.1016/j.molliq.2017.05.053

Balbi T, Caratto V, Fabbri R et al (2017) Photocatalytic Fe-doped n-TiO_2: from synthesis to utilization of in vitro cell models for screening human and environmental nanosafety. Resour Technol 3:158–165. https://doi.org/10.1016/j.reffit.2017.03.009

Barahimi V, Moghimi H, Taheri RA (2019) Cu doped TiO_2–Bi_2O_3 nanocomposite for degradation of azo dye in aqueous solution: process modeling and optimization using central composite design. J Environ Chem Eng 7:103078. https://doi.org/10.1016/j.jece.2019.103078

Barbosa LV, Marçal L, Nassar EJ et al (2015) Kaolinite-titanium oxide nanocomposites prepared via sol-gel as heterogeneous photocatalysts for dyes degradation. Catal Today 246:133–142. https://doi.org/10.1016/j.cattod.2014.09.019

Barrocas B, Sério S, Rovisco A et al (2016) Removal of rhodamine 6G dye contaminant by visible light driven immobilized $Ca_{1-x}Ln_xMnO_3$ (Ln = Sm, Ho; $0.1 \le x \le 0.4$) photocatalysts. Appl Surf Sci 360:798–806. https://doi.org/10.1016/j.apsusc.2015.11.070

Barzgari Z, Ghazizadeh A, Askari SZ (2016) Preparation of Mn-doped ZnO nanostructured for photocatalytic degradation of Orange G under solar light. Res Chem Intermed 42:4303–4315. https://doi.org/10.1007/s11164-015-2276-y

Basnet P, Inakhunbi Chanu T, Samanta D, Chatterjee S (2018) A review on bio-synthesized zinc oxide nanoparticles using plant extracts as reductants and stabilizing agents. J Photochem Photobiol B Biol 183:201–221. https://doi.org/10.1016/j.jphotobiol.2018.04.036

Batista APL, Carvalho HWP, Luz GHP et al (2010) Preparation of CuO/SiO_2 and photocatalytic activity by degradation of methylene blue. Environ Chem Lett 8:63–67. https://doi.org/10.1007/s10311-008-0192-8

Baylan E, Altintas Yildirim O (2019) Highly efficient photocatalytic activity of stable manganese-doped zinc oxide (Mn:ZnO) nanofibers via electrospinning method. Mater Sci Semicond Process 103:104621. https://doi.org/10.1016/j.mssp.2019.104621

Bellardita M, Di Paola A, Palmisano L et al (2011) Preparation and photoactivity of samarium loaded anatase, brookite and rutile catalysts. Appl Catal B Environ 104:291–299. https://doi.org/10.1016/j.apcatb.2011.03.016

Bello MM, Raman AAA (2019) Synergy of adsorption and advanced oxidation processes in recalcitrant wastewater treatment. Environ Chem Lett 17(2):1125–1142. https://doi.org/10.1007/s10311-018-00842-0

Bento RMF, Almeida MR, Bharmoria P et al (2020) Improvements in the enzymatic degradation of textile dyes using ionic-liquid-based surfactants. Sep Purif Technol 235:116191. https://doi.org/10.1016/j.seppur.2019.116191

Bhanvase BA, Shende TP, Sonawane SH (2017) A review on graphene–TiO_2 and doped graphene–TiO_2 nanocomposite photocatalyst for water and wastewater treatment. Environ Technol Rev 6:1–14. https://doi.org/10.1080/21622515.2016.1264489

Bilal Tahir M, Sagir M (2019) Carbon nanodots and rare metals (RM = La, Gd, Er) doped tungsten oxide nanostructures for photocatalytic dyes degradation and hydrogen production. Sep Purif Technol 209:94–102. https://doi.org/10.1016/j.seppur.2018.07.029

Bomila R, Srinivasan S, Gunasekaran S, Manikandan A (2018) Enhanced photocatalytic degradation of methylene blue dye, opto-magnetic and antibacterial behaviour of pure and La-doped ZnO nanoparticles. J Supercond Nov Magn 31:855–864. https://doi.org/10.1007/s10948-017-4261-8

Borlaf M, Colomer MT, de Andrés A et al (2014) TiO_2/Eu^{3+} thin films with high photoluminescence emission prepared by electrophoretic deposition from nanoparticulate sols. Eur J Inorg Chem 2014:5152–5159. https://doi.org/10.1002/ejic.201402445

Boruah B, Gupta R, Modak JM, Madras G (2019) Novel insights into the properties of $AgBiO_3$ photocatalyst and its application in immobilized state for 4-nitrophenol degradation and bacteria inactivation. J Photochem Photobiol A Chem 373:105–115. https://doi.org/10.1016/j.jphotochem.2018.11.001

Bourgeault A, Legros V, Gonnet F et al (2017) Interaction of TiO_2 nanoparticles with proteins from aquatic organisms: the case of gill mucus from blue mussel. Environ Sci Pollut Res 24:13474–13483. https://doi.org/10.1007/s11356-017-8801-3

Brindha A, Sivakumar T (2017) Visible active N, S co-doped TiO_2/graphene photocatalysts for the degradation of hazardous dyes. J Photochem Photobiol A Chem 340:146–156. https://doi.org/10.1016/j.jphotochem.2017.03.010

Bubacz K, Choina J, Dolat D, Morawski AW (2010) Methylene blue and phenol photocatalytic degradation on nanoparticles of anatase TiO_2. Pol J Environ Stud 19:685–691

Bumajdad A, Madkour M (2014) Understanding the superior photocatalytic activity of noble metals modified titania under UV and visible light irradiation. Phys Chem Chem Phys 16:7146. https://doi.org/10.1039/c3cp54411g

Cao M, Wang P, Ao Y et al (2016) Visible light activated photocatalytic degradation of tetracycline by a magnetically separable composite photocatalyst: graphene oxide/magnetite/cerium-doped titania. J Colloid Interface Sci 467:129–139. https://doi.org/10.1016/j.jcis.2016.01.005

Cao Y, Mao S, Li M et al (2017) Metal/porous carbon composites for heterogeneous catalysis: old catalysts with improved performance promoted by N-doping. ACS Catal 7:8090–8112. https://doi.org/10.1021/acscatal.7b02335

Cao Z, Wen X, Chen P et al (2018) Synthesis of a novel heterogeneous fenton catalyst and promote the degradation of methylene blue by fast regeneration of Fe^{2+}. Colloids Surf A Physicochem Eng Asp 549:94–104. https://doi.org/10.1016/j.colsurfa.2018.04.009

Cao X, Han Y, Li F et al (2019) Impact of protein-nanoparticle interactions on gastrointestinal fate of ingested nanoparticles: not just simple protein corona effects. NanoImpact 13:37–43. https://doi.org/10.1016/j.impact.2018.12.002

Cargnello M, Montini T, Smolin SY et al (2016) Engineering titania nanostructure to tune and improve its photocatalytic activity. Proc Natl Acad Sci 113:3966–3971. https://doi.org/10.1073/pnas.1524806113

Caschera D, Federici F, de Caro T et al (2018) Fabrication of Eu–TiO_2 NCs functionalized cotton textile as a multifunctional photocatalyst for dye pollutants degradation. Appl Surf Sci 427:81–91. https://doi.org/10.1016/j.apsusc.2017.08.015

Chai B, Yan J, Wang C et al (2017) Enhanced visible light photocatalytic degradation of Rhodamine B over phosphorus doped graphitic carbon nitride. Appl Surf Sci 391:376–383. https://doi.org/10.1016/j.apsusc.2016.06.180

Chakrabarti S, Dutta B (2004) Photocatalytic degradation of model textile dyes in wastewater using ZnO as semiconductor catalyst. J Hazard Mater 112:269–278. https://doi.org/10.1016/j.jhazmat.2004.05.013

Chang H (2000) A kinetic model for photocatalytic degradation of organic contaminants in a thin-film TiO_2 catalyst. Water Res 34:407–416. https://doi.org/10.1016/S0043-1354(99)00247-X

Chang C-J, Chao P-Y, Lin K-S (2019) Flower-like BiOBr decorated stainless steel wire-mesh as immobilized photocatalysts for photocatalytic degradation applications. Appl Surf Sci 494:492–500. https://doi.org/10.1016/j.apsusc.2019.07.203

Chaudhari SM, Gawal PM, Sane PK et al (2018) Solar light-assisted photocatalytic degradation of methylene blue with Mo/TiO_2: a comparison with Cr- and Ni-doped TiO_2. Res Chem Intermed 44:3115–3134. https://doi.org/10.1007/s11164-018-3296-1

Chaudhary JP, Mahto A, Vadodariya N et al (2016) Fabrication of carbon and sulphur-doped nanocomposites with seaweed polymer carrageenan as an efficient catalyst for rapid degradation of dye pollutants using a solar concentrator. RSC Adv 6:61716–61724. https://doi.org/10.1039/C6RA10317K

Chauhan PS, Kant R, Rai A et al (2019) Facile synthesis of ZnO/GO nanoflowers over Si substrate for improved photocatalytic decolorization of MB dye and industrial wastewater under solar irradiation. Mater Sci Semicond Process 89:6–17. https://doi.org/10.1016/j.mssp.2018.08.022

Chen H, Chen K-F, Lai S-W et al (2015) Photoelectrochemical oxidation of azo dye and generation of hydrogen via CN co-doped TiO_2 nanotube arrays. Sep Purif Technol 146:143–153. https://doi.org/10.1016/j.seppur.2015.03.026

Chen Y, Liu H, Geng B et al (2017) A reusable surface-quaternized nanocellulose-based hybrid cryogel loaded with N-doped TiO_2 for self-integrated adsorption/photo-degradation of methyl orange dye. RSC Adv 7:17279–17288. https://doi.org/10.1039/C7RA00450H

Chen F, Wu C, Wang J et al (2019) Highly efficient Z-scheme structured visible-light photocatalyst constructed by selective doping of Ag@AgBr and Co_3O_4 separately on 010 and 110 facets of $BiVO_4$: pre-separation channel and hole-sink effects. Appl Catal B Environ 250:31–41. https://doi.org/10.1016/j.apcatb.2019.03.023

Cheng M, Zeng G, Huang D, Lai C, Xu P, Zhang C, Liu Y (2016) Hydroxyl radicals based advanced oxidation processes (AOPs) for remediation of soils contaminated with organic compounds: a review. Chem Eng J 284:582–598

Chithira PR, Theresa John T (2020) Correlation among oxygen vacancy and doping concentration in controlling the properties of cobalt doped ZnO nanoparticles. J Magn Magn Mater 496:165928. https://doi.org/10.1016/j.jmmm.2019.165928

Choi YI, Jeon KH, Kim HS et al (2016) TiO_2/BiOX (X = Cl, Br, I) hybrid microspheres for artificial waste water and real sample treatment under visible light irradiation. Sep Purif Technol 160:28–42. https://doi.org/10.1016/j.seppur.2016.01.009

Chong MN, Tneu ZY, Poh PE et al (2015) Synthesis, characterisation and application of TiO_2–zeolite nanocomposites for the advanced treatment of industrial dye wastewater. J Taiwan Inst Chem Eng 50:288–296. https://doi.org/10.1016/j.jtice.2014.12.013

Chung Y-C, Chen C-Y (2009) Degradation of azo dye reactive violet 5 by TiO_2 photocatalysis. Environ Chem Lett 7:347–352. https://doi.org/10.1007/s10311-008-0178-6

Ci S, Cai P, Wen Z, Li J (2015) Graphene-based electrode materials for microbial fuel cells. Sci China Mater 58:496–509. https://doi.org/10.1007/s40843-015-0061-2

Cinelli G, Cuomo F, Ambrosone L et al (2017) Photocatalytic degradation of a model textile dye using carbon-doped titanium dioxide and visible light. J Water Process Eng 20:71–77. https://doi.org/10.1016/j.jwpe.2017.09.014

Ciocarlan R-G, Seftel EM, Gavrila R et al (2020) Spinel nanoparticles on stick-like Freudenbergite nanocomposites as effective smart-removal photocatalysts for the degradation of organic pollutants under visible light. J Alloys Compd 820:153403. https://doi.org/10.1016/j.jallcom.2019.153403

Colmenares JC, Varma RS, Lisowski P (2016) Sustainable hybrid photocatalysts: titania immobilized on carbon materials derived from renewable and biodegradable resources. Green Chem 18:5736–5750. https://doi.org/10.1039/C6GC02477G

Colombo E, Ashokkumar M (2017) Comparison of the photocatalytic efficiencies of continuous stirred tank reactor (CSTR) and batch systems using a dispersed micron sized photocatalyst. RSC Adv 7:48222–48229. https://doi.org/10.1039/C7RA09753K

Corsi I, Cherr GN, Lenihan HS et al (2014) Common strategies and technologies for the ecosafety assessment and design of nanomaterials entering the marine environment. ACS Nano 8:9694–9709. https://doi.org/10.1021/nn504684k

Corsi I, Winther-Nielsen M, Sethi R et al (2018) Ecofriendly nanotechnologies and nanomaterials for environmental applications: key issue and consensus recommendations for sustainable and ecosafe nanoremediation. Ecotoxicol Environ Saf 154:237–244. https://doi.org/10.1016/j.ecoenv.2018.02.037

Crini G, Lichtfouse E (2019) Advantages and disadvantages of techniques used for wastewater treatment. Environ Chem Lett 17:145–155. https://doi.org/10.1007/s10311-018-0785-9

Cui G, Xin Y, Jiang X et al (2015) Safety profile of TiO_2-based photocatalytic nanofabrics for indoor formaldehyde degradation. Int J Mol Sci 16:27721–27729. https://doi.org/10.3390/ijms161126055

Cui X, Jiang G, Zhao Z et al (2016) Facile regulation of crystalline phases and exposed facets on Ti^{3+} self-doped TiO_2 for efficient photocatalytic hydrogen evolution. J Mater Sci 51:10819–10832. https://doi.org/10.1007/s10853-016-0293-x

Dalhatou S, Pétrier C, Laminsi S et al (2015) Sonochemical removal of naphthol blue black azo dye: influence of parameters and effect of mineral ions. Int J Environ Sci Technol 12:35–44. https://doi.org/10.1007/s13762-013-0432-8

Das S, Mahalingam H (2020) Novel immobilized ternary photocatalytic polymer film based airlift reactor for efficient degradation of complex phthalocyanine dye wastewater. J Hazard Mater 383:121219. https://doi.org/10.1016/j.jhazmat.2019.121219

de Brites-Nóbrega FF, Polo ANB, Benedetti AM et al (2013) Evaluation of photocatalytic activities of supported catalysts on NaX zeolite or activated charcoal. J Hazard Mater 263:61–66. https://doi.org/10.1016/j.jhazmat.2013.07.061

de Sá DS, Vasconcellos LE, de Souza JR et al (2018) Intensification of photocatalytic degradation of organic dyes and phenol by scale-up and numbering-up of meso- and microfluidic TiO_2 reactors for wastewater treatment. J Photochem Photobiol A Chem 364:59–75. https://doi.org/10.1016/j.jphotochem.2018.05.020

de Sá DS, de Andrade Bustamante R, Rodrigues Rocha CE et al (2019) Fabrication of lignocellulose-based microreactors: copper-functionalized bamboo for continuous-flow CuAAC click reactions. ACS Sustain Chem Eng 7:3267–3273. https://doi.org/10.1021/acssuschemeng.8b05273

de Sousa Filho IA, Arana LR, Doungmo G et al (2020) $SrSnO_3$/g-C_3N_4 and sunlight: photocatalytic activity and toxicity of degradation byproducts. J Environ Chem Eng 8:103633. https://doi.org/10.1016/j.jece.2019.103633

Demircivi P, Simsek EB (2018) Fabrication of Zr doped TiO_2/chitosan composite catalysts with enhanced visible-light-mediated photoactivity for the degradation of Orange II dye. Water Sci Technol. https://doi.org/10.2166/wst.2018.298

Desa AL, Hairom NHH, Sidik DAB et al (2019) A comparative study of ZnO-PVP and ZnO-PEG nanoparticles activity in membrane photocatalytic reactor (MPR) for industrial dye wastewater treatment under different membranes. J Environ Chem Eng 7:103143. https://doi.org/10.1016/j.jece.2019.103143

Dhanalakshmi M, Saravanakumar K, Prabavathi SL, Muthuraj V (2020) Iridium doped ZnO nanocomposites: synergistic effect induced photocatalytic degradation of methylene blue and crystal violet. Inorg Chem Commun 111:107601. https://doi.org/10.1016/j.inoche.2019.107601

Di J, Xia J, Chen X et al (2017) Tunable oxygen activation induced by oxygen defects in nitrogen doped carbon quantum dots for sustainable boosting photocatalysis. Carbon N Y 114:601–607. https://doi.org/10.1016/j.carbon.2016.12.030

Do Nascimento WJ, Aquino RVS, Barbosa AA, Rocha OR (2019) Development of a new PET flow reactor applied to food dyes removal with advanced oxidative processes. J Water Process Eng 31:100823. https://doi.org/10.1016/j.jwpe.2019.100823

Dodoo-Arhin D, Buabeng FP, Mwabora JM et al (2018) The effect of titanium dioxide synthesis technique and its photocatalytic degradation of organic dye pollutants. Heliyon 4:e00681. https://doi.org/10.1016/j.heliyon.2018.e00681

Dong H, Zeng G, Tang L et al (2015) An overview on limitations of TiO_2-based particles for photocatalytic degradation of organic pollutants and the corresponding countermeasures. Water Res 79:128–146. https://doi.org/10.1016/j.watres.2015.04.038

Dutta SK, Mehetor SK, Pradhan N (2015) Metal semiconductor heterostructures for photocatalytic conversion of light energy. J Phys Chem Lett 6:936–944. https://doi.org/10.1021/acs.jpclett.5b00113

Ebrahimi R, Maleki A, Zandsalimi Y et al (2019) Photocatalytic degradation of organic dyes using WO_3-doped ZnO nanoparticles fixed on a glass surface in aqueous solution. J Ind Eng Chem 73:297–305. https://doi.org/10.1016/j.jiec.2019.01.041

Ebrahimzadeh MA, Mortazavi-Derazkola S, Zazouli MA (2020) Eco-friendly green synthesis of novel magnetic Fe_3O_4/SiO_2/ZnO-Pr_6O_{11} nanocomposites for photocatalytic degradation of organic pollutant. J Rare Earths 38:13–20. https://doi.org/10.1016/j.jre.2019.07.004

Egerton TA, Mattinson JA (2010) Effects of particle dispersion on photocatalysis probed by the effect of platinum on dichloroacetic acid oxidation by P25 and nanoparticulate rutile. Appl Catal B Environ 99:407–412. https://doi.org/10.1016/j.apcatb.2010.05.008

El-Bindary AA, El-Marsafy SM, El-Maddah AA (2019) Enhancement of the photocatalytic activity of ZnO nanoparticles by silver doping for the degradation of AY99 contaminants. J Mol Struct 1191:76–84. https://doi.org/10.1016/j.molstruc.2019.04.064

Elias M, Amin MK, Firoz SH et al (2017) Microwave-assisted synthesis of Ce-doped ZnO/CNT composite with enhanced photocatalytic activity. Ceram Int 43:84–91. https://doi.org/10.1016/j.ceramint.2016.09.114

Eskandari N, Nabiyouni G, Masoumi S, Ghanbari D (2019) Preparation of a new magnetic and photo-catalyst $CoFe_2O_4$–$SrTiO_3$ perovskite nanocomposite for photo-degradation of toxic dyes under

short time visible irradiation. Compos Part B Eng 176:107343. https://doi.org/10.1016/j.compositesb.2019.107343
Fakhri A, Nejad PA (2016) Antimicrobial, antioxidant and cytotoxic effect of molybdenum trioxide nanoparticles and application of this for degradation of ketamine under different light illumination. J Photochem Photobiol B Biol 159:211–217. https://doi.org/10.1016/j.jphotobiol.2016.04.002
Fakhri H, Mahjoub AR, Aghayan H (2017) Effective removal of methylene blue and cerium by a novel pair set of heteropoly acids based functionalized graphene oxide: adsorption and photocatalytic study. Chem Eng Res Des 120:303–315. https://doi.org/10.1016/j.cherd.2017.02.030
Fan M, Song C, Chen T et al (2016) Visible-light-drived high photocatalytic activities of Cu/g-C_3N_4 photocatalysts for hydrogen production. RSC Adv 6:34633–34640. https://doi.org/10.1039/C5RA27755H
Fan Q, Liu J, Yu Y et al (2017) A simple fabrication for sulfur doped graphitic carbon nitride porous rods with excellent photocatalytic activity degrading RhB dye. Appl Surf Sci 391:360–368. https://doi.org/10.1016/j.apsusc.2016.04.055
Fang Z, Weng S, Ye X et al (2015) Defect engineering and phase junction architecture of wide-bandgap ZnS for conflicting visible light activity in photocatalytic H_2 evolution. ACS Appl Mater Interfaces 7:13915–13924. https://doi.org/10.1021/acsami.5b02641
Faraldos M, Bahamonde A (2017) Environmental applications of titania-graphene photocatalysts. Catal Today 285:13–28. https://doi.org/10.1016/j.cattod.2017.01.029
Fernandes A, Makoś P, Khan JA, Boczkaj G (2019) Pilot scale degradation study of 16 selected volatile organic compounds by hydroxyl and sulfate radical based advanced oxidation processes. J Clean Prod 208:54–64
Fessi N, Nsib MF, Chevalier Y et al (2019) Photocatalytic degradation enhancement in pickering emulsions stabilized by solid particles of bare TiO_2. Langmuir 35:2129–2136. https://doi.org/10.1021/acs.langmuir.8b03806
Fiyadh SS, AlSaadi MA, Jaafar WZ et al (2019) Review on heavy metal adsorption processes by carbon nanotubes. J Clean Prod 230:783–793. https://doi.org/10.1016/j.jclepro.2019.05.154
Fowsiya J, Madhumitha G, Al-Dhabi NA, Arasu MV (2016) Photocatalytic degradation of Congo red using *Carissa edulis* extract capped zinc oxide nanoparticles. J Photochem Photobiol B Biol 162:395–401. https://doi.org/10.1016/j.jphotobiol.2016.07.011
Franco P, Sacco O, De Marco I, Vaiano V (2019) Zinc oxide nanoparticles obtained by supercritical antisolvent precipitation for the photocatalytic degradation of crystal violet dye. Catalysts 9:346. https://doi.org/10.3390/catal9040346
Fu J, Tian Y, Chang B et al (2013) Soft-chemical synthesis of mesoporous nitrogen-modified titania with superior photocatalytic performance under visible light irradiation. Chem Eng J 219:155–161. https://doi.org/10.1016/j.cej.2013.01.032
Gadah RH, Basaleh AS (2020) Influence of doped platinum nanoparticles on photocatalytic performance of CuO–SiO_2 for degradation of Acridine orange dye. Ceram Int 46:1690–1696. https://doi.org/10.1016/j.ceramint.2019.09.141
Gajera HP, Bambharolia RP, Hirpara DG et al (2015) Molecular identification and characterization of novel Hypocrea koningii associated with azo dyes decolorization and biodegradation of textile dye effluents. Process Saf Environ Prot 98:406–416. https://doi.org/10.1016/j.psep.2015.10.005
Gallo A, Manfra L, Boni R et al (2018) Cytotoxicity and genotoxicity of CuO nanoparticles in sea urchin spermatozoa through oxidative stress. Environ Int 118:325–333. https://doi.org/10.1016/j.envint.2018.05.034
Gnanasekaran L, Hemamalini R, Saravanan R et al (2017) Synthesis and characterization of metal oxides (CeO_2, CuO, NiO, Mn_3O_4, SnO_2 and ZnO) nanoparticles as photo catalysts for degradation of textile dyes. J Photochem Photobiol B Biol 173:43–49. https://doi.org/10.1016/j.jphotobiol.2017.05.027
Gonell F, Puga AV, Julián-López B et al (2016) Copper-doped titania photocatalysts for simultaneous reduction of CO_2 and production of H_2 from aqueous sulfide. Appl Catal B Environ 180:263–270. https://doi.org/10.1016/j.apcatb.2015.06.019
González-Casamachin DA, Rivera De la Rosa J, Lucio-Ortiz CJ et al (2019) Visible-light photocatalytic degradation of acid violet 7 dye in a continuous annular reactor using ZnO/PPy photocatalyst: synthesis, characterization, mass transfer effect evaluation and kinetic analysis. Chem Eng J 373:325–337. https://doi.org/10.1016/j.cej.2019.05.032
Goutham R, Badri Narayan R, Srikanth B, Gopinath KP (2019) Supporting materials for immobilisation of nano-photocatalysts. In: Inamuddin, Sharma G, Kumar A, Lichtfouse E, Asiri A (eds) Nanophotocatalysis and environmental applications. Environmental chemistry for a sustainable World. Springer, Cham, pp 49–82
Guo J, Khan S, Cho S-H, Kim J (2019) Preparation and immobilization of zinc sulfide (ZnS) nanoparticles on polyvinylidene fluoride pellets for photocatalytic degradation of methylene blue in wastewater. Appl Surf Sci 473:425–432. https://doi.org/10.1016/j.apsusc.2018.12.103
Hamad HA, Sadik WA, Abd El-latif MM et al (2016) Photocatalytic parameters and kinetic study for degradation of dichlorophenol-indophenol (DCPIP) dye using highly active mesoporous TiO_2 nanoparticles. J Environ Sci 43:26–39. https://doi.org/10.1016/j.jes.2015.05.033
Hamaloğlu KÖ, Sağ E, Tuncel A (2017) Bare, gold and silver nanoparticle decorated, monodisperse-porous titania microbeads for photocatalytic dye degradation in a newly constructed microfluidic, photocatalytic packed-bed reactor. J Photochem Photobiol A Chem 332:60–65. https://doi.org/10.1016/j.jphotochem.2016.08.015
Han J, Zhu G, Hojamberdiev M et al (2016a) Synergetic effects of surface adsorption and photodegradation on removal of organic pollutants by Er^{3+}-doped BiOI ultrathin nanosheets with exposed 001 facets. J Mater Sci 51:2057–2071. https://doi.org/10.1007/s10853-015-9516-9
Han X, Dong S, Yu C et al (2016b) Controllable synthesis of Sn-doped BiOCl for efficient photocatalytic degradation of mixed-dye wastewater under natural sunlight irradiation. J Alloys Compd 685:997–1007. https://doi.org/10.1016/j.jallcom.2016.06.298
Han F, Kambala VSR, Dharmarajan R et al (2018) Photocatalytic degradation of azo dye acid orange 7 using different light sources over Fe^{3+}-doped TiO_2 nanocatalysts. Environ Technol Innov 12:27–42. https://doi.org/10.1016/j.eti.2018.07.004
Hanifehpour Y, Soltani B, Amani-Ghadim AR et al (2016) Synthesis and characterization of samarium-doped ZnS nanoparticles: a novel visible light responsive photocatalyst. Mater Res Bull 76:411–421. https://doi.org/10.1016/j.materresbull.2015.12.035
Hao X, Jin Z, Min S, Lu G (2016) Modulating photogenerated electron transfer with selectively exposed Co–Mo facets on a novel amorphous g-C_3N_4/$Co_xMo_{1-x}S_2$ photocatalyst. RSC Adv 6:23709–23717. https://doi.org/10.1039/C5RA22102A
Hao L, Huang H, Guo Y, Zhang Y (2018) Multifunctional Bi_2O_2(OH)(NO_3) nanosheets with 001 active exposing facets: efficient photocatalysis, dye-sensitization, and piezoelectric-catalysis. ACS Sustain Chem Eng 6:1848–1862. https://doi.org/10.1021/acssuschemeng.7b03223
Hasnat M, Siddiquey IA, Nuruddin N (2005) Comparative photocatalytic studies of degradation of a cationic and an anionic dye. Dye Pigment 66:185–188. https://doi.org/10.1016/j.dyepig.2004.09.020

Hassan SM, Mannaa MA (2016) Photocatalytic degradation of brilliant green dye by SnO_2/TiO_2 nanocatalysts. Int J Nano Mater Sci 5:9–19

Hatat-Fraile M, Liang R, Arlos MJ et al (2017) Concurrent photocatalytic and filtration processes using doped TiO_2 coated quartz fiber membranes in a photocatalytic membrane reactor. Chem Eng J 330:531–540. https://doi.org/10.1016/j.cej.2017.07.141

He R, Cao S, Yu J, Yang Y (2016) Microwave-assisted solvothermal synthesis of $Bi_4O_5I_2$ hierarchical architectures with high photocatalytic performance. Catal Today 264:221–228. https://doi.org/10.1016/j.cattod.2015.07.029

He D, Zhang Z, Qu J et al (2018) Facile one-step synthesis of black phosphorus via microwave irradiation with excellent photocatalytic activity. Part Part Syst Charact 35:1800306. https://doi.org/10.1002/ppsc.201800306

Hidayanto E, Sutanto H, Wibowo S, Irwanto M (2017) Morphology and degradation kinetics of N-doped TiO_2 nano particle synthesized using sonochemical method. Solid State Phenom 266:95–100. https://doi.org/10.4028/www.scientific.net/SSP.266.95

Hir ZAM, Moradihamedani P, Abdullah AH, Mohamed MA (2017) Immobilization of TiO_2 into polyethersulfone matrix as hybrid film photocatalyst for effective degradation of methyl orange dye. Mater Sci Semicond Process 57:157–165. https://doi.org/10.1016/j.mssp.2016.10.009

Hoffmann MR, Martin ST, Choi W, Bahnemann DW (1995) Environmental applications of semiconductor photocatalysis. Chem Rev 95:69–96. https://doi.org/10.1021/cr00033a004

Hofstadler K, Bauer R, Novalic S, Heisler G (1994) New reactor design for photocatalytic wastewater treatment with TiO_2 immobilized on fused-silica glass fibers: photomineralization of 4-chlorophenol. Environ Sci Technol 28:670–674. https://doi.org/10.1021/es00053a021

Horie M, Sugino S, Kato H et al (2016) Does photocatalytic activity of TiO_2 nanoparticles correspond to photo-cytotoxicity? Cellular uptake of TiO_2 nanoparticles is important in their photocytotoxicity. Toxicol Mech Methods 26:284–294. https://doi.org/10.1080/15376516.2016.1175530

Hossain MA, Elias M, Sarker DR et al (2018) Synthesis of Fe- or Ag-doped TiO_2–MWCNT nanocomposite thin films and their visible-light-induced catalysis of dye degradation and antibacterial activity. Res Chem Intermed 44:2667–2683. https://doi.org/10.1007/s11164-018-3253-z

Hou Q, Li W, Ju M et al (2016) One-pot synthesis of sulfonated graphene oxide for efficient conversion of fructose into HMF. RSC Adv 6:104016–104024. https://doi.org/10.1039/C6RA23420H

Hu Q, Liu B, Zhang Z et al (2010) Temperature effect on the photocatalytic degradation of methyl orange under UV–Vis light irradiation. J Wuhan Univ Technol Sci Ed 25:210–213. https://doi.org/10.1007/s11595-010-2210-5

Hu S, Li F, Fan Z et al (2015) Band gap-tunable potassium doped graphitic carbon nitride with enhanced mineralization ability. Dalt Trans 44:1084–1092. https://doi.org/10.1039/C4DT02658F

Huang F, Yan A, Zhao H (2016) Influences of doping on photocatalytic properties of TiO_2 photocatalyst. In: Cao W (ed) Semiconductor photocatalysis—materials, mechanisms and applications. InTech, Rijeka

Huo Y, Chen X, Zhang J et al (2014) Ordered macroporous Bi_2O_3/TiO_2 film coated on a rotating disk with enhanced photocatalytic activity under visible irradiation. Appl Catal B Environ 148–149:550–556. https://doi.org/10.1016/j.apcatb.2013.11.040

Huo P, Zhou M, Tang Y et al (2016) Incorporation of N-ZnO/CdS/graphene oxide composite photocatalyst for enhanced photocatalytic activity under visible light. J Alloys Compd 670:198–209. https://doi.org/10.1016/j.jallcom.2016.01.247

Iannone F, Casiello M, Monopoli A et al (2017) Ionic liquids/ZnO nanoparticles as recyclable catalyst for polycarbonate depolymerization. J Mol Catal A: Chem 426:107–116. https://doi.org/10.1016/j.molcata.2016.11.006

Iglesias O, Rivero MJ, Urtiaga AM, Ortiz I (2016) Membrane-based photocatalytic systems for process intensification. Chem Eng J 305:136–148. https://doi.org/10.1016/j.cej.2016.01.047

Indrawirawan S, Sun H, Duan X, Wang S (2015) Low temperature combustion synthesis of nitrogen-doped graphene for metal-free catalytic oxidation. J Mater Chem A 3:3432–3440. https://doi.org/10.1039/C4TA05940A

Isari AA, Payan A, Fattahi M et al (2018) Photocatalytic degradation of rhodamine B and real textile wastewater using Fe-doped TiO_2 anchored on reduced graphene oxide (Fe–TiO_2/rGO): characterization and feasibility, mechanism and pathway studies. Appl Surf Sci 462:549–564. https://doi.org/10.1016/j.apsusc.2018.08.133

Iveland J, Martinelli L, Peretti J et al (2013) Direct measurement of auger electrons emitted from a semiconductor light-emitting diode under electrical injection: identification of the dominant mechanism for efficiency droop. Phys Rev Lett 110:177406. https://doi.org/10.1103/PhysRevLett.110.177406

Jabeen U, Shah SM, Khan SU (2017) Photo catalytic degradation of Alizarin red S using ZnS and cadmium doped ZnS nanoparticles under unfiltered sunlight. Surf Interfaces 6:40–49. https://doi.org/10.1016/j.surfin.2016.11.002

Jafari H, Afshar S, Zabihi O, Naebe M (2016) Enhanced photocatalytic activities of TiO_2–SiO_2 nanohybrids immobilized on cement-based materials for dye degradation. Res Chem Intermed 42:2963–2978. https://doi.org/10.1007/s11164-015-2190-3

Janczarek M, Kowalska E, Ohtani B (2016) Decahedral-shaped anatase titania photocatalyst particles: synthesis in a newly developed coaxial-flow gas-phase reactor. Chem Eng J 289:502–512. https://doi.org/10.1016/j.cej.2016.01.008

Jawad AH, Mubarak NSA, Ishak MAM et al (2016) Kinetics of photocatalytic decolourization of cationic dye using porous TiO_2 film. J Taibah Univ Sci 10:352–362. https://doi.org/10.1016/j.jtusci.2015.03.007

Jayamohan H, Smith YR, Hansen LC et al (2015) Anodized titania nanotube array microfluidic device for photocatalytic application: experiment and simulation. Appl Catal B Environ 174–175:167–175. https://doi.org/10.1016/j.apcatb.2015.02.041

Jayamohan H, Smith YR, Gale BK et al (2016) Photocatalytic microfluidic reactors utilizing titania nanotubes on titanium mesh for degradation of organic and biological contaminants. J Environ Chem Eng 4:657–663. https://doi.org/10.1016/j.jece.2015.12.018

Jeyachitra R, Senthilnathan V, Senthil TS (2018) Studies on electrical behavior of Fe doped ZnO nanoparticles prepared via co-precipitation approach for photo-catalytic application. J Mater Sci: Mater Electron 29:1189–1197. https://doi.org/10.1007/s10854-017-8021-0

Ji K, Deng J, Zang H et al (2015) Fabrication and high photocatalytic performance of noble metal nanoparticles supported on 3DOM $InVO_4$–$BiVO_4$ for the visible-light-driven degradation of rhodamine B and methylene blue. Appl Catal B Environ 165:285–295. https://doi.org/10.1016/j.apcatb.2014.10.005

Jia Z, Miao J, Lu HB et al (2016) Photocatalytic degradation and absorption kinetics of cibacron brilliant yellow 3G-P by nanosized ZnO catalyst under simulated solar light. J Taiwan Inst Chem Eng 60:267–274. https://doi.org/10.1016/j.jtice.2015.10.012

Jin Z, Duan W, Liu B et al (2015) Fabrication of efficient visible light activated Cu–P25–graphene ternary composite for photocatalytic degradation of methyl blue. Appl Surf Sci 356:707–718. https://doi.org/10.1016/j.apsusc.2015.08.122

Jo W-K, Tayade RJ (2016) Facile photocatalytic reactor development using nano-TiO_2 immobilized mosquito net and energy efficient UVLED for industrial dyes effluent treatment. J Environ Chem Eng 4:319–327. https://doi.org/10.1016/j.jece.2015.11.024

Joseph HM, Sugunan S, Gurrala L et al (2019) New insights into surface functionalization and preparation methods of MWCNT based semiconductor photocatalysts. Ceram Int 45:14490–14499. https://doi.org/10.1016/j.ceramint.2019.04.058

Jouali A, Salhi A, Aguedach A et al (2019) Photo-catalytic degradation of methylene blue and reactive blue 21 dyes in dynamic mode using TiO_2 particles immobilized on cellulosic fibers. J Photochem Photobiol A Chem 383:112013. https://doi.org/10.1016/j.jphotochem.2019.112013

Juntrapirom S, Tantraviwat D, Suntalelat S et al (2017) Visible light photocatalytic performance and mechanism of highly efficient SnS/BiOI heterojunction. J Colloid Interface Sci 504:711–720. https://doi.org/10.1016/j.jcis.2017.06.019

Kadam AN, Dhabbe RS, Kokate MR et al (2014) Preparation of N doped TiO_2 via microwave-assisted method and its photocatalytic activity for degradation of Malathion. Spectrochim Acta Part A Mol Biomol Spectrosc 133:669–676. https://doi.org/10.1016/j.saa.2014.06.020

Kalam A, Al-Sehemi AG, Assiri M et al (2018) Modified solvothermal synthesis of cobalt ferrite ($CoFe_2O_4$) magnetic nanoparticles photocatalysts for degradation of methylene blue with H_2O_2/visible light. Results Phys 8:1046–1053. https://doi.org/10.1016/j.rinp.2018.01.045

Kang X, Sun X, Han B (2016) Synthesis of functional nanomaterials in ionic liquids. Adv Mater 28:1011–1030. https://doi.org/10.1002/adma.201502924

Karimi L, Zohoori S, Yazdanshenas ME (2014) Photocatalytic degradation of azo dyes in aqueous solutions under UV irradiation using nano-strontium titanate as the nanophotocatalyst. J Saudi Chem Soc 18:581–588. https://doi.org/10.1016/j.jscs.2011.11.010

Karimi-Shamsabadi M, Behpour M, Babaheidari AK, Saberi Z (2017) Efficiently enhancing photocatalytic activity of NiO–ZnO doped onto nanozeoliteX by synergistic effects of p–n heterojunction, supporting and zeolite nanoparticles in photo-degradation of eriochrome black T and methyl orange. J Photochem Photobiol A Chem 346:133–143. https://doi.org/10.1016/j.jphotochem.2017.05.038

Karnan T, Selvakumar SAS (2016) Biosynthesis of ZnO nanoparticles using rambutan (*Nephelium lappaceum* L.) peel extract and their photocatalytic activity on methyl orange dye. J Mol Struct 1125:358–365. https://doi.org/10.1016/j.molstruc.2016.07.029

Karousis N, Tagmatarchis N, Tasis D (2010) Current progress on the chemical modification of carbon nanotubes. Chem Rev 110:5366–5397. https://doi.org/10.1021/cr100018g

Karthika V, Arumugam A (2017) Synthesis and characterization of MWCNT/TiO_2/Au nanocomposite for photocatalytic and antimicrobial activity. IET Nanobiotechnol 11:113–118. https://doi.org/10.1049/iet-nbt.2016.0072

Kaur M, Umar A, Mehta SK, Kansal SK (2019) Reduced graphene oxide-CdS heterostructure: an efficient fluorescent probe for the sensing of Ag(I) and sunset yellow and a visible-light responsive photocatalyst for the degradation of levofloxacin drug in aqueous phase. Appl Catal B Environ 245:143–158. https://doi.org/10.1016/j.apcatb.2018.12.042

Kayani ZN, Abbas E, Saddiqe Z et al (2018) Photocatalytic, antibacterial, optical and magnetic properties of Fe-doped ZnO nanoparticles prepared by sol-gel. Mater Sci Semicond Process 88:109–119. https://doi.org/10.1016/j.mssp.2018.08.003

Kazeminezhad I, Sadollahkhani A (2016) Influence of pH on the photocatalytic activity of ZnO nanoparticles. J Mater Sci: Mater Electron 27:4206–4215. https://doi.org/10.1007/s10854-016-4284-0

Khaki MRD, Shafeeyan MS, Raman AAA, Daud WMAW (2017) Application of doped photocatalysts for organic pollutant degradation—a review. J Environ Manag 198:78–94

Khaletskaya K, Pougin A, Medishetty R et al (2015) Fabrication of gold/titania photocatalyst for CO_2 reduction based on pyrolytic conversion of the metal-organic framework NH_2-MIL-125(Ti) loaded with gold nanoparticles. Chem Mater 27:7248–7257. https://doi.org/10.1021/acs.chemmater.5b03017

Khalil M, Anggraeni ES, Ivandini TA, Budianto E (2019) Exposing TiO_2 (001) crystal facet in nano Au–TiO_2 heterostructures for enhanced photodegradation of methylene blue. Appl Surf Sci 487:1376–1384. https://doi.org/10.1016/j.apsusc.2019.05.232

Khan Z, Chetia TR, Vardhaman AK et al (2012) Visible light assisted photocatalytic hydrogen generation and organic dye degradation by CdS–metal oxide hybrids in presence of graphene oxide. RSC Adv 2:12122–12128. https://doi.org/10.1039/c2ra21596a

Khan M, Gul SR, Li J, Cao W (2015a) Variations in the structural, electronic and optical properties of N-doped TiO_2 with increasing N doping concentration. Mod Phys Lett B 29:1550022. https://doi.org/10.1142/S0217984915500220

Khan MM, Adil SF, Al-Mayouf A (2015b) Metal oxides as photocatalysts. J Saudi Chem Soc 19:462–464. https://doi.org/10.1016/j.jscs.2015.04.003

Khan J, Ilyas S, Akram B et al (2018) Zno/NiO coated multi-walled carbon nanotubes for textile dyes degradation. Arab J Chem 11:880–896. https://doi.org/10.1016/j.arabjc.2017.12.020

Khataee A, Arefi-Oskoui S, Fathinia M et al (2015) Synthesis, characterization and photocatalytic properties of Er-doped PbSe nanoparticles as a visible light-activated photocatalyst. J Mol Catal A: Chem 398:255–267. https://doi.org/10.1016/j.molcata.2014.11.009

Khataee A, Gholami P, Sheydaei M (2016) Heterogeneous Fenton process by natural pyrite for removal of a textile dye from water: effect of parameters and intermediate identification. J Taiwan Inst Chem Eng 58:366–373. https://doi.org/10.1016/j.jtice.2015.06.015

Khataee A, Mohamadi FT, Rad TS, Vahid B (2018) Heterogeneous sonocatalytic degradation of anazolene sodium by synthesized dysprosium doped CdSe nanostructures. Ultrason Sonochem 40:361–372. https://doi.org/10.1016/j.ultsonch.2017.07.021

Khosroshahi AG, Mehrizad A (2019) Optimization, kinetics and thermodynamics of photocatalytic degradation of Acid Red 1 by Sm-doped CdS under visible light. J Mol Liq 275:629–637. https://doi.org/10.1016/j.molliq.2018.11.122

Koh PW, Yuliati L, Lee SL (2019) Kinetics and optimization studies of photocatalytic degradation of methylene blue over Cr-doped TiO_2 using response surface methodology. Iran J Sci Technol Trans A Sci 43:95–103. https://doi.org/10.1007/s40995-017-0407-6

Krishnakumar V, Ranjith R, Jayaprakash J et al (2017) Enhancement of photocatalytic degradation of methylene blue under visible light using transparent Mg-doped CdS–PVA nanocomposite films. J Mater Sci: Mater Electron 28:13990–13999. https://doi.org/10.1007/s10854-017-7249-z

Kumar S, Parthasarathy R, Singh AP et al (2017) Dominant 100 facet selectivity for enhanced photocatalytic activity of $NaNbO_3$ in $NaNbO_3$/CdS core/shell heterostructures. Catal Sci Technol 7:481–495. https://doi.org/10.1039/C6CY02098D

Kumar A, Thakur PR, Sharma G et al (2019) Carbon nitride, metal nitrides, phosphides, chalcogenides, perovskites and carbides nanophotocatalysts for environmental applications. Environ Chem Lett 17:655–682. https://doi.org/10.1007/s10311-018-0814-8

Kumari P, Bahadur N, Dumée LF (2020) Photo-catalytic membrane reactors for the remediation of persistent organic pollutants—a review. Sep Purif Technol 230:115878. https://doi.org/10.1016/j.seppur.2019.115878

Kundu A, Mondal A (2019) Kinetics, isotherm, and thermodynamic studies of methylene blue selective adsorption and photocatalysis of malachite green from aqueous solution using layered Na-intercalated Cu-doped Titania. Appl Clay Sci 183:105323. https://doi.org/10.1016/j.clay.2019.105323

Kuvarega AT, Khumalo N, Dlamini D, Mamba BB (2018) Polysulfone/N, Pd co-doped TiO_2 composite membranes for photocatalytic dye degradation. Sep Purif Technol 191:122–133. https://doi.org/10.1016/j.seppur.2017.07.064

Kwong T-L, Yung K-F (2015) Surfactant-free microwave-assisted synthesis of Fe-doped ZnO nanostars as photocatalyst for degradation of tropaeolin O in water under visible light. J Nanomater 2015:1–9. https://doi.org/10.1155/2015/190747

Landi S, Carneiro J, Ferdov S et al (2017) Photocatalytic degradation of Rhodamine B dye by cotton textile coated with SiO_2–TiO_2 and SiO_2–TiO_2–HY composites. J Photochem Photobiol A Chem 346:60–69. https://doi.org/10.1016/j.jphotochem.2017.05.047

Landi S, Carneiro J, Soares OSGP et al (2019) Photocatalytic performance of N-doped TiO_2nano–SiO_2–HY nanocomposites immobilized over cotton fabrics. J Mater Res Technol 8:1933–1943. https://doi.org/10.1016/j.jmrt.2018.06.025

Lavand AB, Malghe YS, Singh SH (2015) synthesis, characterization, and investigation of visible light photocatalytic activity of C doped TiO_2/CdS core–shell nanocomposite. Indian J Mater Sci 2015:1–9. https://doi.org/10.1155/2015/690568

Lavand AB, Bhatu MN, Malghe YS (2019) Visible light photocatalytic degradation of malachite green using modified titania. J Mater Res Technol 8:299–308. https://doi.org/10.1016/j.jmrt.2017.05.019

Lebedev A, Anariba F, Li X et al (2019) Ag/Ag_2O/$BiNbO_4$ structure for simultaneous photocatalytic degradation of mixed cationic and anionic dyes. Sol Energy 178:257–267. https://doi.org/10.1016/j.solener.2018.12.040

Lee G-J, Wu JJ (2017) Recent developments in ZnS photocatalysts from synthesis to photocatalytic applications—a review. Powder Technol 318:8–22. https://doi.org/10.1016/j.powtec.2017.05.022

Lee KM, Lai CW, Ngai KS, Juan JC (2016a) Recent developments of zinc oxide based photocatalyst in water treatment technology: a review. Water Res 88:428–448. https://doi.org/10.1016/j.watres.2015.09.045

Lee S, Park Y, Pradhan D, Sohn Y (2016b) AgX (X = Cl, Br, I)/BiOX nanoplates and microspheres for pure and mixed (methyl orange, rhodamine B and methylene blue) dyes. J Ind Eng Chem 35:231–252. https://doi.org/10.1016/j.jiec.2015.12.040

Li Y, Gao W, Ci L et al (2010) Catalytic performance of Pt nanoparticles on reduced graphene oxide for methanol electro-oxidation. Carbon N Y 48:1124–1130. https://doi.org/10.1016/j.carbon.2009.11.034

Li M, Zhang S, Peng Y et al (2015) Enhanced visible light responsive photocatalytic activity of TiO_2-based nanocrystallites: impact of doping sequence. RSC Adv 5:7363–7369. https://doi.org/10.1039/C4RA10604K

Li T, Hu X, Liu C et al (2016) Efficient photocatalytic degradation of organic dyes and reaction mechanism with Ag_2CO_3/$Bi_2O_2CO_3$ photocatalyst under visible light irradiation. J Mol Catal A: Chem. https://doi.org/10.1016/j.molcata.2016.10.001

Li Q, Guan Z, Wu D et al (2017) Z-scheme BiOCl–Au–CdS heterostructure with enhanced sunlight-driven photocatalytic activity in degrading water dyes and antibiotics. ACS Sustain Chem Eng. https://doi.org/10.1021/acssuschemeng.7b01157

Li B, Chu J, Li Y et al (2018) Preparation and performance of visible-light-driven Bi_2O_3/ZnS heterojunction functionalized porous CA membranes for effective degradation of rhodamine B. Phys Status Solidi 215:1701061. https://doi.org/10.1002/pssa.201701061

Li Q, Zhao T, Li M et al (2019) One-step construction of pickering emulsion via commercial TiO_2 nanoparticles for photocatalytic dye degradation. Appl Catal B Environ 249:1–8. https://doi.org/10.1016/j.apcatb.2019.02.057

Liau LCK, Huang JS (2017) Energy-level variations of Cu-doped ZnO fabricated through sol–gel processing. J Alloys Comp 702:153–160

Lin L, Wang H, Xu P (2017) Immobilized TiO_2-reduced graphene oxide nanocomposites on optical fibers as high performance photocatalysts for degradation of pharmaceuticals. Chem Eng J 310:389–398. https://doi.org/10.1016/j.cej.2016.04.024

Liu G, Yu JC, Lu GQ, Cheng H-M (2011) Crystal facet engineering of semiconductor photocatalysts: motivations, advances and unique properties. Chem Commun 47:6763–6783. https://doi.org/10.1039/c1cc10665a

Liu H, Yu L, Chen W, Li Y (2012) The progress of nanocrystals doped with rare earth ions. J Nanomater 2012:1–9. https://doi.org/10.1155/2012/235879

Liu Z, Tian J, Zeng D et al (2017) A facile microwave-hydrothermal method to fabricate B doped $ZnWO_4$ nanorods with high crystalline and highly efficient photocatalytic activity. Mater Res Bull 94:298–306. https://doi.org/10.1016/j.materresbull.2017.06.021

Liu A-L, Li Z-Q, Wu Z-Q, Xia X-H (2018) Study on the photocatalytic reaction kinetics in a TiO_2 nanoparticles coated microreactor integrated microfluidics device. Talanta 182:544–548. https://doi.org/10.1016/j.talanta.2018.02.028

Liu B, Sun H, Peng T, Zhao X (2019) Effect of microwave irradiation time on structure, morphology, and supercapacitor properties of functionalized graphene. JOM 71:613–620. https://doi.org/10.1007/s11837-018-3139-y

Lofrano G, Libralato G, Carotenuto M et al (2016) Emerging concern from short-term textile leaching: a preliminary ecotoxicological survey. Bull Environ Contam Toxicol 97:646–652. https://doi.org/10.1007/s00128-016-1937-x

Louangsouphom B, Wang X, Song J, Wang X (2019) Low-temperature preparation of a N–TiO_2/macroporous resin photocatalyst to degrade organic pollutants. Environ Chem Lett 17:1061–1066. https://doi.org/10.1007/s10311-018-00827-z

Lu D, Zhao B, Fang P et al (2015) Facile one-pot fabrication and high photocatalytic performance of vanadium doped TiO_2-based nanosheets for visible-light-driven degradation of RhB or Cr(VI). Appl Surf Sci 359:435–448. https://doi.org/10.1016/j.apsusc.2015.10.138

Luna AL, Novoseltceva E, Louarn E et al (2016) Synergetic effect of Ni and Au nanoparticles synthesized on titania particles for efficient photocatalytic hydrogen production. Appl Catal B Environ 191:18–28. https://doi.org/10.1016/j.apcatb.2016.03.008

Luo J, Zhang N, Lai J et al (2015) Tannic acid functionalized graphene hydrogel for entrapping gold nanoparticles with high catalytic performance toward dye reduction. J Hazard Mater 300:615–623. https://doi.org/10.1016/j.jhazmat.2015.07.079

Lv J, Li D, Dai K et al (2017) Multi-walled carbon nanotube supported CdS-DETA nanocomposite for efficient visible light photocatalysis. Mater Chem Phys 186:372–381. https://doi.org/10.1016/j.matchemphys.2016.11.008

Madhumitha G, Fowsiya J, Gupta N et al (2019) Green synthesis, characterization and antifungal and photocatalytic activity of *Pithecellobium dulce* peel-mediated ZnO nanoparticles. J Phys Chem Solids 127:43–51. https://doi.org/10.1016/j.jpcs.2018.12.005

Magdalane CM, Kaviyarasu K, Vijaya JJ et al (2017) Evaluation on the heterostructured CeO_2/Y_2O_3 binary metal oxide nanocomposites for UV/Vis light induced photocatalytic degradation of Rhodamine-B dye for textile engineering application. J Alloys Compd 727:1324–1337. https://doi.org/10.1016/j.jallcom.2017.08.209

Malika M, Rao CV, Das RK et al (2016) Evaluation of bimetal doped TiO_2 in dye fragmentation and its comparison to mono-metal doped and bare catalysts. Appl Surf Sci 368:316–324. https://doi.org/10.1016/j.apsusc.2016.01.230

Malini B, Allen Gnana Raj G (2018) C, N and S-doped TiO_2-characterization and photocatalytic performance for rose bengal dye degradation under day light. J Environ Chem Eng 6:5763–5770. https://doi.org/10.1016/j.jece.2018.09.002

Malwal D, Gopinath P (2016) Enhanced photocatalytic activity of hierarchical three dimensional metal oxide@CuO nanostructures towards the degradation of Congo red dye under solar radiation. Catal Sci Technol 6:4458–4472. https://doi.org/10.1039/C6CY00128A

Mamba G, Mbianda XY, Mishra AK (2015) Photocatalytic degradation of the diazo dye naphthol blue black in water using MWCNT/Gd, N, S-TiO_2 nanocomposites under simulated solar light. J Environ Sci 33:219–228. https://doi.org/10.1016/j.jes.2014.06.052

Manenti DR, Soares PA, Silva TFCV et al (2015) Performance evaluation of different solar advanced oxidation processes applied to the treatment of a real textile dyeing wastewater. Environ Sci Pollut Res 22:833–845. https://doi.org/10.1007/s11356-014-2767-1

Manjunath K, Reddy Yadav LS, Jayalakshmi T et al (2018) Ionic liquid assisted hydrothermal synthesis of TiO_2 nanoparticles: photocatalytic and antibacterial activity. J Mater Res Technol 7:7–13. https://doi.org/10.1016/j.jmrt.2017.02.001

Marschall R, Wang L (2014) Non-metal doping of transition metal oxides for visible-light photocatalysis. Catal Today 225:111–135. https://doi.org/10.1016/j.cattod.2013.10.088

Mazierski P, Bajorowicz B, Grabowska E, Zaleska-Medynska A (2016) Photoreactor design aspects and modeling of light. In: Colmenares J, Xu YJ (eds) Heterogeneous photocatalysis. Green chemistry and sustainable technology. Springer, Berlin, pp 211–248

McBride K, Bennington-Gray S, Cook J et al (2017) Improving the crystallinity and magnetocaloric effect of the perovskite $La_{0.65}Sr_{0.35}MnO_3$ using microwave irradiation. CrystEngComm 19:3776–3791. https://doi.org/10.1039/C7CE00882A

McManamon C, O'Connell J, Delaney P et al (2015) A facile route to synthesis of S-doped TiO_2 nanoparticles for photocatalytic activity. J Mol Catal A: Chem 406:51–57. https://doi.org/10.1016/j.molcata.2015.05.002

Mehrali M, Latibari ST, Mehrali M et al (2013) Preparation and properties of highly conductive palmitic acid/graphene oxide composites as thermal energy storage materials. Energy 58:628–634. https://doi.org/10.1016/j.energy.2013.05.050

Melvin Ng HK, Leo CP, Abdullah AZ (2017) Selective removal of dyes by molecular imprinted TiO_2 nanoparticles in polysulfone ultrafiltration membrane. J Environ Chem Eng 5:3991–3998. https://doi.org/10.1016/j.jece.2017.07.075

Meng X, Qian Z, Wang H et al (2008) Sol–gel immobilization of SiO_2/TiO_2 on hydrophobic clay and its removal of methyl orange from water. J Sol-Gel Sci Technol 46:195–200. https://doi.org/10.1007/s10971-008-1677-4

Meng Z, Zhang X, Qin J (2013) A high efficiency microfluidic-based photocatalytic microreactor using electrospun nanofibrous TiO_2 as a photocatalyst. Nanoscale 5:4687. https://doi.org/10.1039/c3nr00775h

Mesgari Z, Saien J (2017) Pollutant degradation over dye sensitized nitrogen doped titania substances in different configurations of visible light helical flow photoreactor. Sep Purif Technol 185:129–139. https://doi.org/10.1016/j.seppur.2017.05.032

Meshesha DS, Matangi RC, Tirukkovalluri SR, Bojja S (2017) Synthesis, characterization and visible light photocatalytic activity of Mg^{2+} and Zr^{4+} co-doped TiO_2 nanomaterial for degradation of methylene blue. J Asian Ceram Soc 5:136–143. https://doi.org/10.1016/j.jascer.2017.03.006

Meshram SP, Adhyapak PV, Pardeshi SK et al (2017) Sonochemically generated cerium doped ZnO nanorods for highly efficient photocatalytic dye degradation. Powder Technol 318:120–127. https://doi.org/10.1016/j.powtec.2017.05.044

Mirhoseini F, Salabat A (2015) Ionic liquid based microemulsion method for the fabrication of poly(methyl methacrylate)–TiO_2 nanocomposite as a highly efficient visible light photocatalyst. RSC Adv 5:12536–12545. https://doi.org/10.1039/C4RA14612C

Mohaghegh N, Tasviri M, Rahimi E, Gholami MR (2015) A novel p–n junction Ag_3PO_4/$BiPO_4$-based stabilized Pickering emulsion for highly efficient photocatalysis. RSC Adv 5:12944–12955. https://doi.org/10.1039/C4RA14294B

Mohamed RM, Mohamed MM (2008) Copper (II) phthalocyanines immobilized on alumina and encapsulated inside zeolite-X and their applications in photocatalytic degradation of cyanide: a comparative study. Appl Catal A Gen 340:16–24. https://doi.org/10.1016/j.apcata.2008.01.029

Mohamed RM, Shawky A (2018) CNT supported Mn-doped ZnO nanoparticles: simple synthesis and improved photocatalytic activity for degradation of malachite green dye under visible light. Appl Nanosci 8:1179–1188. https://doi.org/10.1007/s13204-018-0742-8

Mohamed MJS, Shenoy US, Bhat DK (2018) Novel NRGO–$CoWO_4$–Fe_2O_3 nanocomposite as an efficient catalyst for dye degradation and reduction of 4-nitrophenol. Mater Chem Phys 208:112–122. https://doi.org/10.1016/j.matchemphys.2018.01.012

Mohanta O, Singhbabu YN, Giri SK et al (2013) Degradation of Congo red pollutants using microwave derived $SrFe_{12}O_{19}$: an efficient magnetic photocatalyst under visible light. J Alloys Compd 564:78–83. https://doi.org/10.1016/j.jallcom.2013.02.074

Mohite SV, Ganbavle VV, Rajpure KY (2017) Photoelectrocatalytic activity of immobilized Yb doped WO_3 photocatalyst for degradation of methyl orange dye. J Energy Chem 26:440–447. https://doi.org/10.1016/j.jechem.2017.01.001

Molinari R, Lavorato C, Argurio P (2017) Recent progress of photocatalytic membrane reactors in water treatment and in synthesis of organic compounds. A review. Catal Today 281:144–164. https://doi.org/10.1016/j.cattod.2016.06.047

Momeni MM, Ghayeb Y, Ghonchegi Z (2015) Fabrication and characterization of copper doped TiO_2 nanotube arrays by in situ electrochemical method as efficient visible-light photocatalyst. Ceram Int 41:8735–8741. https://doi.org/10.1016/j.ceramint.2015.03.094

Mondal D, Das S, Paul BK et al (2019) Size engineered Cu-doped α-MnO_2 nanoparticles for exaggerated photocatalytic activity and energy storage application. Mater Res Bull 115:159–169. https://doi.org/10.1016/j.materresbull.2019.03.023

Moradi H, Eshaghi A, Hosseini SR, Ghani K (2016) Fabrication of Fe-doped TiO_2 nanoparticles and investigation of photocatalytic decolorization of reactive red 198 under visible light irradiation. Ultrason Sonochem 32:314–319. https://doi.org/10.1016/j.ultsonch.2016.03.025

Moradi M, Haghighi M, Allahyari S (2017) Precipitation dispersion of Ag–ZnO nanocatalyst over functionalized multiwall carbon nanotube used in degradation of Acid Orange from wastewater. Process Saf Environ Prot 107:414–427. https://doi.org/10.1016/j.psep.2017.03.010

Mosleh S, Rahimi MR, Ghaedi M et al (2017) Ag_3PO_4/AgBr/Ag-HKUST-1-MOF composites as novel blue LED light active photocatalyst for enhanced degradation of ternary mixture of dyes in a rotating packed bed reactor. Chem Eng Process Process Intensif 114:24–38. https://doi.org/10.1016/j.cep.2017.01.009

Mosleh S, Rahimi MR, Ghaedi M et al (2018) Sonochemical-assisted synthesis of CuO/Cu_2O/Cu nanoparticles as efficient photocatalyst for simultaneous degradation of pollutant dyes in rotating packed bed reactor: LED illumination and central composite design optimization. Ultrason Sonochem 40:601–610. https://doi.org/10.1016/j.ultsonch.2017.08.007

Moussa H, Girot E, Mozet K et al (2016) ZnO rods/reduced graphene oxide composites prepared via a solvothermal reaction for efficient sunlight-driven photocatalysis. Appl Catal B Environ 185:11–21. https://doi.org/10.1016/j.apcatb.2015.12.007

Movahed SK, Piraman Z, Dabiri M (2018) A nitrogen-doped porous carbon derived from copper phthalocyanines on/in ZIF-8 as an

efficient photocatalyst for the degradation of dyes and the C H activation of formamides. J Photochem Photobiol A Chem 351:208–224. https://doi.org/10.1016/j.jphotochem.2017.10.026

Mozia S (2010) Photocatalytic membrane reactors (PMRs) in water and wastewater treatment. A review. Sep Purif Technol 73:71–91. https://doi.org/10.1016/j.seppur.2010.03.021

Munawar T, Iqbal F, Yasmeen S et al (2020) Multi metal oxide NiO–CdO–ZnO nanocomposite–synthesis, structural, optical, electrical properties and enhanced sunlight driven photocatalytic activity. Ceram Int 46:2421–2437. https://doi.org/10.1016/j.ceramint.2019.09.236

Najjar R, Shokri M, Farsadi S (2015) Preparation of Pd-doped nano-TiO_2 in microemulsion and their application in photodegradation of C.I. Acid Yellow 23. Desalin Water Treat 54:2581–2591. https://doi.org/10.1080/19443994.2014.899927

Nan Q, Huang S, Zhou Y et al (2018) Ionic liquid-assisted synthesis of porous BiOBr microspheres with enhanced visible light photocatalytic performance. Appl Organomet Chem 32:e4596. https://doi.org/10.1002/aoc.4596

Naseri A, Samadi M, Mahmoodi NM et al (2017) Tuning composition of electrospun ZnO/CuO nanofibers: toward controllable and efficient solar photocatalytic degradation of organic pollutants. J Phys Chem C 121:3327–3338. https://doi.org/10.1021/acs.jpcc.6b10414

Nasirian M, Bustillo-Lecompte CF, Mehrvar M (2017) Photocatalytic efficiency of Fe_2O_3/TiO_2 for the degradation of typical dyes in textile industries: effects of calcination temperature and UV-assisted thermal synthesis. J Environ Manag 196:487–498. https://doi.org/10.1016/j.jenvman.2017.03.030

Natarajan TS, Lee JY, Bajaj HC et al (2017) Synthesis of multiwall carbon nanotubes/TiO_2 nanotube composites with enhanced photocatalytic decomposition efficiency. Catal Today 282:13–23. https://doi.org/10.1016/j.cattod.2016.03.018

Nawaz M, Miran W, Jang J, Lee DS (2017) Stabilization of Pickering emulsion with surface-modified titanium dioxide for enhanced photocatalytic degradation of Direct Red 80. Catal Today 282:38–47. https://doi.org/10.1016/j.cattod.2016.02.017

Nenavathu BP, Kandula S, Verma S (2018) Visible-light-driven photocatalytic degradation of safranin-T dye using functionalized graphene oxide nanosheet (FGS)/ZnO nanocomposites. RSC Adv 8:19659–19667. https://doi.org/10.1039/C8RA02237B

Ng CT, Yong LQ, Hande MP et al (2017) Zinc oxide nanoparticles exhibit cytotoxicity and genotoxicity through oxidative stress responses in human lung fibroblasts and *Drosophila melanogaster*. Int J Nanomed 12:1621–1637. https://doi.org/10.2147/IJN.S124403

Nguyen XS, Ngo KD (2018) The role of metal-doped into magnetite catalysts for the photo-fenton degradation of organic pollutants. J Surf Eng Mater Adv Technol 08:1–14. https://doi.org/10.4236/jsemat.2018.81001

Nguyen Thi Thu T, Nguyen Thi N, Tran Quang V et al (2016) Synthesis, characterisation, and effect of pH on degradation of dyes of copper-doped TiO_2. J Exp Nanosci 11:226–238. https://doi.org/10.1080/17458080.2015.1053541

Nguyen CH, Fu C-C, Juang R-S (2018) Degradation of methylene blue and methyl orange by palladium-doped TiO_2 photocatalysis for water reuse: efficiency and degradation pathways. J Clean Prod 202:413–427. https://doi.org/10.1016/j.jclepro.2018.08.110

Nidheesh PV, Zhou M, Oturan MA (2018) An overview on the removal of synthetic dyes from water by electrochemical advanced oxidation processes. Chemosphere 197:210–227

Nipane SV, Korake PV, Gokavi GS (2015) Graphene-zinc oxide nanorod nanocomposite as photocatalyst for enhanced degradation of dyes under UV light irradiation. Ceram Int 41:4549–4557. https://doi.org/10.1016/j.ceramint.2014.11.151

Nsabimana A, Kitte SA, Wu F et al (2019) Multifunctional magnetic Fe_3O_4/nitrogen-doped porous carbon nanocomposites for removal of dyes and sensing applications. Appl Surf Sci 467–468:89–97. https://doi.org/10.1016/j.apsusc.2018.10.119

Oblak R, Kete M, Štangar UL, Tasbihi M (2018) Alternative support materials for titania photocatalyst towards degradation of organic pollutants. J Water Process Eng 23:142–150. https://doi.org/10.1016/j.jwpe.2018.03.015

Ola O, Maroto-Valer MM (2015) Review of material design and reactor engineering on TiO_2 photocatalysis for CO_2 reduction. J Photochem Photobiol C Photochem Rev 24:16–42. https://doi.org/10.1016/j.jphotochemrev.2015.06.001

Ollis DF, Pelizzetti E, Serpone N (1991) Photocatalyzed destruction of water contaminants. Environ Sci Technol 25:1522–1529. https://doi.org/10.1021/es00021a001

Osman H, Su Z, Ma X (2017) Efficient photocatalytic degradation of Rhodamine B dye using ZnO/graphitic C_3N_4 nanocomposites synthesized by microwave. Environ Chem Lett 15:435–441. https://doi.org/10.1007/s10311-017-0604-8

Ozmen N, Erdemoglu S, Gungordu A et al (2018) Photocatalytic degradation of azo dye using core@shell nano-TiO_2 particles to reduce toxicity. Environ Sci Pollut Res 25:29493–29504. https://doi.org/10.1007/s11356-018-2942-x

Padmapriya G, Manikandan A, Krishnasamy V et al (2016) Spinel $Ni_xZn_{1-x}Fe_2O_4$ ($0.0 \le x \le 1.0$) nano-photocatalysts: synthesis, characterization and photocatalytic degradation of methylene blue dye. J Mol Struct 1119:39–47. https://doi.org/10.1016/j.molstruc.2016.04.049

Palanivel B, Jayaraman V, Ayyappan C, Alagiri M (2019) Magnetic binary metal oxide intercalated g-C_3N_4: energy band tuned p–n heterojunction towards Z-scheme photo-Fenton phenol reduction and mixed dye degradation. J Water Process Eng 32:100968. https://doi.org/10.1016/j.jwpe.2019.100968

Pan G, Jing X, Ding X et al (2019) Synergistic effects of photocatalytic and electrocatalytic oxidation based on a three-dimensional electrode reactor toward degradation of dyes in wastewater. J Alloys Compd 809:151749. https://doi.org/10.1016/j.jallcom.2019.151749

Panahian Y, Arsalani N (2017) Synthesis of hedgehoglike F–TiO_2(B)/CNT nanocomposites for sonophotocatalytic and photocatalytic degradation of malachite green (MG) under visible light: kinetic study. J Phys Chem A 121:5614–5624. https://doi.org/10.1021/acs.jpca.7b02580

Panthi G, Barakat NAM, Park M et al (2015) Fabrication of PdS/ZnS NPs doped PVAc hybrid electrospun nanofibers: effective and reusable catalyst for dye photodegradation. J Ind Eng Chem 21:298–302. https://doi.org/10.1016/j.jiec.2014.02.036

Parthibavarman M, Sathishkumar S, Prabhakaran S et al (2018a) High visible light-driven photocatalytic activity of large surface area Cu doped SnO_2 nanorods synthesized by novel one-step microwave irradiation method. J Iran Chem Soc 15:2789–2801. https://doi.org/10.1007/s13738-018-1466-0

Parthibavarman M, Sathishkumar S, Prabhakaran S (2018b) Enhanced visible light photocatalytic activity of tin oxide nanoparticles synthesized by different microwave optimum conditions. J Mater Sci: Mater Electron 29:2341–2350. https://doi.org/10.1007/s10854-017-8152-3

Pascariu P, Airinei A, Olaru N et al (2016) Photocatalytic degradation of Rhodamine B dye using ZnO–SnO_2 electrospun ceramic nanofibers. Ceram Int 42:6775–6781. https://doi.org/10.1016/j.ceramint.2016.01.054

Pascariu P, Homocianu M, Cojocaru C et al (2019) Preparation of La doped ZnO ceramic nanostructures by electrospinning–calcination method: effect of La^{3+} doping on optical and photocatalytic properties. Appl Surf Sci 476:16–27. https://doi.org/10.1016/j.apsusc.2019.01.077

Patel JD, Vu TTD, Mighri F (2017) Preparation and characterization of CdS coated multiwalled carbon nanotubes. Mater Lett 196:161–164. https://doi.org/10.1016/j.matlet.2017.03.046

Patil SM, Deshmukh SP, More KV et al (2019) Sulfated TiO_2/WO_3 nanocomposite: an efficient photocatalyst for degradation of Congo red and methyl red dyes under visible light irradiation. Mater Chem Phys 225:247–255. https://doi.org/10.1016/j.matchemphys.2018.12.041

Patil S, Anantharaju KS, Rangappa D et al (2020) Magnetic Eu-doped $MgFe_2O_4$ nanomaterials: an investigation of their structural, optical and enhanced visible-light-driven photocatalytic performance. Environ Nanotechnol Monit Manag 13:100268. https://doi.org/10.1016/j.enmm.2019.100268

Patiño Y, Díaz E, Ordóñez S et al (2015) Adsorption of emerging pollutants on functionalized multiwall carbon nanotubes. Chemosphere 136:174–180. https://doi.org/10.1016/j.chemosphere.2015.04.089

Paul S, Choudhury A (2014) Investigation of the optical property and photocatalytic activity of mixed phase nanocrystalline titania. Appl Nanosci 4:839–847. https://doi.org/10.1007/s13204-013-0264-3

Peter CN, Anku WW, Sharma R et al (2019) N-doped ZnO/graphene oxide: a photostable photocatalyst for improved mineralization and photodegradation of organic dye under visible light. Ionics (Kiel) 25:327–339. https://doi.org/10.1007/s11581-018-2571-x

Pham VP, Yeom GY (2016) Recent advances in doping of molybdenum disulfide: industrial applications and future prospects. Adv Mater 28:9024–9059. https://doi.org/10.1002/adma.201506402

Pickering JW, Bhethanabotla VR, Kuhn JN (2017) Plasmonic photocatalytic reactor design: use of multilayered films for improved organic degradation rates in a recirculating flow reactor. Chem Eng J 314:11–18. https://doi.org/10.1016/j.cej.2016.12.112

Pirinejad L, Maleki A, Shahmoradi B et al (2019) Synthesis and application of Fe–N–Cr–TiO_2 nanocatalyst for photocatalytic degradation of Acid Black 1 under LED light irradiation. J Mol Liq 279:232–240. https://doi.org/10.1016/j.molliq.2019.01.135

Pol R, Guerrero M, García-Lecina E et al (2016) Ni-, Pt- and (Ni/Pt)-doped TiO_2 nanophotocatalysts: a smart approach for sustainable degradation of Rhodamine B dye. Appl Catal B Environ 181:270–278. https://doi.org/10.1016/j.apcatb.2015.08.006

Pozzo RL, Baltanás MA, Cassano AE (1997) Supported titanium oxide as photocatalyst in water decontamination: state of the art. Catal Today 39:219–231. https://doi.org/10.1016/S0920-5861(97)00103-X

Prabakaran E, Pillay K (2019) Synthesis of N-doped ZnO nanoparticles with cabbage morphology as a catalyst for the efficient photocatalytic degradation of methylene blue under UV and visible light. RSC Adv 9:7509–7535. https://doi.org/10.1039/C8RA09962F

Prabhakarrao N, Chandra MR, Rao TS (2017) Synthesis of Zr doped TiO_2/reduced graphene oxide (rGO) nanocomposite material for efficient photocatalytic degradation of Eosin Blue dye under visible light irradiation. J Alloys Compd 694:596–606. https://doi.org/10.1016/j.jallcom.2016.09.329

Prekodravac J, Vasiljević B, Marković Z et al (2019) Green and facile microwave assisted synthesis of (metal-free) N-doped carbon quantum dots for catalytic applications. Ceram Int 45:17006–17013. https://doi.org/10.1016/j.ceramint.2019.05.250

Priyanka, Srivastava VC (2013) Photocatalytic oxidation of dye bearing wastewater by iron doped zinc oxide. Ind Eng Chem Res 52:17790–17799. https://doi.org/10.1021/ie401973r

Punnoose A, Dodge K, Rasmussen JW et al (2014) Cytotoxicity of ZnO nanoparticles can be tailored by modifying their surface structure: a green chemistry approach for safer nanomaterials. ACS Sustain Chem Eng 2:1666–1673. https://doi.org/10.1021/sc500140x

Qi YL, Zheng YF, Yin HY, Song XC (2017) Enhanced visible light photocatalytic activity of AgBr on 001 facets exposed to BiOCl. J Alloys Compd 712:535–542. https://doi.org/10.1016/j.jallcom.2017.04.126

Qian J, Shen C, Yan J et al (2018) Tailoring the electronic properties of graphene quantum dots by P doping and their enhanced performance in metal-free composite photocatalyst. J Phys Chem C 122:349–358. https://doi.org/10.1021/acs.jpcc.7b08702

Rahmanian N, Eskandani M, Barar J, Omidi Y (2017) Recent trends in targeted therapy of cancer using graphene oxide-modified multifunctional nanomedicines. J Drug Target 25:202–215. https://doi.org/10.1080/1061186X.2016.1238475

Rajabi HR, Arjmand H, Kazemdehdashti H, Farsi M (2016) A comparison investigation on photocatalytic activity performance and adsorption efficiency for the removal of cationic dye: quantum dots vs. magnetic nanoparticles. J Environ Chem Eng 4:2830–2840. https://doi.org/10.1016/j.jece.2016.05.029

Ramya S, Ruth Nithila SD, George RP et al (2013) Antibacterial studies on Eu–Ag codoped TiO_2 surfaces. Ceram Int 39:1695–1705. https://doi.org/10.1016/j.ceramint.2012.08.012

Rangel R, Cedeño V, Ramos-Corona A et al (2017) Tailoring surface and photocatalytic properties of ZnO and nitrogen-doped ZnO nanostructures using microwave-assisted facile hydrothermal synthesis. Appl Phys A 123:552. https://doi.org/10.1007/s00339-017-1137-5

Rani MP, Manjunatha P (2018) Review on the photocatalytic degradation of dyes and antibacterial activities of pure and doped-ZnO. Int J Res Innov Appl Sci 4:2252–2264

Rao BG, Mukherjee D, Reddy BM (2017) Novel approaches for preparation of nanoparticles. In: Ficai D, Grumezescu A (eds) Nanostructures for novel therapy. Elsevier, Amsterdam, pp 1–36

Rashmi Pradhan S, Colmenares-Quintero RF, Colmenares Quintero JC (2019) Designing microflowreactors for photocatalysis using sonochemistry: a systematic review article. Molecules 24:3315. https://doi.org/10.3390/molecules24183315

Rauf MA, Ashraf SS (2009) Fundamental principles and application of heterogeneous photocatalytic degradation of dyes in solution. Chem Eng J 151:10–18. https://doi.org/10.1016/j.cej.2009.02.026

Rauf MA, Bukallah SB, Hamadi A et al (2007) The effect of operational parameters on the photoinduced decoloration of dyes using a hybrid catalyst V_2O_5/TiO_2. Chem Eng J 129:167–172. https://doi.org/10.1016/j.cej.2006.10.031

Ravishankar TN, de Vaz MO, Ramakrishnappa T et al (2019) Ionic liquid–assisted hydrothermal synthesis of Nb/TiO_2 nanocomposites for efficient photocatalytic hydrogen production and photodecolorization of Rhodamine B under UV–visible and visible light illuminations. Mater Today Chem 12:373–385. https://doi.org/10.1016/j.mtchem.2019.04.001

Raza W, Faisal SM, Owais M et al (2016) Facile fabrication of highly efficient modified ZnO photocatalyst with enhanced photocatalytic, antibacterial and anticancer activity. RSC Adv 6:78335–78350. https://doi.org/10.1039/C6RA06774C

Reddy PAK, Reddy PVL, Kwon E et al (2016) Recent advances in photocatalytic treatment of pollutants in aqueous media. Environ Int 91:94–103. https://doi.org/10.1016/j.envint.2016.02.012

Reddy IN, Reddy CV, Shim J et al (2020) Excellent visible-light driven photocatalyst of (Al, Ni) co-doped ZnO structures for organic dye degradation. Catal Today 340:277–285. https://doi.org/10.1016/j.cattod.2018.07.030

Ren X, Feng J, Si P et al (2018) Enhanced heterogeneous activation of peroxydisulfate by S, N co-doped graphene via controlling S, N functionalization for the catalytic decolorization of dyes in water. Chemosphere 210:120–128. https://doi.org/10.1016/j.chemosphere.2018.07.011

Renuka L, Anantharaju KS, Sharma SC et al (2016) Hollow microspheres Mg-doped ZrO_2 nanoparticles: green assisted synthesis and applications in photocatalysis and photoluminescence. J Alloys Compd 672:609–622. https://doi.org/10.1016/j.jallcom.2016.02.124

Reszczyńska J, Grzyb T, Sobczak JW et al (2015) Visible light activity of rare earth metal doped (Er^{3+}, Yb^{3+} or Er^{3+}/Yb^{3+}) titania photocatalysts. Appl Catal B Environ 163:40–49. https://doi.org/10.1016/j.apcatb.2014.07.010

Réti B, Major Z, Szarka D et al (2016) Influence of TiO_2 phase composition on the photocatalytic activity of TiO_2/MWCNT composites prepared by combined sol–gel/hydrothermal method. J Mol Catal A: Chem 414:140–147. https://doi.org/10.1016/j.molcata.2016.01.016

Reza KM, Kurny ASW, Gulshan F (2017) Parameters affecting the photocatalytic degradation of dyes using TiO_2: a review. Appl Water Sci 7:1569–1578. https://doi.org/10.1007/s13201-015-0367-y

Rodrigues J, Hatami T, Rosa JM et al (2020) Photocatalytic degradation using ZnO for the treatment of RB 19 and RB 21 dyes in industrial effluents and mathematical modeling of the process. Chem Eng Res Des 153:294–305. https://doi.org/10.1016/j.cherd.2019.10.021

Rokhsat E, Akhavan O (2016) Improving the photocatalytic activity of graphene oxide/ZnO nanorod films by UV irradiation. Appl Surf Sci 371:590–595. https://doi.org/10.1016/j.apsusc.2016.02.222

Rome'as V, Pichat P, Guillard C et al (1999) Degradation of palmitic (hexadecanoic) acid deposited on TiO_2-coated self-cleaning glass: kinetics of disappearance, intermediate products and degradation pathways. New J Chem 23:365–374. https://doi.org/10.1039/a901342c

Rossetti I, Compagnoni M (2016) Chemical reaction engineering, process design and scale-up issues at the frontier of synthesis: flow chemistry. Chem Eng J 296:56–70. https://doi.org/10.1016/j.cej.2016.02.119

Rothenberger G, Moser J, Graetzel M et al (1985) Charge carrier trapping and recombination dynamics in small semiconductor particles. J Am Chem Soc 107:8054–8059. https://doi.org/10.1021/ja00312a043

Rout L, Kumar A, Satish K, Achary L et al (2019) Ionic liquid assisted combustion synthesis of ZnO and its modification by Au Sn bimetallic nanoparticles: an efficient photocatalyst for degradation of organic contaminants. Mater Chem Phys 232:339–353. https://doi.org/10.1016/j.matchemphys.2019.04.063

Ruzimuradov O, Hojamberdiev M, Fasel C, Riedel R (2017) Fabrication of lanthanum and nitrogen – co-doped $SrTiO_3$–TiO_2 heterostructured macroporous monolithic materials for photocatalytic degradation of organic dyes under visible light. J Alloys Compd 699:144–150. https://doi.org/10.1016/j.jallcom.2016.12.355

Saeed M, Muneer M, Mumtaz N et al (2018) Ag–Co_3O_4: synthesis, characterization and evaluation of its photo-catalytic activity towards degradation of rhodamine B dye in aqueous medium. Chin J Chem Eng 26:1264–1269. https://doi.org/10.1016/j.cjche.2018.02.024

Saggioro EM, Oliveira AS, Buss DF et al (2015) Photo-decolorization and ecotoxicological effects of solar compound parabolic collector pilot plant and artificial light photocatalysis of indigo carmine dye. Dye Pigment 113:571–580. https://doi.org/10.1016/j.dyepig.2014.09.029

Sai Saraswathi V, Santhakumar K (2017) Photocatalytic activity against azo dye and cytotoxicity on MCF-7 cell lines of zirconium oxide nanoparticle mediated using leaves of Lagerstroemia speciosa. J Photochem Photobiol B Biol 169:47–55. https://doi.org/10.1016/j.jphotobiol.2017.02.023

Saleh NB, Milliron DJ, Aich N et al (2016) Importance of doping, dopant distribution, and defects on electronic band structure alteration of metal oxide nanoparticles: implications for reactive oxygen species. Sci Total Environ 568:926–932. https://doi.org/10.1016/j.scitotenv.2016.06.145

Sambur JB, Chen P (2016) Distinguishing direct and indirect photoelectrocatalytic oxidation mechanisms using quantitative single-molecule reaction imaging and photocurrent measurements. J Phys Chem C 120:20668–20676. https://doi.org/10.1021/acs.jpcc.6b01848

Sancheti SV, Saini C, Ambati R, Gogate PR (2018) Synthesis of ultrasound assisted nanostuctured photocatalyst (NiO supported over CeO_2) and its application for photocatalytic as well as sonocatalytic dye degradation. Catal Today 300:50–57. https://doi.org/10.1016/j.cattod.2017.02.047

Sangchay W (2016) The self-cleaning and photocatalytic properties of TiO_2 doped with SnO_2 thin films preparation by sol–gel method. Energy Procedia 89:170–176

Sanjeev Kumar R, Veeravazhuthi V, Muthukumarasamy N et al (2019) Effect of gadolinium doped ZnS nanoparticles: ferro magnetic photocatalyst for efficient dye degradation. SN Appl Sci 1:268. https://doi.org/10.1007/s42452-019-0283-0

Sankar S, Sharma SK, An N et al (2016) Photocatalytic properties of Mn-doped NiO spherical nanoparticles synthesized from sol–gel method. Optik (Stuttg) 127:10727–10734. https://doi.org/10.1016/j.ijleo.2016.08.126

Sathish Kumar K, Rohit Narayanan KR, Siddarth S et al (2018) Synthesis of MgO/TiO_2 nanocomposite and its application in photocatalytic dye degradation. Int J Chem React Eng. https://doi.org/10.1515/ijcre-2017-0136

Sayed AE-DH, Soliman HAM (2017) Developmental toxicity and DNA damaging properties of silver nanoparticles in the catfish (*Clarias gariepinus*). Mutat Res Toxicol Environ Mutagen 822:34–40. https://doi.org/10.1016/j.mrgentox.2017.07.002

Senthilraja A, Krishnakumar B, Subash B et al (2016) Sn loaded Au–ZnO photocatalyst for the degradation of AR 18 dye under UV-A light. J Ind Eng Chem 33:51–58. https://doi.org/10.1016/j.jiec.2015.09.010

Serna-Galvis EA, Botero-Coy AM, Martínez-Pachón D, Moncayo-Lasso A, Ibáñez M, Hernández F, Torres-Palma RA (2019) Degradation of seventeen contaminants of emerging concern in municipal wastewater effluents by sonochemical advanced oxidation processes. Water Res 154:349–360

Serpone N, Emeline AV (2012) Semiconductor photocatalysis—past, present, and future outlook. J Phys Chem Lett 3:673–677. https://doi.org/10.1021/jz300071j

Serrà A, Zhang Y, Sepúlveda B et al (2020) Highly reduced ecotoxicity of ZnO-based micro/nanostructures on aquatic biota: influence of architecture, chemical composition, fixation, and photocatalytic efficiency. Water Res 169:115210. https://doi.org/10.1016/j.watres.2019.115210

Shah JH, Fiaz M, Athar M et al (2019) Facile synthesis of N/B-double-doped Mn_2O_3 and WO_3 nanoparticles for dye degradation under visible light. Environ Technol. https://doi.org/10.1080/09593330.2019.1567604

Shams S, Khan AU, Yuan Q et al (2019) Facile and eco-benign synthesis of Au@Fe_2O_3 nanocomposite: efficient photocatalytic, antibacterial and antioxidant agent. J Photochem Photobiol B Biol 199:111632. https://doi.org/10.1016/j.jphotobiol.2019.111632

Shanmugapriya B, Shanthi M, Dhamodharan P et al (2020) Enhancement of photocatalytic degradation of methylene blue dye using Ti^{3+} doped In_2O_3 nanocubes prepared by hydrothermal method. Optik (Stuttg) 202:163662. https://doi.org/10.1016/j.ijleo.2019.163662

Shao L, Liu H, Zeng W et al (2019) Immobilized and photocatalytic performances of PDMS-SiO_2-chitosan@TiO_2 composites on pumice under simulated sunlight irradiation. Appl Surf Sci 478:1017–1026. https://doi.org/10.1016/j.apsusc.2019.02.060

Shao L, Liu Y, Wang L et al (2020) Electronic structure tailoring of BiOBr (0 1 0) nanosheets by cobalt doping for enhanced visible-light photocatalytic activity. Appl Surf Sci 502:143895. https://doi.org/10.1016/j.apsusc.2019.143895

Sharma RK, Chouryal YN, Chaudhari S et al (2017) Adsorption-driven catalytic and photocatalytic activity of phase tuned In_2S_3 nanocrystals synthesized via ionic liquids. ACS Appl Mater Interfaces 9:11651–11661. https://doi.org/10.1021/acsami.7b01092

Sharma S, Pathak AK, Singh VN et al (2018) Excellent mechanical properties of long multiwalled carbon nanotube bridged Kevlar fabric. Carbon N Y 137:104–117. https://doi.org/10.1016/j.carbon.2018.05.017

Sharma HK, Archana R, Sankar Ganesh R et al (2019) Substitution of Al^{3+} to Zn^{2+} sites of ZnO enhanced the photocatalytic degradation of methylene blue under irradiation of visible light. Solid State Sci 94:45–53. https://doi.org/10.1016/j.solidstatesciences.2019.05.011

Sharon M, Modi F, Sharon M (2016) Titania based nanocomposites as a photocatalyst: a review. AIMS Mater Sci 3:1236–1254. https://doi.org/10.3934/matersci.2016.3.1236

Shende TP, Bhanvase BA, Rathod AP et al (2018) Sonochemical synthesis of graphene–Ce–TiO_2 and graphene–Fe–TiO_2 ternary hybrid photocatalyst nanocomposite and its application in degradation of crystal violet dye. Ultrason Sonochem 41:582–589. https://doi.org/10.1016/j.ultsonch.2017.10.024

Shende AG, Ghugal SG, Vidyasagar D et al (2019) Magnetically separable indium doped ZnS $NiFe_2O_4$ heterostructure photocatalyst for mineralization of acid violet 7 dye. Mater Chem Phys 221:483–492. https://doi.org/10.1016/j.matchemphys.2018.09.032

Sheng Y, Yang J, Wang F et al (2019) Sol-gel synthesized hexagonal boron nitride/titania nanocomposites with enhanced photocatalytic activity. Appl Surf Sci 465:154–163. https://doi.org/10.1016/j.apsusc.2018.09.137

Shet A, Vidya SK (2016) Solar light mediated photocatalytic degradation of phenol using Ag core–TiO_2 shell (Ag@TiO_2) nanoparticles in batch and fluidized bed reactor. Sol Energy 127:67–78. https://doi.org/10.1016/j.solener.2015.12.049

Sheydaei M, Fattahi M, Ghalamchi L, Vatanpour V (2019) Systematic comparison of sono-synthesized Ce-, La- and Ho-doped ZnO nanoparticles and using the optimum catalyst in a visible light assisted continuous sono-photocatalytic membrane reactor. Ultrason Sonochem 56:361–371. https://doi.org/10.1016/j.ultsonch.2019.04.031

Shi X, Zhang Y, Liu X et al (2019a) A mild in situ method to construct Fe-doped cauliflower-like rutile TiO_2 photocatalysts for degradation of organic dye in wastewater. Catalysts 9:426. https://doi.org/10.3390/catal9050426

Shi Y, Zhang Q, Liu Y et al (2019b) Preparation of amphiphilic TiO_2 Janus particles with highly enhanced photocatalytic activity. Chin J Catal 40:786–794. https://doi.org/10.1016/S1872-2067(19)63332-2

Shkir M, Yahia IS, AlFaify S et al (2016) Facile synthesis of lead iodide nanostructures by microwave irradiation technique and their structural, morphological, photoluminescence and dielectric studies. J Mol Struct 1110:83–90. https://doi.org/10.1016/j.molstruc.2016.01.014

Siddiqa A, Masih D, Anjum D, Siddiq M (2015) Cobalt and sulfur co-doped nano-size TiO_2 for photodegradation of various dyes and phenol. J Environ Sci 37:100–109. https://doi.org/10.1016/j.jes.2015.04.024

Singh S (2019) Zinc oxide nanoparticles impacts: cytotoxicity, genotoxicity, developmental toxicity, and neurotoxicity. Toxicol Mech Methods 29:300–311. https://doi.org/10.1080/15376516.2018.1553221

Snoussi Y, Bastide S, Abderrabba M, Chehimi MM (2018) Sonochemical synthesis of Fe_3O_4@NH_2-mesoporous silica@Polypyrrole/Pd: a core/double shell nanocomposite for catalytic applications. Ultrason Sonochem 41:551–561. https://doi.org/10.1016/j.ultsonch.2017.10.021

Sobhani S, Zarifi F, Skibsted J (2017) Ionic liquids grafted onto graphene oxide as a new multifunctional heterogeneous catalyst and its application in the one-pot multi-component synthesis of hexahydroquinolines. New J Chem 41:6219–6225. https://doi.org/10.1039/C7NJ00063D

Sompalli NK, Das A, De Syamal S et al (2020) Mesoporous monolith designs of mixed phased titania codoped Sm^{3+}/Er^{3+} composites: a super responsive visible light photocatalysts for organic pollutant clean-up. Appl Surf Sci 504:144350. https://doi.org/10.1016/j.apsusc.2019.144350

Sood S, Umar A, Kumar Mehta S et al (2015) Efficient photocatalytic degradation of brilliant green using Sr-doped TiO_2 nanoparticles. Ceram Int 41:3533–3540. https://doi.org/10.1016/j.ceramint.2014.11.010

Sorbiun M, Shayegan Mehr E, Ramazani A, Taghavi Fardood S (2018) Green synthesis of zinc oxide and copper oxide nanoparticles using aqueous extract of oak fruit hull (jaft) and comparing their photocatalytic degradation of basic violet 3. Int J Environ Res 12:29–37. https://doi.org/10.1007/s41742-018-0064-4

Souza RP, Freitas TKFS, Domingues FS et al (2016) Photocatalytic activity of TiO_2, ZnO and Nb_2O_5 applied to degradation of textile wastewater. J Photochem Photobiol A Chem 329:9–17. https://doi.org/10.1016/j.jphotochem.2016.06.013

Sreelekha N, Subramanyam K, Amaranatha Reddy D et al (2016) Structural, optical, magnetic and photocatalytic properties of Co doped CuS diluted magnetic semiconductor nanoparticles. Appl Surf Sci 378:330–340. https://doi.org/10.1016/j.apsusc.2016.04.003

Srikanth B, Goutham R, Badri Narayan R et al (2017) Recent advancements in supporting materials for immobilised photocatalytic applications in waste water treatment. J Environ Manage 200:60–78. https://doi.org/10.1016/j.jenvman.2017.05.063

Štrbac D, Aggelopoulos CA, Štrbac G et al (2018) Photocatalytic degradation of naproxen and methylene blue: comparison between ZnO, TiO_2 and their mixture. Process Saf Environ Prot 113:174–183. https://doi.org/10.1016/j.psep.2017.10.007

Su Y, Kuijpers K, Hessel V, Noël T (2016) A convenient numbering-up strategy for the scale-up of gas–liquid photoredox catalysis in flow. React Chem Eng 1:73–81. https://doi.org/10.1039/C5RE00021A

Su Y, Li H, Ma H et al (2017) Controlling surface termination and facet orientation in Cu_2O nanoparticles for high photocatalytic activity: a combined experimental and density functional theory study. ACS Appl Mater Interfaces 9:8100–8106. https://doi.org/10.1021/acsami.6b15648

Sudrajat H, Babel S (2017) A novel visible light active N-doped ZnO for photocatalytic degradation of dyes. J Water Process Eng 16:309–318. https://doi.org/10.1016/j.jwpe.2016.11.006

Sudrajat H, Babel S, Sakai H, Takizawa S (2016) Rapid enhanced photocatalytic degradation of dyes using novel N-doped ZrO_2. J Environ Manag 165:224–234. https://doi.org/10.1016/j.jenvman.2015.09.036

Sun H, Liu S, Zhou G et al (2012) Reduced graphene oxide for catalytic oxidation of aqueous organic pollutants. ACS Appl Mater Interfaces 4:5466–5471. https://doi.org/10.1021/am301372d

Sun L, Shao Q, Zhang Y et al (2020) N self-doped ZnO derived from microwave hydrothermal synthesized zeolitic imidazolate framework-8 toward enhanced photocatalytic degradation of methylene blue. J Colloid Interface Sci 565:142–155. https://doi.org/10.1016/j.jcis.2019.12.107

Sundar KP, Kanmani S (2020) Progression of Photocatalytic reactors and it's comparison: a review. Chem Eng Res Des 154:135–150. https://doi.org/10.1016/j.cherd.2019.11.035

Sushma C, Girish Kumar S (2017) Advancements in the zinc oxide nanomaterials for efficient photocatalysis. Chem Pap 71:2023–2042. https://doi.org/10.1007/s11696-017-0217-5

Sutanto H, Hidayanto E, Mukholit et al (2017) The physical and photocatalytic properties of N-doped TiO_2 polycrystalline synthesized by a single step sonochemical method at room temperature. Mater Sci Forum 890:121–126. https://doi.org/10.4028/www.scientific.net/MSF.890.121

Tanji K, Navio JA, Naja J et al (2019) Extraordinary visible photocatalytic activity of a $Co_{0.2}Zn_{0.8}O$ system studied in the Remazol BB oxidation. J Photochem Photobiol A Chem 382:111877. https://doi.org/10.1016/j.jphotochem.2019.111877

Tanwar R, Kumar S, Mandal UK (2017) Photocatalytic activity of PANI/Fe^0 doped BiOCl under visible light-degradation of Congo red dye. J Photochem Photobiol A Chem 333:105–116. https://doi.org/10.1016/j.jphotochem.2016.10.022

Thejaswini TV, Prabhakaran D, Maheswari MA (2016) Soft synthesis of Bi Doped and Bi–N co-doped TiO_2 nanocomposites: a comprehensive mechanistic approach towards visible light induced ultra-fast photocatalytic degradation of fabric dye pollutant. J Environ Chem Eng 4:1308–1321. https://doi.org/10.1016/j.jece.2016.01.031

Thennarasu G, Sivasamy A (2016) Enhanced visible photocatalytic activity of cotton ball like nano structured Cu doped ZnO for the degradation of organic pollutant. Ecotoxicol Environ Saf 134:412–420. https://doi.org/10.1016/j.ecoenv.2015.10.030

Tomei MC, Soria Pascual J, Mosca Angelucci D (2016) Analysing performance of real textile wastewater bio-decolourization under different reaction environments. J Clean Prod 129:468–477. https://doi.org/10.1016/j.jclepro.2016.04.028

Tong T, Binh CTT, Kelly JJ et al (2013) Cytotoxicity of commercial nano-TiO_2 to *Escherichia coli* assessed by high-throughput screening: effects of environmental factors. Water Res 47:2352–2362. https://doi.org/10.1016/j.watres.2013.02.008

Trapalis A, Todorova N, Giannakopoulou T et al (2016) TiO_2/graphene composite photocatalysts for NOx removal: a comparison of surfactant-stabilized graphene and reduced graphene oxide. Appl Catal B Environ 180:637–647. https://doi.org/10.1016/j.apcatb.2015.07.009

Turchi CS, Ollis DF (1990) Photocatalytic degradation of organic water contaminants: mechanisms involving hydroxyl radical attack. J Catal 122:178–192. https://doi.org/10.1016/0021-9517(90)90269-P

Usman M, Byrne JM, Chaudhary A et al (2018) Magnetite and green rust: synthesis, properties, and environmental applications of mixed-valent iron minerals. Chem Rev 118:3251–3304. https://doi.org/10.1021/acs.chemrev.7b00224

Vaiano V, Sacco O, Sannino D et al (2017a) Influence of aggregate size on photoactivity of N-doped TiO_2 particles in aqueous suspensions under visible light irradiation. J Photochem Photobiol A Chem 336:191–197. https://doi.org/10.1016/j.jphotochem.2017.01.009

Vaiano V, Sacco O, Sannino D et al (2017b) Enhanced performances of a photocatalytic reactor for wastewater treatment using controlled modulation of LEDs light. Chem Eng Trans. https://doi.org/10.3303/CET1757093

Vasantharaj S, Sathiyavimal S, Senthilkumar P et al (2019) Biosynthesis of iron oxide nanoparticles using leaf extract of *Ruellia tuberosa*: antimicrobial properties and their applications in photocatalytic degradation. J Photochem Photobiol B Biol 192:74–82. https://doi.org/10.1016/j.jphotobiol.2018.12.025

Veldurthi NK, Palla S, Velchuri R et al (2015) Degradation of mixed dyes in aqueous wastewater using a novel visible light driven $LiMg_{0.5}Mn_{0.5}O_2$ photocatalyst. Mater Express 5:445–450. https://doi.org/10.1166/mex.2015.1255

Verma P, Samanta SK (2018) Microwave-enhanced advanced oxidation processes for the degradation of dyes in water. Environ Chem Lett 16:969–1007. https://doi.org/10.1007/s10311-018-0739-2

Wagner S, Bloh J, Kasper C, Bahnemann D (2011) Toxicological issues of nanoparticles employed in photocatalysis. Green. https://doi.org/10.1515/green.2011.013

Wang J, Xie Y, Zhang Z et al (2010) Photocatalytic degradation of organic dyes by Er^{3+}:$YAlO_3$/TiO_2 composite under solar light. Environ Chem Lett 8:87–93. https://doi.org/10.1007/s10311-008-0196-4

Wang Y, Fang H-B, Ye R-Q et al (2016) Functionalization of ZnO aggregate films via iodine-doping and TiO_2 decorating for enhanced visible-light-driven photocatalytic activity and stability. RSC Adv 6:24430–24437. https://doi.org/10.1039/C6RA00903D

Wang C, Wu Y, Lu J et al (2017) Bioinspired synthesis of photocatalytic nanocomposite membranes based on synergy of Au–TiO_2 and polydopamine for degradation of tetracycline under visible light. ACS Appl Mater Interfaces 9:23687–23697. https://doi.org/10.1021/acsami.7b04902

Wang D, Han D, Yang J et al (2018a) Controlled preparation of superparamagnetic Fe_3O_4@SiO_2@ZnO–Au core–shell photocatalyst with superior activity: RhB degradation and working mechanism. Powder Technol 327:489–499. https://doi.org/10.1016/j.powtec.2017.12.088

Wang J-C, Lou H-H, Xu Z-H et al (2018b) Natural sunlight driven highly efficient photocatalysis for simultaneous degradation of rhodamine B and methyl orange using I/C codoped TiO_2 photocatalyst. J Hazard Mater 360:356–363. https://doi.org/10.1016/j.jhazmat.2018.08.008

Wattanawikkam C, Kansa-ard T, Pecharapa W (2019) X-ray absorption spectroscopy analysis and photocatalytic behavior of $ZnTiO_3$ nanoparticles doped with Co and Mn synthesized by sonochemical method. Appl Surf Sci 474:169–176. https://doi.org/10.1016/j.apsusc.2018.03.175

Wei L, Zhang Y, Chen S et al (2019) Synthesis of nitrogen-doped carbon nanotubes-$FePO_4$ composite from phosphate residue and its application as effective Fenton-like catalyst for dye degradation. J Environ Sci 76:188–198. https://doi.org/10.1016/j.jes.2018.04.024

Wen J, Xie J, Chen X, Li X (2017) A review on g-C_3N_4-based photocatalysts. Appl Surf Sci 391:72–123

Wu C-H, Chang H-W, Chern J-M (2006) Basic dye decomposition kinetics in a photocatalytic slurry reactor. J Hazard Mater 137:336–343. https://doi.org/10.1016/j.jhazmat.2006.02.002

Wu Y, Wang P, Zhu X et al (2018) Composite of $CH_3NH_3PbI_3$ with reduced graphene oxide as a highly efficient and stable visible-light photocatalyst for hydrogen evolution in aqueous HI solution. Adv Mater 30:1704342. https://doi.org/10.1002/adma.201704342

Xia X-H, Jia Z-J, Yu Y et al (2007) Preparation of multi-walled carbon nanotube supported TiO_2 and its photocatalytic activity in the reduction of CO_2 with H_2O. Carbon N Y 45:717–721. https://doi.org/10.1016/j.carbon.2006.11.028

Xing X, Du Z, Zhuang J, Wang D (2018) Removal of ciprofloxacin from water by nitrogen doped TiO_2 immobilized on glass spheres: rapid screening of degradation products. J Photochem Photobiol A Chem 359:23–32. https://doi.org/10.1016/j.jphotochem.2018.03.026

Xu P (2001) Polymer–ceramic nanocomposites: ceramic phases. In: Buschow KHJ (ed) Encyclopedia of materials: science and technology. Elsevier, Amsterdam, pp 7565–7570

Xu R, Li J, Wang J et al (2010) Photocatalytic degradation of organic dyes under solar light irradiation combined with Er^{3+}:$YAlO_3$/

Fe- and Co-doped TiO_2 coated composites. Sol Energy Mater Sol Cells 94:1157–1165. https://doi.org/10.1016/j.solmat.2010.03.003

Xu H, Zeiger BW, Suslick KS (2013) Sonochemical synthesis of nanomaterials. Chem Soc Rev 42:2555–2567. https://doi.org/10.1039/C2CS35282F

Xuan Z, Shiyue Y, Yumei L et al (2015) Microwave-assisted synthesis and enhanced visible-light-driven photocatalytic property of g-C_3N_4/Bi_2S_3 nanocomposite. Mater Lett 145:23–26. https://doi.org/10.1016/j.matlet.2015.01.084

Xue J, Song F, Dong X et al (2019) Controlling self-assembly of cellulose nanocrystal to synergistically regulate (001) reactive facets and hierarchical pore structure of anatase nano-TiO_2 for high photocatalytic activity. ACS Sustain Chem Eng 7:1973–1979. https://doi.org/10.1021/acssuschemeng.8b04171

Yan W-Y, Zhou Q, Chen X et al (2016) Size-controlled TiO_2 nanocrystals with exposed 001 and 101 facets strongly linking to graphene oxide via p-phenylenediamine for efficient photocatalytic degradation of fulvic acids. J Hazard Mater 314:41–50. https://doi.org/10.1016/j.jhazmat.2016.04.026

Yan X, Ye K, Zhang T et al (2017) Formation of three-dimensionally ordered macroporous TiO_2@nanosheet SnS_2 heterojunctions for exceptional visible-light driven photocatalytic activity. New J Chem 41:8482–8489. https://doi.org/10.1039/C7NJ01421J

Yang S, Yang L, Liu X et al (2015) TiO_2-doped Fe_3O_4 nanoparticles as high-performance Fenton-like catalyst for dye decoloration. Sci China Technol Sci 58:858–863. https://doi.org/10.1007/s11431-015-5801-8

Yang Q, Chen F, Li X et al (2016) Self-assembly Z-scheme heterostructured photocatalyst of Ag_2O@Ag-modified bismuth vanadate for efficient photocatalytic degradation of single and dual organic pollutants under visible light irradiation. RSC Adv 6:60291–60307. https://doi.org/10.1039/C6RA04862E

Yang W, Shen H, Min H, Ge J (2020) Enhanced visible light-driven photodegradation of rhodamine B by Ti^{3+} self-doped TiO_2@Ag nanoparticles prepared using Ti vapor annealing. J Mater Sci 55:701–712. https://doi.org/10.1007/s10853-019-03996-6

Yao Y, Qin J, Chen H et al (2015) One-pot approach for synthesis of N-doped TiO_2/$ZnFe_2O_4$ hybrid as an efficient photocatalyst for degradation of aqueous organic pollutants. J Hazard Mater 291:28–37. https://doi.org/10.1016/j.jhazmat.2015.02.042

Yao Y, Chen H, Lian C et al (2016) Fe Co, Ni nanocrystals encapsulated in nitrogen-doped carbon nanotubes as Fenton-like catalysts for organic pollutant removal. J Hazard Mater 314:129–139. https://doi.org/10.1016/j.jhazmat.2016.03.089

Ye Y, Feng Y, Bruning H et al (2018) Photocatalytic degradation of metoprolol by TiO_2 nanotube arrays and UV-LED: effects of catalyst properties, operational parameters, commonly present water constituents, and photo-induced reactive species. Appl Catal B Environ 220:171–181. https://doi.org/10.1016/j.apcatb.2017.08.040

Yildirim OA (2018) Synthesis of Ag-doped ZnO nanofibers using electrospinning method and their photocatalytic activities. Selcuk Univ J Eng Sci Technol 6:633–642. https://doi.org/10.15317/Scitech.2018.157

Yu X, Hou T, Sun X, Li Y (2012) The influence of defects on Mo-doped TiO_2 by first-principles studies. ChemPhysChem 13:1514–1521. https://doi.org/10.1002/cphc.201101012

Yu C, He H, Fan Q et al (2019) Novel B-doped BiOCl nanosheets with exposed (001) facets and photocatalytic mechanism of enhanced degradation efficiency for organic pollutants. Sci Total Environ 694:133727. https://doi.org/10.1016/j.scitotenv.2019.133727

Yun HH, Kim JS, Kim EH et al (2015) Enhanced photocatalytic activity of TiO_2@mercapto-functionalized silica toward colored organic dyes. J Mater Sci 50:2577–2586. https://doi.org/10.1007/s10853-015-8823-5

Yusof NSM, Babgi B, Alghamdi Y et al (2016) Physical and chemical effects of acoustic cavitation in selected ultrasonic cleaning applications. Ultrason Sonochem 29:568–576. https://doi.org/10.1016/j.ultsonch.2015.06.013

Yusuf A, Garlisi C, Palmisano G (2018) Overview on microfluidic reactors in photocatalysis: applications of graphene derivatives. Catal Today 315:79–92. https://doi.org/10.1016/j.cattod.2018.05.041

Zada N, Khan I, Saeed K (2017) Synthesis of multiwalled carbon nanotubes supported manganese and cobalt zinc oxides nanoparticles for the photodegradation of malachite green. Sep Sci Technol 52:1477–1485. https://doi.org/10.1080/01496395.2017.1285920

Zeng T, Yu M, Zhang H et al (2017) In situ synthesis of cobalt ferrites-embedded hollow N-doped carbon as an outstanding catalyst for elimination of organic pollutants. Sci Total Environ 593–594:286–296. https://doi.org/10.1016/j.scitotenv.2017.03.180

Zeng Y, Liu X, Liu C et al (2018) Scalable one-step production of porous oxygen-doped g-C_3N_4 nanorods with effective electron separation for excellent visible-light photocatalytic activity. Appl Catal B Environ 224:1–9. https://doi.org/10.1016/j.apcatb.2017.10.042

Zhang Y, Tang Z-R, Fu X, Xu Y-J (2010) TiO_2 – graphene nanocomposites for gas-phase photocatalytic degradation of volatile aromatic pollutant: is TiO_2 – graphene truly different from other TiO_2 – carbon composite materials? ACS Nano 4:7303–7314. https://doi.org/10.1021/nn1024219

Zhang Y, Tang Z-R, Fu X, Xu Y-J (2011) Engineering the unique 2D mat of graphene to achieve graphene-TiO_2 nanocomposite for photocatalytic selective transformation: what advantage does graphene have over its forebear carbon nanotube? ACS Nano 5:7426–7435. https://doi.org/10.1021/nn202519j

Zhang X, Dong S, Zhou X et al (2015a) A facile one-pot synthesis of Er–Al co-doped ZnO nanoparticles with enhanced photocatalytic performance under visible light. Mater Lett 143:312–314. https://doi.org/10.1016/j.matlet.2014.12.094

Zhang X, Qin J, Hao R et al (2015b) Carbon-doped ZnO nanostructures: facile synthesis and visible light photocatalytic applications. J Phys Chem C 119:20544–20554. https://doi.org/10.1021/acs.jpcc.5b07116

Zhang W, Ding L, Luo J et al (2016) Membrane fouling in photocatalytic membrane reactors (PMRs) for water and wastewater treatment: a critical review. Chem Eng J 302:446–458. https://doi.org/10.1016/j.cej.2016.05.071

Zhang Y, Hu H, Chang M et al (2017) Non-uniform doping outperforms uniform doping for enhancing the photocatalytic efficiency of Au-doped TiO_2 nanotubes in organic dye degradation. Ceram Int 43:9053–9059. https://doi.org/10.1016/j.ceramint.2017.04.050

Zhang D, Wang F, Cao S, Duan X (2018) Rapid microwave irradiation synthesis and characterization of $Bi_7O_9I_3$ photocatalyst for the degradation of bisphenol A. Mater Lett 218:32–35. https://doi.org/10.1016/j.matlet.2018.01.105

Zhao H, Liu X, Cao Z et al (2016) Adsorption behavior and mechanism of chloramphenicols, sulfonamides, and non-antibiotic pharmaceuticals on multi-walled carbon nanotubes. J Hazard Mater 310:235–245. https://doi.org/10.1016/j.jhazmat.2016.02.045

Zhao S, Zhang Y, Zhou Y et al (2017a) Ionic liquid-assisted photochemical synthesis of ZnO/Ag_2O heterostructures with enhanced visible light photocatalytic activity. Appl Surf Sci 410:344–353. https://doi.org/10.1016/j.apsusc.2017.03.051

Zhao Y, Zhang Y, Liu A et al (2017b) Construction of three-dimensional hemin-functionalized graphene hydrogel with high mechanical stability and adsorption capacity for enhancing photodegradation of methylene blue. ACS Appl Mater Interfaces 9:4006–4014. https://doi.org/10.1021/acsami.6b10959

Zhao P, Qin N, Wen JZ, Ren CL (2017c) Photocatalytic performances of ZnO nanoparticle film and vertically aligned nanorods in chamber-based microfluidic reactors: reaction kinetics and flow effects. Appl Catal B Environ 209:468–475. https://doi.org/10.1016/j.apcatb.2017.03.020

Zheng B, Guo Q, Wang D et al (2015) Energy-transfer modulation for enhanced photocatalytic activity of near-infrared upconversion photocatalyst. J Am Ceram Soc 98:136–140. https://doi.org/10.1111/jace.13232

Zheng X, Shen Z-P, Shi L et al (2017) Photocatalytic membrane reactors (PMRs) in water treatment: configurations and influencing factors. Catalysts 7:224. https://doi.org/10.3390/catal7080224

Zhong D, Liu W, Tan P et al (2018) Insights into the synergy effect of anisotropic 001 and {230}facets of $BaTiO_3$ nanocubes sensitized with CdSe quantum dots for photocatalytic water reduction. Appl Catal B Environ 227:1–12. https://doi.org/10.1016/j.apcatb.2018.01.009

Zhou F, Yan C, Liang T et al (2018) Photocatalytic degradation of Orange G using sepiolite-TiO_2 nanocomposites: optimization of physicochemical parameters and kinetics studies. Chem Eng Sci 183:231–239. https://doi.org/10.1016/j.ces.2018.03.016

Zhu S, Wang J, Fan W (2015) Graphene-based catalysis for biomass conversion. Catal Sci Technol 5:3845–3858. https://doi.org/10.1039/C5CY00339C

Zhu D, Liu S, Chen M et al (2018) Flower-like-flake Fe_3O_4/g-C_3N_4 nanocomposite: facile synthesis, characterization, and enhanced photocatalytic performance. Colloids Surf A Physicochem Eng Asp 537:372–382. https://doi.org/10.1016/j.colsurfa.2017.10.053

Zhu Z, Yang P, Li X et al (2020) Green preparation of palm powder-derived carbon dots co-doped with sulfur/chlorine and their application in visible-light photocatalysis. Spectrochim Acta Part A Mol Biomol Spectrosc 227:117659. https://doi.org/10.1016/j.saa.2019.117659

Zou J, Yu Y, Yan W et al (2019) A facile route to synthesize boron-doped g-C_3N_4 nanosheets with enhanced visible-light photocatalytic activity. J Mater Sci 54:6867–6881. https://doi.org/10.1007/s10853-019-03384-0

Zouzelka R, Kusumawati Y, Remzova M et al (2016) Photocatalytic activity of porous multiwalled carbon nanotube-TiO_2 composite layers for pollutant degradation. J Hazard Mater 317:52–59. https://doi.org/10.1016/j.jhazmat.2016.05.056